1983-12

The effect of interior motion on seasonal thermocline evolution.

Garner, Janice P.

NAVAL POSTGRADUATE SCHOOL
Monterey, California

THESIS

THE EFFECT OF INTERIOR MOTION
ON
SEASONAL THERMOCLINE EVOLUTION

by

Janice P. Garner

December 1983

Thesis Advisor: R. W. Garwood,Jr.

Approved for public release; distribution unlimited

SECURITY CLASSIFICATION OF THIS PAGE (When Data Entered)

REPORT DOCUMENTATION PAGE		READ INSTRUCTIONS BEFORE COMPLETING FORM
1. REPORT NUMBER	2. GOVT ACCESSION NO.	3. RECIPIENT'S CATALOG NUMBER
4. TITLE (and Subtitle) The Effect of Interior Motion on Seasonal Thermocline Evolution		5. TYPE OF REPORT & PERIOD COVERED Master's Thesis December 1983 6. PERFORMING ORG. REPORT NUMBER
7. AUTHOR(s) Janice P. Garner		8. CONTRACT OR GRANT NUMBER(s)
9. PERFORMING ORGANIZATION NAME AND ADDRESS Naval Postgraduate School Monterey, California 93943		10. PROGRAM ELEMENT, PROJECT, TASK AREA & WORK UNIT NUMBERS
11. CONTROLLING OFFICE NAME AND ADDRESS Naval Postgraduate School Monterey, California 93943		12. REPORT DATE December 1983 13. NUMBER OF PAGES 85
14. MONITORING AGENCY NAME & ADDRESS(if different from Controlling Office)		15. SECURITY CLASS. (of this report) Unclassified 15a. DECLASSIFICATION/DOWNGRADING SCHEDULE

16. DISTRIBUTION STATEMENT (of this Report)

Approved for public release, distribution unlimited.

17. DISTRIBUTION STATEMENT (of the abstract entered in Block 20, if different from Report)

18. SUPPLEMENTARY NOTES

19. KEY WORDS (Continue on reverse side if necessary and identify by block number)

mixed layer modelling, vertical advection,
long period interior motion.

20. ABSTRACT (Continue on reverse side if necessary and identify by block number)

The response of the seasonal thermocline formation and mixing to prescribed vertical interior motion is examined. For the annual and shorter period interior motion cases studied, the response was strongest for the annual period. For an oscillatory vertical motion having a 15 m amplitude

DD FORM 1 JAN 73 1473 EDITION OF 1 NOV 65 IS OBSOLETE
S/N 0102-LF-014-6601

at a 75 m depth, warm sea surface temperature anomalies of up to 2.16 C and cold anomalies of up to 2.04 C are found, depending on the phase difference between the interior motion and the annual heat cycle. The net phase-averaged effect on the mixed layer for annual period interior motion is a reduction in vertical mixing. Higher frequency motion produces a net enhancement of the mixing.

The Effect of Interior Motion on Seasonal Thermocline Evolution

by

Janice P. Garner
Lieutenant, United States Navy
B.A., Montclair State College, 1972
M.A., Indiana University, 1974

Submitted in partial fulfillment of the
requirements for the degree of

MASTER OF SCIENCE IN METEOROLOGY AND OCEANOGRAPHY

from the

NAVAL POSTGRADUATE SCHOOL
December 1983

ABSTRACT

The response of the seasonal thermocline formation and mixing to prescribed vertical interior motion is examined. For the annual and shorter period interior motion cases studied, the response was strongest for the annual period. For an oscillatory vertical motion having a 15 m amplitude at a 75 m depth, warm sea surface temperature anomalies of up to 2.16°C and cold anomalies of up to 2.04°C are found, depending on the phase difference between the interior motion and the annual heat cycle. The net phase-averaged effect on the mixed layer for annual period interior motion is a reduction in vertical mixing. Higher frequency motion produces a net enhancement of the mixing.

TABLE OF CONTENTS

LIST OF FIGURES

ACKNOWLEDGMENT

I wish to thank Professors R.W. Garwood and A.J. Willmott for their valuable help and encouragement during the undertaking of this thesis.

I. INTRODUCTION

Interior vertical motion can play a significant role in the mechanical energy budget of the ocean boundary layer. Linden (1975) carried out experiments to observe mixed layer deepening in a stratified fluid. He found that internal waves are important in the energetics of the mixed layer and that the mixing process may provide a significant source of energy for the generation of internal waves. In this thesis the interior motion is prescribed and not affected by the mixed layer processes. However, the modelling of the interaction of free internal waves with mixed layer processes is an important area for future study. Linden points out that he did not account for waves generated elsewhere which propagate into the region of consideration. Also, the internal waves considered by Linden were of relatively high frequency.

De Szoeke (1980) found wind stress curl-driven vertical advection to be as important as the entrainment rate in mixed layer dynamics. Cushman-Roisin (1981) likewise found wind-driven advection to be as important as wind-driven mixing in mixed layer dynamics and temperature front formation.

Much work has been done to study the ocean response to storms. Price et al. (1978), in their work on the mixed layer response to storms, found it necessary to include vertical advection. Price (1981) found that upwelling will significantly enhance the sea-surface temperature response to a slowly moving hurricane. Adamec et al. (1981), using a two-dimensional model to study the oceanic response to a hurricane, found a strong interdependence between mixing and advection. Greatbatch (1983) also found advection to be

important in increasing maximum cooling due to the passage of a storm.

Only recently has much been done to include long period interior motion in mixed layer models. Stevenson (1980,1981) examined the response of the mixed layer when perturbed by linear Rossby waves. He found no mixed layer response during the first half of the heating season while the mixed layer is shallowing and a maximum sea surface temperature response at the end of the heating season and beginning of the cooling season. Stevenson found that the maximum response of mixed layer depth to the wave occurred at or near the end of the cooling season. Also, he found that the lowest frequency waves produced the greatest mixed layer depth and temperature responses. This study differs from that of Stevenson in that a finite amplitude prescribed interior motion is used rather than a linear Rossby wave. This produces a phase dependent asymmetry in the mixed layer response to the interior motion.

Burger (1982) successfully introduced tidal period vertical advection into the Garwood (1976,1977) one-dimensional mixed layer model. He found that the interior motion had a significant effect on the near-surface temperature field and that the inclusion of the interior motion can improve the model for single station forecasting.

In this study, the Garwood (1976,1977) one-dimensional ocean planetary boundary layer model is used. Vertical advection was added to the model. The annual heat cycle is a sine function and wind stress is held constant at one dyne per square centimeter. By keeping the surface boundary conditions simple, the effect of the interior motion can be more readily observed.

The interior vertical motion is a prescribed, forced interior wave which is linear with depth and sinusoidal in time:

$$\bar{w}(z,t) = \frac{z}{D} W_o \sin\left(\frac{2\pi t}{T} + \phi\right), \qquad (1.1)$$

where D is a reference depth, 200 meters, and W_o is the amplitude of the prescribed vertical motion at depth, D. The periods, T, studied are one year, one-half year, one-third year and one-quarter year. The phase difference, ϕ, between the interior motion and the annual heating cycle is varied from 0° to 360° at increments of 22.5°. This interior motion is general and may be representative of a number of possible long period phenomena, for example, internal Rossby waves or perhaps Ekman pumping on seasonal scales.

The oceanic variables of interest are mixed layer depth, h, sea surface temperature which equals mixed layer temperature, $\bar{T}_{ML}$, the heat content, H, and the potential energy, P. These variables are contoured as functions of time and phase for each of the periods studied. Also, contours are made of the differences of these variables relative to the case of no interior motion. These contours are used to observe the effect of the interior motion on the mixed layer processes.

Furthermore, the phase, ϕ, in equation (1.1) can be replaced by the expression:

$$\phi = \frac{2\pi x}{L}, \qquad (1.2)$$

where x is horizontal displacement and L is some typical wavelength. Then, at any fixed x, equation (1.2) represents the vertical motion due to the passage of a travelling wave. The wavelength, L, might be, for example, 300 km for an annual baroclinic Rossby wave in the central north Pacific (Kang and Magaard, 1980). The phase in equation (1.1) can thus be related to horizontal location. The contours of h, $\bar{T}_{ML}$, H and P versus phase and time then indicate horizontal

structure in these variables due to the presence of the wave.

II. MODEL AND EQUATIONS

A. THE MODEL

1. Some General Considerations

For this study the Garwood (1976,1977) one-dimensional bulk mixed layer model is used. The model is based on the Navier-Stokes equations of motion, assumes the continuity equation for an incompressible fluid and makes the one-dimensional approximation. The Garwood model differs from previous bulk mixed layer models in several features. The time scale for viscous dissipation of turbulent kinetic energy, TKE, is dependent on planetary rotation. This allows for a cyclical steady state on an annual basis by increasing dissipation for deeper mixed layers. Both downward and upward turbulent heat fluxes are important in this model. Furthermore, entrainment depends on the relative distribution of TKE between vertical and horizontal components.

Before continuing, a comment on notation is in order. An overbar on a variable will indicate the horizontally averaged mean. A prime on a variable will indicate the fluctuation about this horizontal mean. Angled brackets, < >, will indicate vertically averaged, mixed layer mean.

2. Equation of State

In the Garwood model, the equation of state has the form:

$$\rho = \rho_0 \left[1 - \alpha (T - T_0) + \beta (S - S_0) \right] . \qquad (2.1)$$

The thermal expansion coefficient, α, is a function of T and is re-computed daily. The constants ρ_0, T_0 and S_0 are typical density, temperature and salinity values, respectively. In this study, salinity is fixed (precipitation and evaporation are disallowed) and set equal to the value of S_0. Equation (2.1) then becomes

$$\rho = \rho_0 \left[1 - \alpha (T - T_0) \right] . \qquad (2.2)$$

B. THE HEAT EQUATION

1. Initial Form

The time rate of change of temperature is given by the one-dimensional heat equation:

$$\frac{\partial \bar{T}}{\partial t} = - \frac{\partial}{\partial z} \left(\overline{w' T'} \right) + \frac{\partial}{\partial z} \left(\frac{Q}{\rho c_p} \right) - \bar{w} \frac{\partial \bar{T}}{\partial z} + \kappa \frac{\partial^2 \bar{T}}{\partial z^2} . \qquad (2.3)$$

The first term on the right is vertical turbulent heat flux, the second is solar insolation, the third is vertical temperature advection and the last, diffusion. All of the solar insolation will be assumed to be absorbed at the surface (in the first few centimeters) of the ocean. Hence, the solar insolation term will be dropped in favor of a surface boundary condition on the turbulent heat flux. Equation (2.3) then becomes

$$\frac{\partial \bar{T}}{\partial t} = - \frac{\partial}{\partial z} \left(\overline{w' T'} \right) - \bar{w} \frac{\partial \bar{T}}{\partial z} + \kappa \frac{\partial^2 \bar{T}}{\partial z^2} . \qquad (2.4)$$

In this model, mixed layer temperature is assumed to be vertically homogeneous. Equation (2.4) then reduces to

$$\frac{\partial \bar{T}_{ML}}{\partial t} = -\frac{\partial}{\partial z}\left(\overline{w'T'}\right) \tag{2.5}$$

for mixed layer temperature, $\bar{T}_{ML}$. Obviously, $\bar{T}_{ML}$ is equal to sea surface temperature because of the vertical homogeneity assumption in the mixed layer.

The surface boundary condition on heat flux is given by:

$$\left(\overline{w'T'}\right) = -\frac{Q}{\rho_o c_p} \tag{2.6}$$

where the zero subscript indicates the value of $\overline{w'T'}$ at z=0. The net surface heat flux, $Q/\rho_o c_p$, is prescribed to be harmonic in time:

$$\frac{Q}{\rho_o c_p} = \frac{Q_o}{\rho_o c_p} \sin\left(\frac{2\pi t}{1\ year}\right). \tag{2.7}$$

The amplitude of this sine function is set equal to a representative mid-latitude value of $4 \cdot 10^{-3}$°C cm/sec. In this study, heat flux is positive downward. Time t=0 is the start of the "heating season", when Q first becomes positive.

The boundary condition on heat flux at the base of the mixed layer is given by the entrainment heat flux,

$$\left(\overline{w'T'}\right)_h = -\Delta T\, w_e \quad , \tag{2.8}$$

where the subscript, h, indicates the value of $\overline{w'T'}$ at z=-h, the base of the mixed layer. The variable, We is the entrainment rate and ΔT is the temperature jump across the entrainment zone at the base of the mixed layer. The turbulent heat flux is linear with depth in the mixed layer (due to the assumption of a well-mixed layer), monotonically decreases with depth in the entrainment zone and is zero below. The profile of turbulent heat flux is shown in Figure 2.1. The net surface heat flux varies from positive

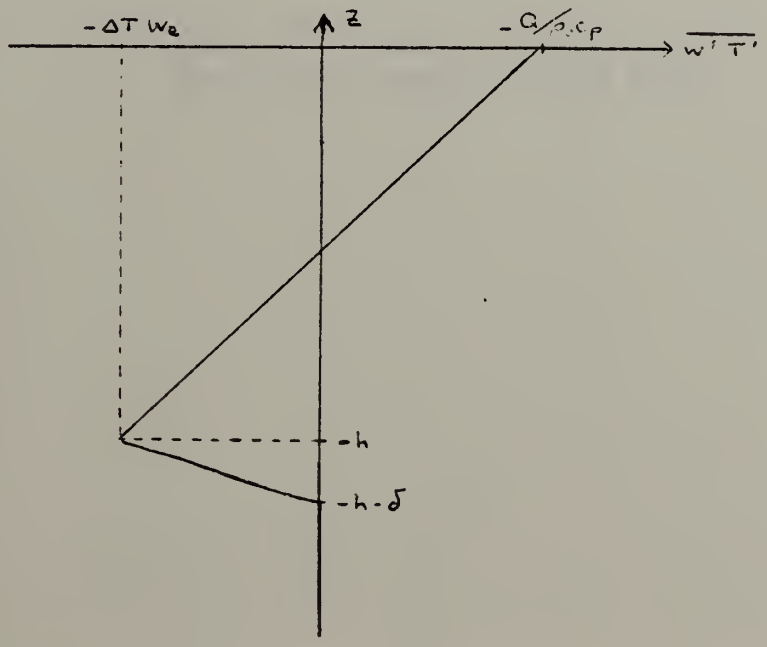

Figure 2.1 Turbulent Heat Flux Profile.

to negative values according to equation (2.7). The entrainment heat flux term, $-\Delta T\, We$, is always negative or zero. This is because the entrainment rate is positive when the mixed layer is deepening but "turns off" and is zero for non-entraining shallowing cases. The thickness of the

entrainment zone, δ, is assumed to be much less than the depth of the mixed layer, h.

Equation (2.5) now becomes

$$\frac{\partial \bar{T}_{ML}}{\partial t} = \frac{Q}{\rho_o c_p h} - \frac{\Delta T \, We}{h} . \qquad (2.9)$$

Note that the advection term is absent. Thus, the interior motion does not directly affect the mixed layer temperature. Instead, the interior motion affects the mixed layer temperature indirectly through the variables h, ΔT and We.

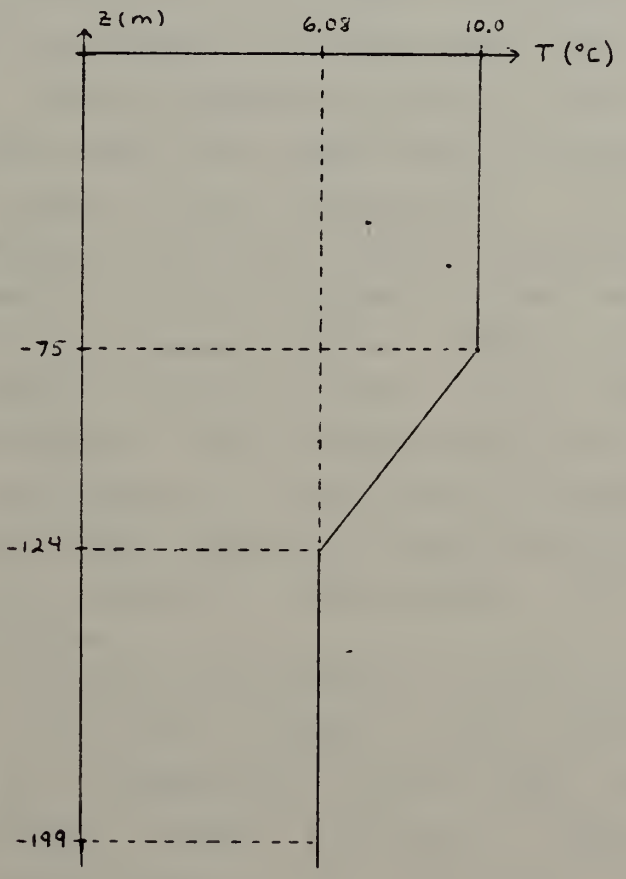

Figure 2.2 Initial Temperature Profile.

The initial temperature profile is given in Figure 2.2. The reference depth, D, is 200 m and will be used in some of the equations in later sections.

2. Scale Analysis and Simplification of the Heat Equation

Consider now the relative magnitudes of the terms of equation (2.4). In the mixed layer, the temperature may change by as much as 10 °C in a half year. The time rate of change of mixed layer temperature would then be on the order of 10^{-6} °C/sec or less. Below the mixed layer the time rate of change of temperature of fluid particles will generally be smaller.

The first term on the right of equation (2.4) is the turbulent heat flux term. In the mixed layer, the only term on the right side of equation (2.5) is the turbulent heat flux. Thus this term will scale with the seasonal time rate of change of mixed layer temperature, 10^{-6} °C/sec. The prescribed surface heat flux boundary condition, $Q/\rho_o c_p$, has extreme values of $\pm 4 \cdot 10^{-3}$ °C cm/sec. The value of h varies from around 30 m to around 100 m. Thus, the first term on the right side of equation (2.9) has a range of values between $\pm 10^{-6}$ °C/sec. The second term on the right of equation (2.9) has roughly the same order of magnitude, but it can only be negative. Below the mixed layer and entrainment zone, that is, below the flux region, the turbulent heat flux term vanishes.

Next consider the advection term in equation (2.4). Recall that this term is zero in the mixed layer. The gradient of the temperature profile just below the mixed layer is initially about 10^{-3} °C/cm. During the heating season the temperature at the top of the thermocline will increase, but the vertical extent of the thermocline will also increase as the mixed layer shallows. This term should

thus be expected to have the same order of magnitude. The amplitude of $\bar{W}$ will be prescribed according to equation (2.19) in section D. The maximum value at 200 m depends on the wave or oscillation frequency, but it will be on the order of 10^{-3} cm/sec. This amplitude will be smaller at lesser depths. The result is that the advection term of equation (2.4) should be of the order of 10^{-6} °C/sec below the mixed layer.

Finally, consider the diffusion term of equation (2.4). This term vanishes in the mixed layer. Below the mixed layer a reasonable scale for the second derivative of temperature is on the order of 4 °C/(5000 cm)^2. A typical range of values for the eddy diffusivity, K, is 0.1 to 0.5 cm^2/sec. Thus, the diffusion term has a magnitude of about 10^{-8} to 10^{-7} °C/sec. The diffusion term is much smaller than the other terms of equation (2.4) and will, from now on, be neglected. The heat equation (2.4) thus can be simplified to

$$\frac{\partial \bar{T}}{\partial t} = - \frac{\partial}{\partial z} \left(\overline{w'T'} \right) - \bar{w} \frac{\partial \bar{T}}{\partial z} , \qquad (2.10)$$

C. MIXED LAYER DEPTH

In the model of Garwood (1977), the mixed layer either shallows to a retreat depth, h_r, or deepens at the entrainment rate, We. The retreat depth is determined by assuming steady state conditions for the turbulent kinetic energy budget, letting entrainment heat flux vanish and letting $\langle \overline{w'^2} \rangle$ approach zero. The resulting equation for retreat depth is

$$h_r = \frac{m_3 u_*^3 - m_1 \langle \bar{E} \rangle^{3/2}}{(\alpha g/\rho)(\overline{w'T'})_0} , \qquad (2.11)$$

(Garwcod, 1977). In this equation, m_1 and m_3 are dimensionless model constants, α is the thermal expansion coefficient and $\langle \bar{E} \rangle$ is the mixed layer mean turbulent kinetic energy. Also, u_*, the friction velocity, is the square root of the surface wind stress divided by density. Throughout this study, it is set equal to one centimeter per second. Since mixed layer mean turbulent kinetic energy depends on surface boundary conditions, the retreat depth is independent of the prescribed interior motion.

In the case of active entrainment, the mixed layer deepening rate in the model depends on the entrainment rate and $\bar{W}_h$, the mean vertical velocity at the bottom of the mixed layer due to the prescribed interior motion:

$$\frac{\partial h}{\partial t} = w_e - \bar{W}_h . \qquad (2.12)$$

The entrainment rate, We, depends on the entrainment zone temperature jump, ΔT, and the entrainment heat flux (see equation (2.8)). The entrainment heat flux is modelled by

$$(\overline{w'T'})_h = \frac{-m_4 (\overline{w'^2})^{1/2} \langle \bar{E} \rangle}{\alpha g h} , \qquad (2.13)$$

(Garwcod, 1977), where m_4 is a model constant. The entrainment rate can then be expressed as

$$w_e = \frac{+m_4 (\overline{w'^2})^{1/2} \langle \bar{E} \rangle}{\alpha g h \Delta T} . \qquad (2.14)$$

Therefore, equations (2.12) and (2.14) give a solution for $\partial h/\partial t$ if $\bar{W}_h$, $\langle\overline{w'^2}\rangle$ and $\langle\bar{E}\rangle$ are known.

For moderately strong wind stress, mixed layer mean turbulent kinetic energy, $\langle\bar{E}\rangle$, depends primarily on surface wind stress, which is held constant here. The vertical component of turbulent kinetic energy, $(\overline{w'^2})^{1/2}$, depends primarily on surface heat flux and surface wind stress. When the surface heat flux becomes large enough, this term becomes zero, stopping the entrainment process and permitting shallowing. These two terms are unaffected by the interior motion. The entrainment rate is affected by the mean vertical motion indirectly as a result of changes in mixed layer depth, h, and entrainment zone temperature jump, ΔT.

D. INTERIOR VERTICAL MOTION

Consider for the moment a two layer, deep ocean with the upper layer about 200 m deep and the lower layer about 5000 m deep. Assuming the fluid is incompressible, the continuity equation is differentiated with respect to z:

$$\frac{\partial^2}{\partial z^2}\overline{w} = -\frac{\partial^2}{\partial x \partial z}\overline{u} - \frac{\partial^2}{\partial y \partial z}\overline{v}\,, \qquad (2.15)$$

where $\bar{U}$, $\bar{V}$ and $\bar{W}$ are the mean velocity components in either layer. Furthermore, assume that horizontal momentum is vertically well mixed in the upper layer. Thus,

$$\frac{\partial \bar{u}}{\partial z} = 0 \quad , \quad \frac{\partial \bar{v}}{\partial z} = 0 \qquad (2.16)$$

Then $\bar{W}$ must be linear with depth in the upper layer. With a rigid-lid approximation, $\bar{W} = 0$ at the surface.

Our interest is confined to the upper 200 m and a linear vertical profile for $\bar{W}$ is a good approximation for long period interior motion. The functional dependence of $\bar{W}$ on z is

$$\bar{W}(z) = - \frac{W_D}{D} z \ , \tag{2.17}$$

where D = 200 m is the reference depth and W_D is the interior vertical motion at 200 m given by a sinusiodal function of time, namely

$$W_D = - W_o \sin\left(\frac{2\pi t}{T} + \phi\right) . \tag{2.18}$$

The amplitude, W_o, is defined by

$$W_o = \frac{2\pi D}{T} \cdot \frac{15\ m}{75\ m} \ . \tag{2.19}$$

For the one-year period interior motion, $W_o = 8 \cdot 10^{-4}$ cm/sec = 69 cm/day. The value of W_o will be 2, 3 and 4 times this for the one-half, one-third and one-quarter year periods, respectively. These values of W_o are selected so that the displacement amplitude at 75 m is approximately 15 m. The actual values of the displacement amplitude depend on phase and will be discussed below.

Combining equations (2.17) and (2.18) yields the equation for the prescribed interior motion,

$$\bar{W}(z,t) = \frac{z}{D} W_o \sin\left(\frac{2\pi t}{T} + \phi\right) . \tag{2.20}$$

The formula for the particle position due to the interior motion can be obtained by noting that $\bar{W} = dz/dt$, and is given by

$$z = z_o \exp\left\{\frac{-T W_o}{2\pi D}\left[\cos\left(\frac{2\pi t}{T} + \phi\right) - \cos\left(\phi\right)\right]\right\} \quad . \qquad (2.21)$$

For any fixed phase the maximum and minimum values of z are given by

$$z_{max} = z_o \exp\left[\frac{-T W_o}{2\pi D}\left(-1 - \cos\phi\right)\right] \qquad (2.22)$$

and

$$z_{min} = z_o \exp\left[\frac{-T W_o}{2\pi D}\left(+1 - \cos\phi\right)\right] \quad . \qquad (2.23)$$

The peak-to-peak displacement amplitude is the difference,

$$z_{max} - z_{min} = z_o \exp\left(\frac{T W_o}{2\pi D}\cos\phi\right)\left[\exp\left(\frac{T W_o}{2\pi D}\right) - \exp\left(\frac{-T W_o}{2\pi D}\right)\right] . \qquad (2.24)$$

The maximum peak-to-peak displacement amplitude will occur when $\cos\phi = +1$ and the minimum when $\cos\phi = -1$. For the vertical motion amplitude given by equation (2.19), a particle with an initial position at z=-75 m will experience a displacement amplitude (half of the peak-to-peak value) between 12.4 and 18.4 m.

The model time step is one hour. This is much smaller than the one-year or even one-quarter year periods considered. Hence, since W_D does not vary significantly over a one hour time step, the integral of (2.17) can be approximated by

$$z_2 \simeq z_1 \exp\left(-\frac{W_D}{D}\Delta t\right) \quad , \tag{2.25}$$

where $\Delta t = t_2 - t_1$ is the time increment (one hour) and W_D is obtained from equation (2.18). In the model, vertical advection is handled by compressing or expanding the vertical grid according to equation (2.25). No significant difference in the results was found between model runs using equation (2.25) and equation (2.21).

The vertical increment is initially one meter, but this varies as a result of the compression or expansion of the vertical grid. This variation in the vertical increment is never more than about 25%. A consequence of this scheme is that the lowest grid point is not always at a depth of 199 m as in the initial profile, Figure 2.2. Care must be taken, therefore, when performing vertical integration from the surface to the reference depth, D = 200 m. The integrals that will be calculated in the next section involve the temperature difference, $\bar{T} - T_o$. Problems with varying the grid size can easily be avoided by setting the reference temperature, T_o, equal to $\bar{T}_D$, the initial temperature at 200 m. This way, $\bar{T} - \bar{T}_D$ will always be zero at the base of the vertical grid. The grid is initially made deep enough so that the seasonal thermocline never reaches the bottom of the grid; hence, $\bar{T}_D$ always equals its initial value, 6.08°C.

Subtracting the reference temperature, $\bar{T}_D$, from temperature, $\bar{T}$, in the integrals in the next section amounts to subtracting the terms:

$$-\int_{-D}^{0} \bar{\bar{T}}_D \, dz = -\bar{\bar{T}}_D \cdot D \tag{2.26}$$

and

$$-\int_{-D}^{0} \bar{T}_D \, z \, dz = \frac{\bar{T}_D D^2}{2} \quad . \tag{2.27}$$

Since $\bar{T}_D$ always remains constant, both expressions, (2.26) and (2.27), will always remain constant. Subtracting $\bar{T}_D$ from $\bar{T}$ will amount to subtracting constants from the integrals in the next section.

E. POTENTIAL ENERGY AND HEAT

The potential energy per unit area for a column of water from the surface to depth, D, is given by

$$\frac{PE}{area} = \int_{-D}^{0} g \rho \, z \, dz. \tag{2.28}$$

Employing equation (2.2) with $\bar{T}_D$ as the reference temperature, allows equation (2.28) to be written as

$$\frac{1}{\alpha g \rho_0} \frac{PE}{area} = -\int_{-D}^{0} (\bar{T} - \bar{T}_D) \, z \, dz + \text{constant}. \tag{2.29}$$

The constant in equation (2.29) is

$$\frac{1}{\alpha g \rho_0} \int_{-D}^{0} g \rho_0 \, z \, dz = -\frac{D^2}{2\alpha} \quad . \tag{2.30}$$

The integral in equation (2.29) will be used for the comparison of the potential energy with and without the interior motion. It will be represented by the variable P with units of °C m² where

$$P = -\int_{-D}^{0} (\bar{T} - \bar{T}_D) \, z \, dz \quad . \tag{2.31}$$

Similarly, heat content will be indicated by the variable H with units °C m where

$$H = \int_{-D}^{0} \left(\bar{T} - \bar{T}_D \right) dz . \tag{2.32}$$

The analysis of the physical effects of the interior motion can be facilitated by developing the expressions for the time rate of change of H and of P. First, differentiating equation (2.32) with respect to time gives

$$\frac{\partial H}{\partial t} = \frac{\partial}{\partial t} \int_{-D}^{0} \left(\bar{T} - \bar{T}_D \right) dz . \tag{2.33}$$

Equation (2.33) can be written as

$$\frac{\partial H}{\partial t} = \int_{-D}^{0} \frac{\partial \bar{T}}{\partial t} \, dz . \tag{2.34}$$

Substituting equation (2.10) for the time rate of change of temperature into equation (2.34) yields

$$\frac{\partial H}{\partial t} = - \int_{-D}^{0} \frac{\partial}{\partial z} \left(\overline{w'T'} \right) dz - \int_{-D}^{0} \bar{w} \frac{\partial \bar{T}}{\partial z} \, dz . \tag{2.35}$$

The first term on the right, when integrated, is just the net surface heat flux. Substituting equation (2.17) into the second term on the right of (2.35) and integrating by parts gives

$$-\int_{-D}^{0} \overline{w}\,\frac{\partial \overline{T}}{\partial z}\,dz = -\frac{w_D}{D}\left(-D\overline{T}_D + \int_{-D}^{0} \overline{T}\,dz\right). \tag{2.36}$$

Using equation (2.26) this can be rewritten as

$$-\int_{-D}^{0} \overline{w}\,\frac{\partial \overline{T}}{\partial z}\,dz = -\frac{w_D}{D}\int_{-D}^{0}\left(\overline{T}-\overline{T}_D\right)dz = -\frac{w_D}{D}\,H. \tag{2.37}$$

Equation (2.35) can now be written as

$$\frac{\partial H}{\partial t} = \frac{G}{\rho_o c_p} - \frac{w_D}{D}\,H. \tag{2.38}$$

The formulation for the time rate of change of the potential energy is similar and is given by

$$\frac{\partial P}{\partial t} = -\int_{-D}^{0} \frac{\partial \overline{T}}{\partial t}\,z\,dz. \tag{2.39}$$

Substituting equation (2.10) into (2.39) yields

$$\frac{\partial P}{\partial t} = +\int_{-D}^{0} z\,\frac{\partial}{\partial z}\left(\overline{w'T'}\right)dz + \int_{-D}^{0} z\,\overline{w}\,\frac{\partial \overline{T}}{\partial z}\,dz. \tag{2.40}$$

The first term in equation (2.40) can be integrated by parts:

$$\int_{-D}^{0} z\,\frac{\partial}{\partial z}\left(\overline{w'T'}\right)dz = z\left(\overline{w'T'}\right)\Big|_{-D}^{0} - \int_{-D}^{0}\left(\overline{w'T'}\right)dz. \tag{2.41}$$

The first term on the right of equation (2.41) vanishes because $\overline{w'T'} = 0$ at $z = -D$. Since $\overline{w'T'}$ is zero below the

entrainment zone, equation (2.41) reduces to

$$\int_{-D}^{0} z \frac{\partial}{\partial z} (\overline{w'T'}) \, dz = - \int_{-h-\delta}^{0} (\overline{w'T'}) \, dz . \tag{2.42}$$

This integral may be broken up over the mixed layer and the entrainment zone, producing

$$\int_{-D}^{0} z \frac{\partial}{\partial z} (\overline{w'T'}) \, dz = -h \langle \overline{w'T'} \rangle - \int_{-h-\delta}^{-h} \overline{w'T'} \, dz \ , \tag{2.43}$$

where $\langle \overline{w'T'} \rangle$ is the vertically averaged mixed layer mean of the turbulent heat flux. Since $\overline{w'T'}$ is linear with respect to z in the mixed layer, this mixed layer mean can be written

$$- \langle \overline{w'T'} \rangle = \frac{1}{2} \left(\frac{Q}{\rho_o c_p} + \Delta T \, w_e \right) . \tag{2.44}$$

Consider the second term on the right side of equation (2.40). Substituting equation (2.17) for $\overline{W}$ and integrating by parts yields

$$\int_{-D}^{0} z \overline{W} \frac{\partial \overline{T}}{\partial z} \, dz = \frac{w_D}{D} \left(+ D^2 \overline{T}_D + 2 \int_{-D}^{0} \overline{T} \, z \, dz \right) ; \tag{2.45}$$

using equation (2.27) this can be rewritten as

$$\int_{-D}^{0} z \overline{W} \frac{\partial \overline{T}}{\partial z} \, dz = \frac{2 w_D}{D} \int_{-D}^{0} (\overline{T} - \overline{T}_D) z \, dz = - \frac{2 w_D}{D} P . \tag{2.46}$$

On combining equations (2.40), (2.43), (2.44) and (2.46), the time rate of change of the potential energy variable now

becomes

$$\frac{\partial P}{\partial \tau} = \frac{h}{2}\left(\frac{G}{\rho_o c_p} + \Delta T w_e\right) - \int_{-h-\delta}^{-h} \overline{w'T'}\, dz - \frac{2w_D}{D} P. \qquad (2.47)$$

Because the turbulent heat flux is monotonic across the entrainment zone, as illustrated in Figure 2.1:

$$\left| \int_{-h-\delta}^{-h} \overline{w'T'}\, dz \right| < \delta \Delta T w_e << h \Delta T w_e . \qquad (2.48)$$

This indicates that the integral term in equation (2.47) should generally be smaller in magnitude than the first term on the right side, unless of course, the surface and entrainment heat fluxes nearly cancel.

Actual values of the terms of equation (2.47) were calculated for one-year period interior motion at two different phases and the second term on the right of the equation was smaller than the first, usually by one order of magnitude. Furthermore, the third term on the right was generally an order of magnitude larger than either of the other two. Equation (2.47) will thus be approximated by

$$\frac{\partial P}{\partial t} \approx \frac{h}{2}\frac{G}{\rho_o c_p} + \frac{1}{2} h \Delta T w_e - \frac{2w_D}{D} P. \qquad (2.49)$$

III. EXPERIMENTS AND RESULTS

A. SUMMARY OF PERTINENT EQUATIONS

The equations for time rate of change of mixed layer depth, mixed layer (and sea surface) temperature, heat and potential energy are

$$\frac{\partial h}{\partial t} = w_e - \overline{w}_h \quad , \tag{3.1}$$

$$\frac{\partial \overline{T}_{ML}}{\partial t} = \frac{Q}{\rho_o c_p h} - \frac{\Delta T w_e}{h} \quad , \tag{3.2}$$

$$\frac{\partial H}{\partial t} = \frac{Q}{\rho_o c_p} - \frac{w_D}{D} H \quad , \tag{3.3}$$

and

$$\frac{\partial P}{\partial t} = \frac{h}{2} \frac{Q}{\rho_o c_p} + \frac{1}{2} h \Delta T w_e - \frac{2 w_D}{D} P \, . \tag{3.4}$$

The retreat depth is given by

$$h_r = \frac{-m_3 u_*^3 + m_1 \langle \overline{E} \rangle^{3/2}}{\frac{\alpha g}{2} \frac{Q}{\rho_o c_p}} \quad , \tag{3.5}$$

where $(\overline{w'T'})_o$ has been replaced by equation (2.6).

The entrainment rate is given by

$$\Delta T\, w_e = \frac{m_4 (\overline{w'^2})^{1/2} \langle E \rangle}{2gh} \quad (3.6)$$

The prescribed net surface heat flux is given by

$$\frac{G}{\rho_o c_p} = \frac{Q_o}{\rho_o c_p} \sin\left(\frac{2\pi t}{1\ \text{year}}\right) \quad (3.7)$$

and is plotted as a function of time in Figure 3.1.

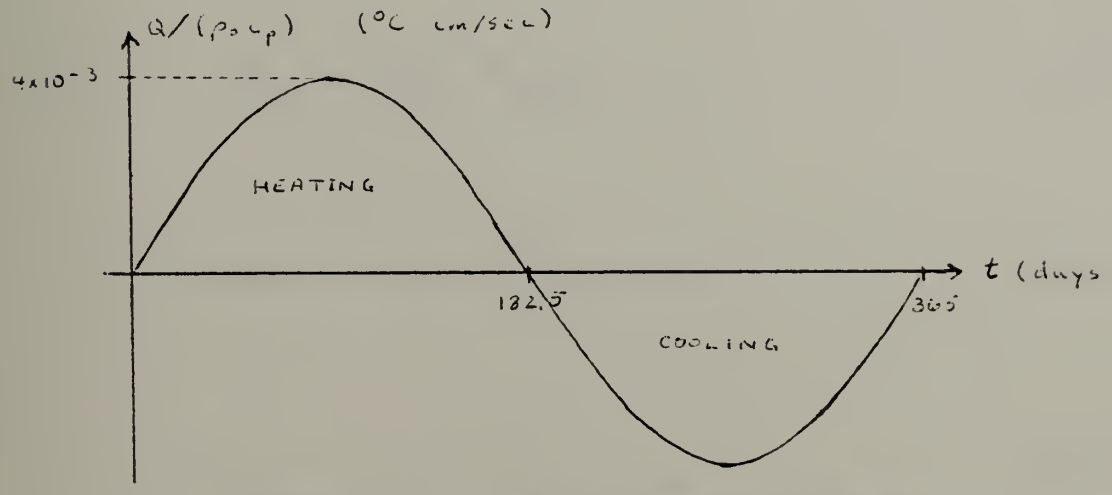

Figure 3.1 Net Surface Heat Flux.

The prescribed vertical motion at the reference depth, D=200 m, is

$$w_D = -w_e \sin\left(\frac{2\pi t}{T} + \phi\right), \quad (3.8)$$

where W_o is defined by equation (2.19). By substituting z=-h into equation (2.17), it can be seen that $\bar{W}_h$ varies directly as h and W_D.

Some additional nctation will be useful for the discussion of the results. To observe the effect of the interior

motion, the values of h, $\bar{T}_{ML}$, H and P are compared to those without interior motion. Contours are plotted of the difference of mixed layer depth with and without the interior motion, likewise for mixed layer temperature, heat and potential energy. Therefore, the following new variables are defined:

$$\Delta h = h - h\big|_{\bar{w}=0} , \tag{3.9}$$

$$\Delta \bar{T}_{ML} = \bar{T}_{ML} - \bar{T}_{ML}\big|_{\bar{w}=0} , \tag{3.10}$$

$$\Delta H = H - H\big|_{\bar{w}=0} , \tag{3.11}$$

$$\Delta P = P - P\big|_{\bar{w}=0} . \tag{3.12}$$

B. RESULTS WITH NO INTERIOR MOTION

The mixed layer depth has been plotted in Figure A.4. Note that the vertical axis scale is inverted for clarity. The year was started at the beginning of the heating season and the mixed layer retreats for the first quarter year. Then the mixed layer deepens slowly for the next half year and more rapidly in the last quarter. In the last few days the mixed layer shallows to the t=0,1 year,...,n-years cyclical steady state value of about 75 m.

The mixed layer temperature, $\bar{T}_{ML}$, is plotted in Figure A.5. As expected, the mixed layer temperature increases during the heating season and decreases during the cooling season, for the most part. However, note that the peak mixed layer temperature occurs around day 170 and $\bar{T}_{ML}$ starts to decrease ten days before the end of the heating season. This is because the entrainment heat flux term has begun to dominate equation (3.2). Some entrainment had already started fifty days earlier. By day 170, towards the end of the heating season, ΔT has reached its largest value, 7.8 °C. On day 170 the cooling of the mixed layer due to entrainment has reached 0.021 °C per day while the surface heating has dropped to 0.030 °C per day.

The heat content, plotted in Figure A.6, depends only on surface heat flux for the case of no interior motion (see equation (3.3)). Any heat lost from the mixed layer due to entrainment will be gained by the region below. Since heat is calculated from the surface to 200 m, entrainment will have no effect on its value.

Potential energy per unit area is plotted in Figure A.7. This, too, generally increases with heating and decreases with cooling. However, note that the peak value occurs at about day 305, 25 days into the cooling season. This is because potential energy is also increased by mixing as indicated by equation (3.4). The entrainment term dominates equation (3.4) from day 170 until day 305, when the net surface heat flux is near zero. A close inspection of Figure A.7 reveals that the potential energy at the end of the year is greater than the initial value. Specifically, the initial value of P is 19608 °C m²; the value at the end of the first model year is 20204 °C m² and at the end of the second year is 20579 °C m². This increase in the potential energy is due to the adjustment of the temperature profile as the ocean approaches cyclical steady state.

Figure A.1 is a plot of temperature versus depth and time. The top of the graph where the temperature contours are vertical is the mixed layer. The mixed layer structure is quite evident after the first quarter year due to the strong temperature gradient at the base of the mixed layer. Note that the temperature profile at any depth below the mixed layer is left unchanged until mixing reaches that depth.

C. ONE-YEAR PERIOD INTERIOR MOTION

The zero contours of the prescribed interior motion have been drawn in Figure A.8 with upwelling and downwelling indicated. The dotted contours indicate when the magnitude of the interior motion drops to half of the maximum value.

During the first quarter year the mixed layer is shallowing. Since the retreat depth depends primarily on surface boundary conditions, mixed layer depth will be unaffected by interior motion at this time. This is borne out by the contours of Δh (defined in equation (3.9)), Figure A.10. The first quarter year shows no difference in mixed layer depth. With little or no effect on mixed layer depth during the first quarter year, there will be little or no difference in the value of the first term of equation (3.2) with and without the interior motion. The second term of equation (3.2) will be zero at this time since entrainment stops during shallowing. Hence, mixed layer temperature will also remain unaffected by the interior motion during the first quarter year. This can be seen in Figure A.12. Heat and potential energy, on the other hand, are influenced by the advection of temperature in the thermocline as indicated by the presence of the last term in equation (3.3) and equation (3.4). Thus, the interior motion will influence heat content and potential energy even during the first quarter year (Figures A.16 and A.18).

1. Effect on Mixed Layer Depth

Equation (3.1) indicates that downwelling will enhance deepening, and upwelling will reduce deepening. In Figure A.9, it can be seen that deepening still does occur after the first quarter year as it did without any interior motion. However, the rate of deepening depends on phase.

At the 90° phase, there is upwelling during the middle half of the model year (see Figure A.2) reducing the rate of deepening. At day 274 downwelling begins and the mixed layer begins to deepen more rapidly. The very rapid deepening in the last quarter of the year for this phase results from both entrainment and downwelling working together. Calculated values of the terms of equation (3.1) indicate that entrainment is the dominant term most of the time during deepening. In this example the entrainment rate has been enhanced by conditions set-up by the interior motion. Equation (3.6) indicates that entrainment rate, We, is inversely proportional to mixed layer depth, h, and entrainment zone temperature jump, ΔT. Compare Figure A.2 to Figure A.1 (the case with no interior motion) and A.3 (the 270° phase case). It can be seen that at the start of the last quarter of the year the 90° phase case has a much lower mixed layer temperature than the other two cases (the reason for this will be discussed in the next section). This lower mixed layer temperature means that the entrainment zone temperature jump will be smaller, allowing for a larger entrainment rate. At the start of the last quarter of the year, the differences in h are not as significant as those in ΔT.

For example, the values of ΔT, h, We and $\overline{W}_k$ have been calculated for these three cases for day 280. The mixed layer depth, h, is about 60 m for the case without interior motion, 65 m for the 90° phase and 68 m for the

270° phase. These values do not greatly differ. However, the temperature jump for the 90° phase case is 1.3°C which is less than half the 2.9°C value for the case with no interior motion which in turn is less than the 4.7°C value for the 270° case. The entrainment rate for the 90° phase case is 90 cm/day compared to 43 cm/day for the no interior motion case and 22 cm/day for the 270° case. For both phases considered, the interior motion is at least an order of magnitude smaller than the entrainment rate. Nevertheless, at day 280, the deepening in the 90° phase case is helped a little by downwelling and in the 270° case, hindered a little by upwelling.

In the last few days of the year, the increase in mixed layer depth begins to take over, particularly for the 90° case. This inhibits further entrainment and the mixed layer then rapidly shallows to the cyclical steady-state value of 75 m (Figure A.9).

In the 270° phase case (Figure A.3) there is downwelling during the middle half of the year, which increases the deepening of the mixed layer. By the start of the last quarter of the year, the mixed layer is warmer than in the case with no interior motion or in the 90° phase case. This leads to a larger value of ΔT and a reduced entrainment rate.

Comparing Figures A.8 and A.9 it can be seen that mid-year upwelling is associated with a reduced rate of deepening and mid-year downwelling is associated with an increased deepening rate. Looking at Figure A.10, it can be seen that the actual decreased or increased values of mixed layer depth lag the start of upwelling or downwelling (respectively) by 90°. The time rate of change of mixed layer depth tracks along with the interior motion in accordance with equation (3.1). However, actual mixed layer depth is the integral of this and integrals of periodic

functions lag them by 90°. Also note that the strong enhancement of and strong hindrance to deepening at the end of the year (Figure A.10) lags the strong decrease and strong increase in mixed layer temperature (Figure A.12) by about 90°.

2. Effect on Mixed Layer Temperature

Consider now the mixed layer heat equation (3.2). The net surface heat flux is prescribed and unaffected by the interior motion. The entrainment heat flux, given by equation (3.6), is inversely proportional to mixed layer depth. The other terms in equation (3.6) depend primarily on surface boundary conditions. So, the first term in equation (3.2) is inversely proportional to mixed layer depth, h, and the second, inversely proportional to the square of h. This implies that an increase in h will reduce the magnitude of mixed layer temperature change; a decrease in h will increase the change in $\bar{T}_{ML}$. This is because, with a deeper mixed layer, a given amount of heat added to or removed from the mixed layer must be spread over a larger mass of water.

This effect is illustrated in the examples shown in Figures A.2 and A.3. In Figure A.2, the mixed layer is shallower than in Figure A.3 from about day 180 to about day 300. This resulted from the mid-year upwelling for the 90° phase case and the mid-year downwelling for the 270° case. The shallower mixed layer in Figure A.2 allows for a much more rapid temperature drop than occurs with the deeper mixed layer of Figure A.3. This can be seen in the enhanced gradients in Figure A.2. After day 300, the rapid deepening of the mixed layer for the 90° phase case and slow deepening for the 270° case reverse the situation.

To see the effect of the interior motion for all of the phases, the $\bar{T}_{ML}$ contours should not be compared directly

to the interior motion contours but rather to the contours of the mixed layer depth difference, Δh (defined by equation (3.9)). Between the 0° and 180° phases, after day 180 there is a region in Figure A.10 where the mixed layer is shallower with the interior motion than without. This causes the mixed layer temperature decrease (the second half of the year is the cooling season) to be greater, resulting in the negative values of $\Delta \bar{T}_{ML}$ in the last quarter year at these phases (Figure A.12). Between the 180° and 360° phases the opposite occurs.

At the end of the year the mixed layer depth returns to 75 m. Mixed layer temperature does not return to its initial value. The second year $\bar{T}_{ML}$ data is plotted in Figures A.13 and A.14. The reduced temperatures for phases 0° to 180° and increased temperatures for phases 180° to 360° are continued into the second year. The mixed layer depth follows the same pattern in the second year as it did in the first. This causes the $\bar{T}_{ML}$ pattern begun in the first year to be enhanced in the second year. Continued pumping of the ocean by this period interior motion enhances this structure. If permitted, it would eventually cause the upper 200 m to become isothermal (in the region of the 90° phase at the end of the year), followed by deepening beyond the limits of what the model can handle. It would not be realistic, however, to have this single period interior motion continue for the several years necessary for this to happen. In reality, the interior motion would probably be damped by interactions with the boundary layer mixing processes. There should also be more than one period present. Furthermore, surface heat flux should be influenced by sea surface temperature. These three possibilities open up avenues for further research.

3. Effect on Heat Content

Equation (3.3) indicates that change in the heat content depends on net surface heat flux and on pumping of the ocean by the interior motion. The net surface heat flux is prescribed and is independent of the interior motion. Subtracting equation (3.3) for the case of no interior motion from the same equation with interior motion gives

$$\frac{\partial \Delta H}{\partial t} = - \frac{w_D}{D} H \,, \tag{3.13}$$

where ΔH is defined by equation (3.11). Equation (3.13) indicates that upwelling will cause ΔH to decrease and downwelling will cause ΔH to increase. This can be observed by comparing Figures A.8 and A.16. The input to heat content due to net surface heat flux alone causes H to increase during the first half of the year and decrease during the second half as shown in Figure A.6. The combination of surface heating with the effect of the interior motion produces the saddle-shaped curve shown in Figure A.15.

The effect of different phases of the interior motion can be demonstrated by the following two simple examples (Figures 3.2 and 3.3). No mixing is permitted and a two-layer ocean is assumed for simplicity.

In the first example shown in Figure 3.2 there is initial downwelling followed by heating, then upwelling followed by cooling and final downwelling to the initial mixed layer depth. When downwelling precedes heating, the heat is distributed over a thicker mixed layer. A fixed amount of heat will produce a smaller increase in T than would have resulted without the downwelling. If this is followed by upwelling before cooling, the thinner mixed

		Heat (°C m)
initial	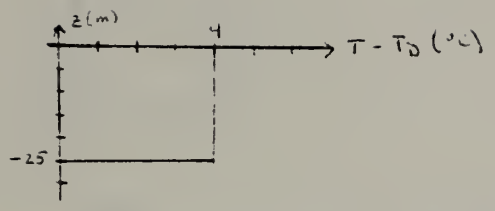	100
downwelling	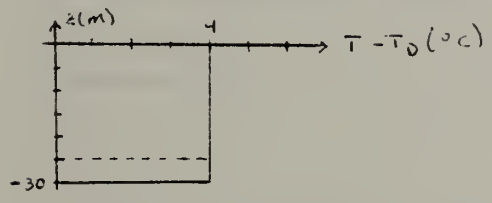	120
heating	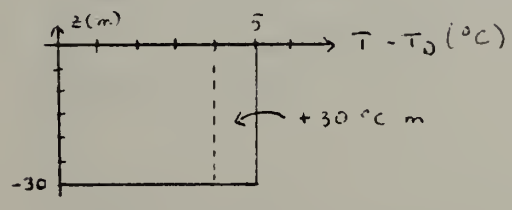	150
upwelling	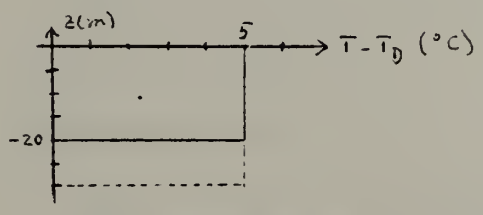	100
cooling	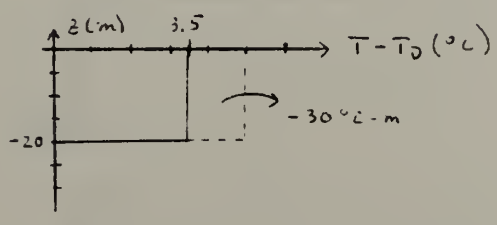	70
downwelling	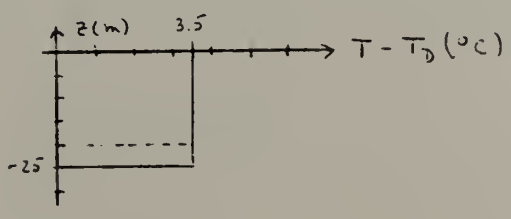	87.5

Figure 3.2 Heat Content Example 1.

		Heat (°C m)
initial	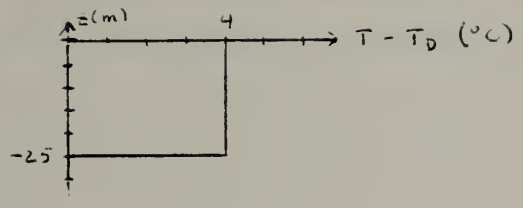	100
upwelling	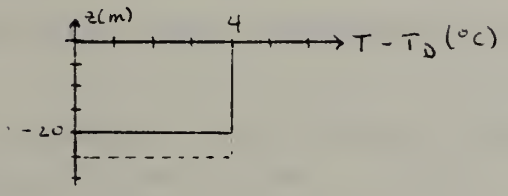	80
heating	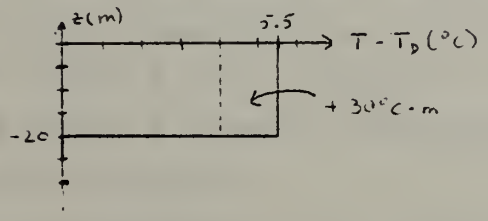	110
downwelling	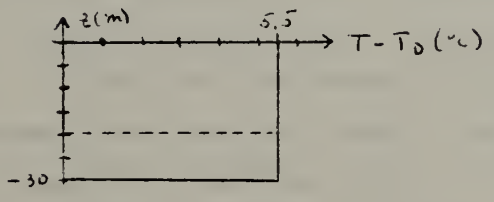	165
cocling	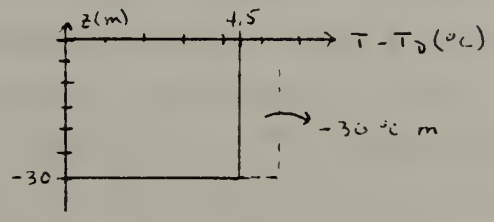	135
upwelling	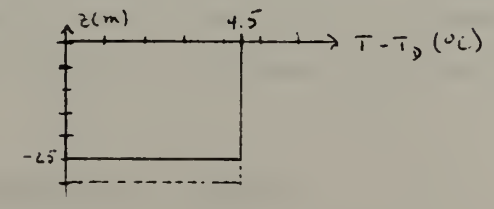	112.5

Figure 3.3 Heat Content Example 2.

layer will reach a lower temperature for a given amount of heat removed. At the end of the complete cycle the mixed layer temperature will be lower. Recall that the heat content is defined by

$$H = \int_{-D}^{0} (T - T_b)\, dz .$$

Therefore the lower mixed layer temperature produces a lower heat content.

Upwelling preceding the heating season distributes the heat over a thinner mixed layer. This allows a greater increase in T than would otherwise occur. If this is followed by downwelling preceding the cooling season, a fixed amount of heat removed will produce a smaller drop in T. The net effect will be a higher temperature in the mixed layer and a higher heat content.

Because of the asymmetry, as illustrated in these examples, heat is not conserved for a particular phase of the interior motion. This can be seen in Figures A.15 and A.16. At some phases the year-end heat content is higher than it was at the beginning of the year, at other phases, lower. However, if the heat content is averaged over all of the phases, the year-end value equals the initial value. The average heat content for sixteen equally spaced phases from 0° to 360° was tabulated. The phase-averaged value of H was 0.07°C m less at the end of the year than it was initially. This small error can be attributed to the coarse resolution of averaging only sixteen phases over the entire 360°.

4. Effect on Potential Energy

Time rate of change of potential energy is given by equation (3.4). From this equation it can be seen that surface heating tends to increase potential energy, surface

cooling tends to decrease it. The net surface heat flux is independent of the interior motion so the effect on ΔP due to this term depends on Δh. If there is an increase in mixed layer depth during heating, the buoyancy added will be mixed deeper, increasing potential energy. If there is an increase in mixed layer depth during cooling the effect will be opposite.

The entrainment heat flux term has a positive sign in equation (3.4). Increased mixing moves buoyant water down and less buoyant water upward, increasing potential energy.

Comparison of values of the terms of equation (3.4) indicates that the third term on the right is generally dominant. The exception is when the interior motion goes to zero, twice a year. The first term of equation (3.4) will not differ greatly with and without interior motion unless there is a large difference in mixed layer depth. Recall that entrainment heat flux is nearly inversely proportional to mixed layer depth (equation (3.6)). Thus, the second term will not vary significantly. So, the potential energy closely follows the interior motion. This can be seen by comparing Figures A.8 and A.18. During downwelling, potential energy increases, during upwelling it decreases.

The physical reasoning behind the effect of the third term of equation (3.4), the pumping term, is that downwelling pushes buoyant surface water downward, whereas, upwelling is in the same direction as the buoyant forces.

5. Summary of Response to One-Year Period Interior Motion

During the first quarter year there is shallowing and the interior motion has little effect on either mixed layer depth or temperature. Mid-year upwelling reduces deepening and mid-year downwelling enhances deepening. The

shallower mixed layer resulting from upwelling will cool faster; the deeper mixed layer resulting from downwelling will cool slower. A cooler mixed layer has a reduced ΔT allowing for a larger entrainment rate and more rapid deepening. A warmer mixed layer deepens more slowly.

Potential energy and heat are both directly affected by the interior motion. Both are increased by downwelling and decreased by upwelling.

Before examining the mixing response to higher frequencies, an observation can be made regarding horizontal structure produced by the interior motion. As noted in chapter one, phase may be related to horizontal displacement by substituting

$$\phi = \frac{2\pi x}{L} \tag{3.14}$$

into equation (2.20) to obtain

$$\overline{w} = \frac{z}{D} W_o \sin\left(\frac{2\pi t}{T} + \frac{2\pi x}{L}\right). \tag{3.15}$$

The wavelength, L, might be on the order of 300 km, large enough for the one-dimensional assumption to be valid.

Figures A.12 and A.14 show the development of horizontal bands of positive and negative mixed layer temperature anomalies which would result from a one-year period interior wave. Because temperature is assumed to be vertically homogeneous in the mixed layer, $\overline{T}_{ML}$ also represents sea surface temperature. Figures A.11 and A.13 show a time sequence of the horizontal sea surface temperature field resulting from the interior motion, the heat cycle and mixing processes. The entire surface warms during the heating season and cools during the cooling season. During

the first half of the first year, there is no significant difference in sea surface temperature along the horizontal axis. After the first half year, the region where there is upwelling at the start of the cooling season becomes and remains cooler than the region where there is downwelling at the start of the cooling season.

D. EFFECT OF SHORTER PERIOD INTERIOR MOTION

Comparison of Figures A.19 and A.21 shows that as before downwelling increases deepening and upwelling reduces deepening. This can also be observed by comparing Figures A.30 and A.32 and by comparing Figures A.39 and A.41. The more rapid variation in mixed layer depth does not yield the strong effect on temperature found for the one-year period interior motion. This can be seen in the weaker gradients of $\Delta\bar{T}_{ML}$ of Figures A.23, A.34 and A.43 compared to that of A.12. Hence, the higher frequency interior motion does not have as strong an effect on the mixed layer as the lower frequency motion does.

The second year temperature data was plotted for the half-year period interior motion in Figures A.24 and A.25. Notice that the same structure seen in the first year reappears in the second, but the cold spots have not grown significantly colder nor the warm spots warmer as in the case of the one-year period motion.

As before, the heat and potential energy differences, ΔH and ΔP, track along with the interior motion as seen in Figures A.27, A.29, A.36, A.38, A.45 and A.47. The resulting contours of H and P appear more complex. This is because the values of H and P without the interior motion follow a one year cycle (Figures A.6 and A.7) and the higher frequency cycles due to the pumping by the interior motion are superimposed on the one year cycle.

For the one-year period interior motion, upwelling lasts long enough to enhance cooling significantly (at phases around 90°) and downwelling lasts long enough to inhibit cooling significantly (at phases around 270°). The shorter periods do not maintain upwelling and downwelling long enough to produce an effect this strong.

E. ASYMMETRY IN ENHANCED AND REDUCED MIXING

In Figures A.48 and A.49 the values of peak enhanced cooling and peak reduced mixed layer cooling are plotted. Both first and second year values are considered (in Figures A.48 and A.49, respectively). Negative values of $\Delta\bar{T}_{ML}$ indicate enhanced cooling due to the interior motion. The maximum absolute value of all of the negative $\Delta\bar{T}_{ML}$ data points was determined to indicate the peak enhanced cooling. Positive values of $\Delta\bar{T}_{ML}$ indicate reduced cooling. The maximum value of all of the positive $\Delta\bar{T}_{ML}$ data points indicates the peak reduced cooling. The positive values do not generally indicate enhanced heating, because the wave has very little effect on the mixed layer temperature during the heating season.

The first obvious observation that can be made from Figures A.48 and A.49 is that the largest peak anomalies occur with the one-year period interior motion. For the one-year period interior motion the peak enhanced and peak reduced mixed layer cooling is 2.04 and 2.16°C, respectively. For the one-half year period motion these values are 1.35 and 1.15°C, respectively. Also, for each of the periods studied, the difference between the peak enhanced cooling and the peak reduced cooling is greater in the second year than in the first. All of the periods studied except the one-year period have greater peak enhanced cooling than peak reduced cooling.

The phase-averaged values of the variables Δh, $\Delta \bar{T}_{m.l.}$, ΔH, and ΔP were computed for sixteen equally spaced phases from 0° to 360°. The phase-averaged values at the end of the first and the end of the second model years are listed in Table I. These values indicate the net effect of the interior motion after each year of interacting with the mixing processes. Consistent with the results shown in Figures A.48 and A.49, the results in Table I indicate that the one-year period interior motion has produced a net reduction of mixed layer cooling. The higher frequency interior motion has produced a net enhancement of mixed layer cooling. For all of the periods studied there has been a net reduction of the mixed layer depth. Heat is conserved, hence the phase-averaged value of ΔH is zero at the end of each year. The effect of the one-year period interior motion was to decrease the potential energy. The higher frequency interior motion produced a net increase in potential energy.

A net increase (decrease) in potential energy indicates that the interior motion has enhanced (reduced) the overall mixing. The amount of deepening required to produce an equivalent increase in potential energy is instructive. This can easily be calculated for the simplified example of a two-layer ocean, illustrated in Figure 3.4 with initial mixed-layer temperature, T_0 and depth, h_0. This mixed layer is deepened to h_1 with new mixed layer temperature, T_1. Heat is conserved, so, using the definition for the heat variable, H, given in equation (2.32):

$$(\bar{T}_1 - \bar{T}_D)h_1 = (\bar{T}_0 - \bar{T}_D)h_0 \qquad (3.16)$$

Using equation (2.31), the change in the potential energy is given by

$$P_1 - P_0 = (T_1 - T_D)\frac{h_1^2}{2} - (T_0 - T_D)\frac{h_0^2}{2} . \qquad (3.17)$$

Substituting equation (3.16) into equation (3.17) yields

$$P_1 - P_0 = \frac{1}{2}(T_0 - T_D)\, h_0 (h_1 - h_0) \qquad (3.18)$$

The term $T_0 - T_D$ is just the initial entrainment zone temperature jump. The increase in potential energy due to deepening with heat conserved is directly proportional to the increase in mixed layer depth for the two-layer example.

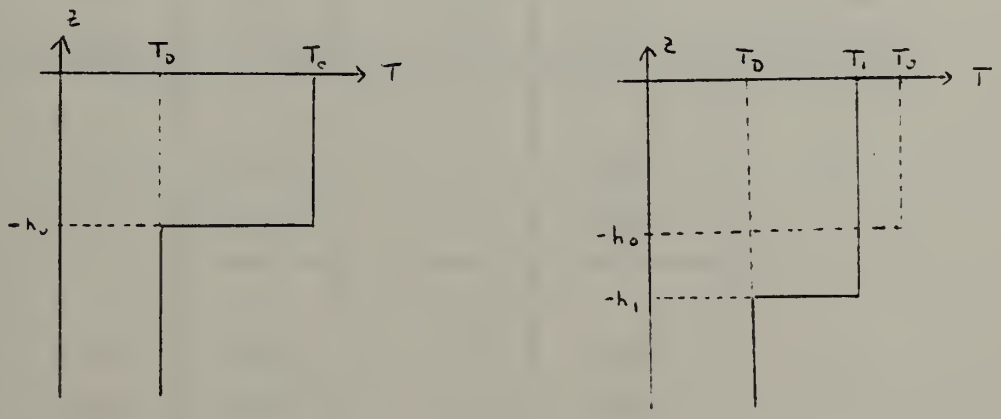

initial profile after mixing

Figure 3.4 Two-Layer Ocean Example.

Consider now the phase-averaged potential energy anomalies at the end of the first year, shown in Table I. Suppose the initial mixed layer depth is 75 m and the initial temperature jump is 4 °C. The net reduction of potential energy for the one-year period interior motion would then be equivalent to a reduced mixed layer depth of

0.73 m. The net increase of potential energy for the one-half, one-third, and one-quarter year period interior motion is equivalent to an increase of mixed layer depth by 1.6, 1.8 and 1.8 m, respectively.

The amount of downwelling and upwelling are the same over the whole year and for all phases. Yet, the net reduction of mixing and mixed layer cooling does not equal the net enhancement of the same. The net effect of the one-year period interior motion is to hinder mixing. The net effect of the shorter period interior motion is to enhance mixing.

TABLE I

Phase-Averaged Mean Anomalies

Day	Phase-averaged mean of: Δh (m)	$\Delta \bar{T}_{ML}$ (°C)	ΔH (°C m)	ΔP (°C m)	Period (years)
0	0.	0.	0.	0.	
365	-0.43	+0.06	0.	-109.	1
730	-0.71	+0.22	0.	-645.	
0	0.	0.	0.	0.	
365	-0.16	-0.05	0.	239.	1/2
730	-0.16	-0.06	0.	381.	
0	0.	0.	0.	0.	
365	-0.23	-0.05	0.	267.	1/3
730	-0.23	-0.07	0.	435.	
0	0.	0.	0.	0.	
365	-0.31	-0.05	0.	275.	1/4
730	-0.31	-0.07	0.	451.	

IV. CONCLUSIONS AND RECOMMENDATIONS

A. CONCLUSIONS

Seasonal-scale interior motion has a significant effect on boundary layer mixing processes. This effect is most pronounced when the period of the interior motion is one year. For this pericd, upwelling between the heating and cooling seasons can strongly enhance mixed layer cooling and subsequent deepening. Downwelling can strongly reduce the same. This effect may produce a significant, observable horizontal pattern in sea surface temperature. Although there is negligible effect on sea surface temperature and mixed layer depth during the beginning of the heating season, the interior motion does affect the potential energy and heat content at this time. Throughout the year the potential energy and heat are directly related to the pumping by the interior motion. Upwelling decreases and downwelling increases both potential energy and heat content.

Higher frequency interior motion does not have as strong an effect. The cycling between upwelling and downwelling during the cooling season prevents the strongly enhanced mixed layer cooling from occurring.

The effect of the interior motion is asymmetric. Generally, the enhancement of mixing and mixed layer cooling exceeds the reduction of the same. The exception to this occurs for the one-year period interior motion.

B. RECOMMENDATIONS

One aspect of this research which departs from reality is in prescribing a single wave for the interior motion. This could be changed quite easily by prescribing

$$w_D = \sum_n w_n \sin\left(\frac{2\pi t}{T_n} + \varphi_n\right). \qquad (4.1)$$

The amplitudes, W_n, and periods, T_n, could be based on the first few dominant frequency components observed in actual wave spectra.

Another way that reality could be more closely approached is by allowing the net surface heat flux to vary depending on the sea surface temperature. This should dampen the strongly enhanced or reduced cooling of the mixed layer temperature seen with the one-year period motion.

An area open to further research is to use a finite depth ocean and an appropriate vertical wave structure. An appropriate wave structure for planetary waves is given by Willmott and Mysak (1980). In their work the vertical motion is linear in the mixed layer:

$$\frac{\partial^2 w}{\partial z^2} = 0, \qquad (4.2)$$

but, below the mixed layer the vertical motion is given by

$$\frac{\partial^2 w}{\partial z^2} + \left(\frac{N^2}{c_n^2}\right) w = 0, \qquad (4.3)$$

where N^2 is the Brunt-Väisälä frequency and c_n represents the speed of propagating long waves in the non-rotating case for mode number n. The solutions of equations (4.2) and (4.3) must be matched at the base of the mixed layer, z=-h, to ensure continuity of the vertical velocity. The boundary conditions are rigid lid and no normal flow through the ocean bottom, so, w=0 at z=0 and at the ocean bottom. At each time step the mixed layer depth is recalculated and so the vertical wave structure problem would also have to be solved for the new w(z). The combination of this sort of

vertical wave structure with the Garwood model for boundary layer mixing processes could provide an interesting area for future study.

In this study the interior motion was prescribed and acted on the mixed layer. The interior motion was not allowed to be changed by the mixed layer processes. If, for example, the wave motion enhances mixing, the increase in potential energy should be balanced by a decrease in wave energy. Although the frequencies considered here are much lower than those in the work by Bell (1978), the processes involved could be similar.

APPENDIX A
FIGURES

Solid contours indicate positive values.
Dashed contours indicate negative values.

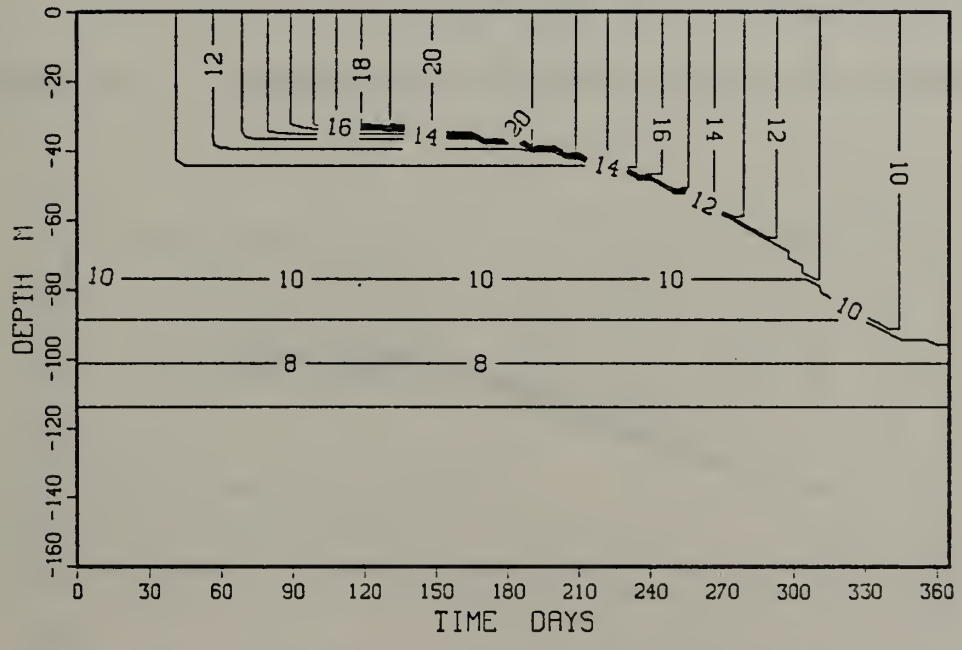

Figure A.1 Temperature, No Interior Motion.

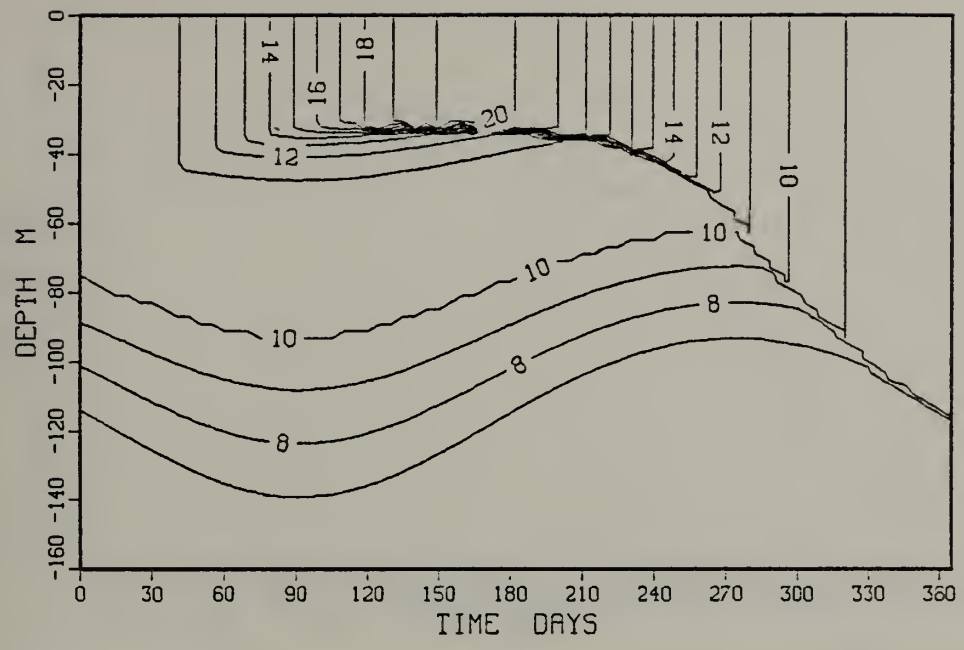

Figure A.2 Temperature, One-Year Period, 90° Phase.

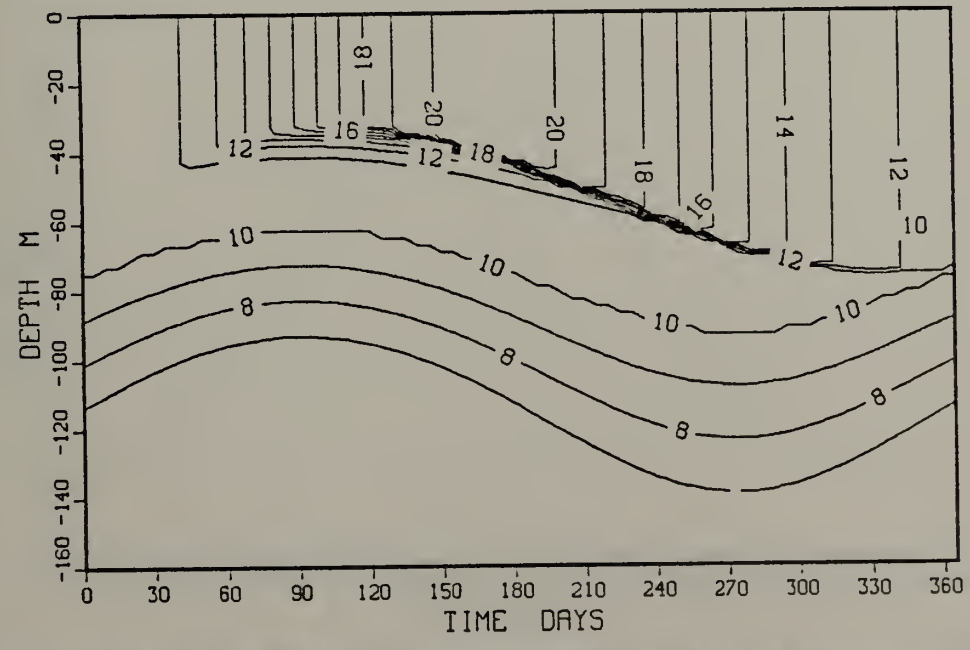

Figure A.3 Temperature, One-Year Period, 270° Phase.

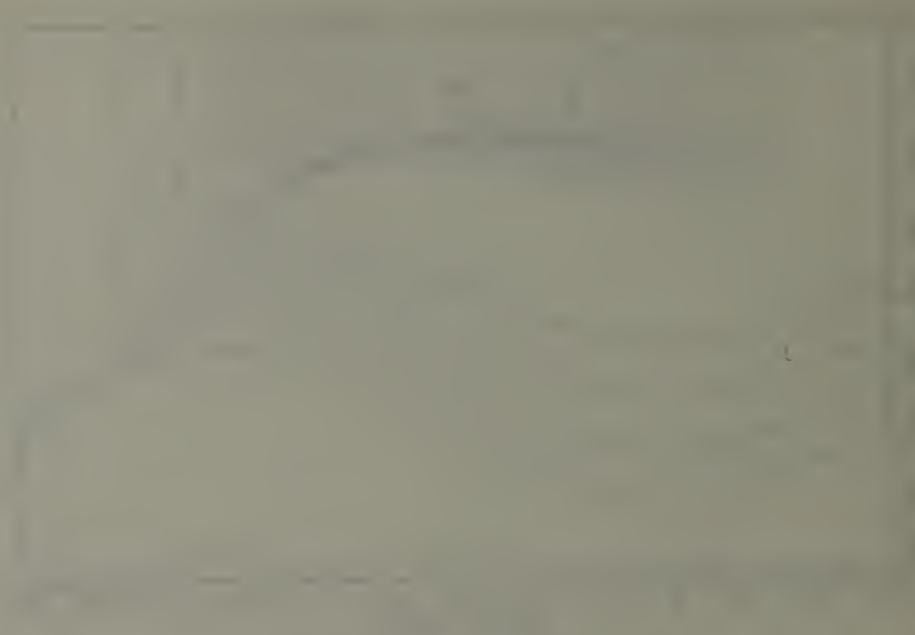

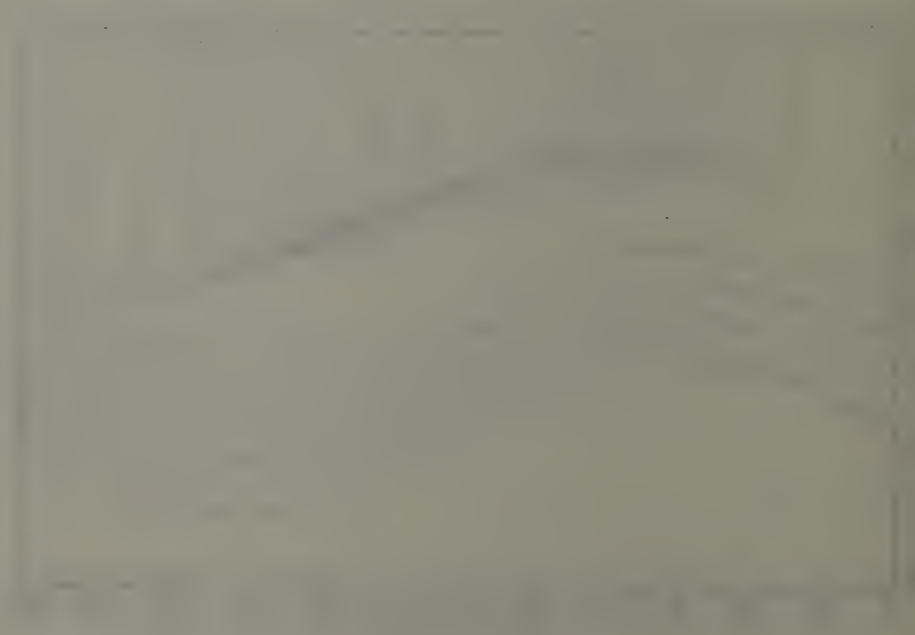

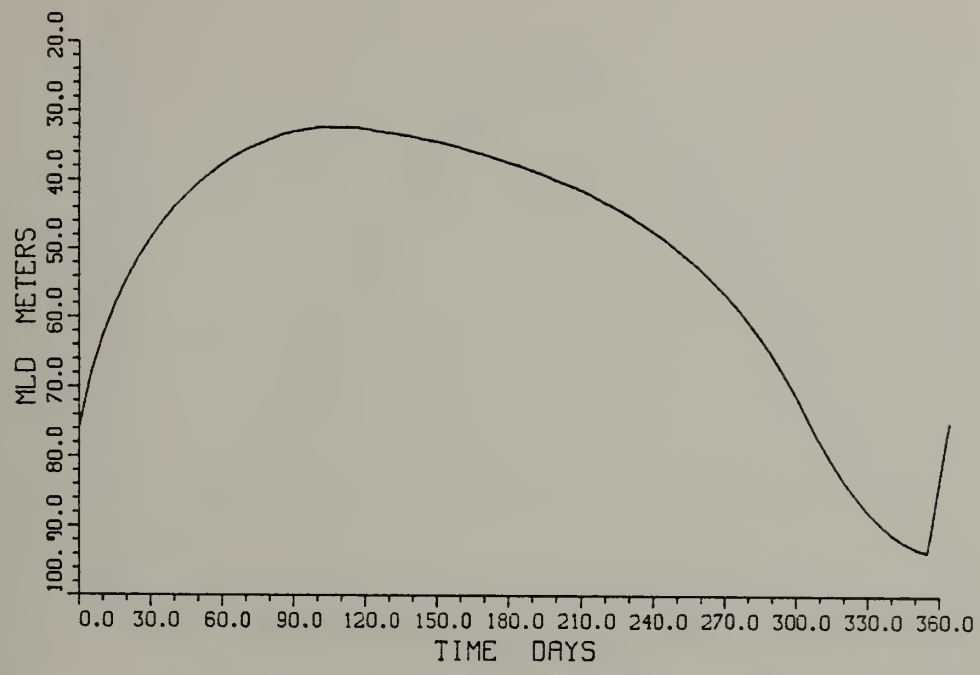

Figure A.4 Mixed Layer Depth, No Interior Motion.

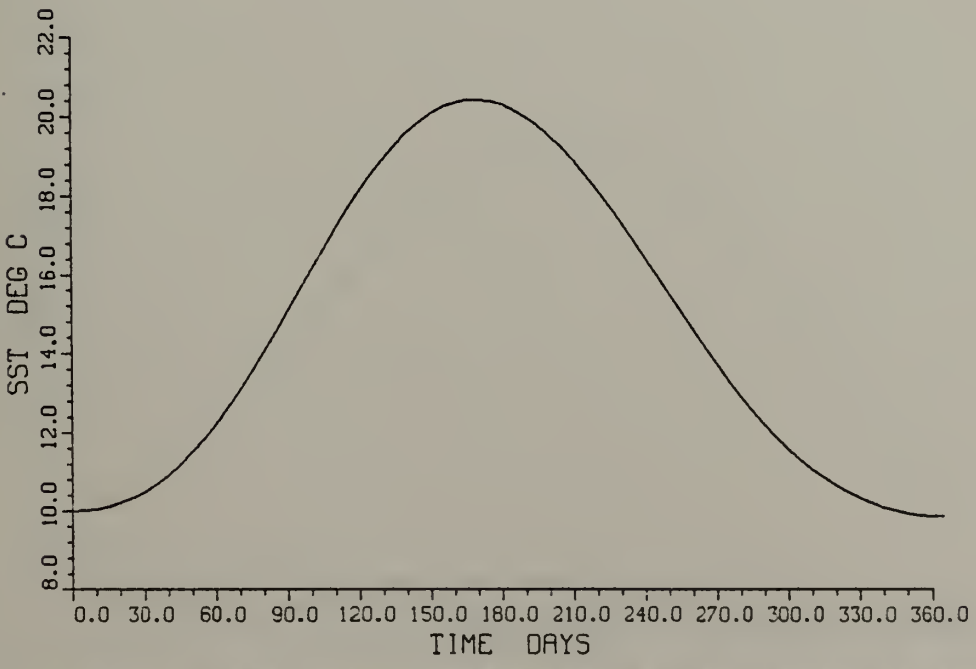

Figure A.5 Mixed Layer Temperature, No Interior Motion.

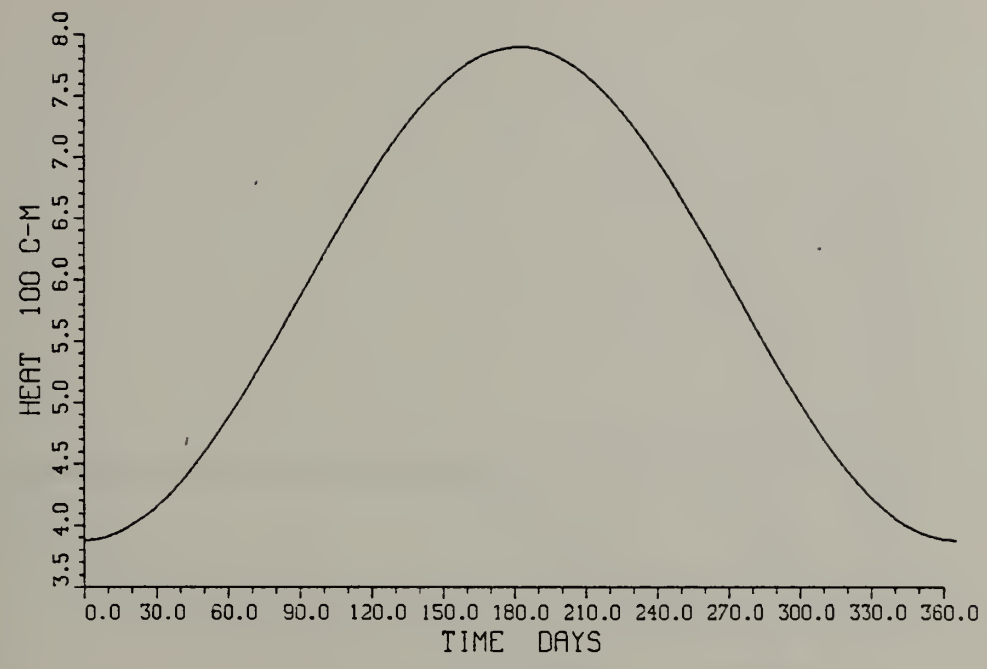

Figure A.6 Heat, No Interior Motion.

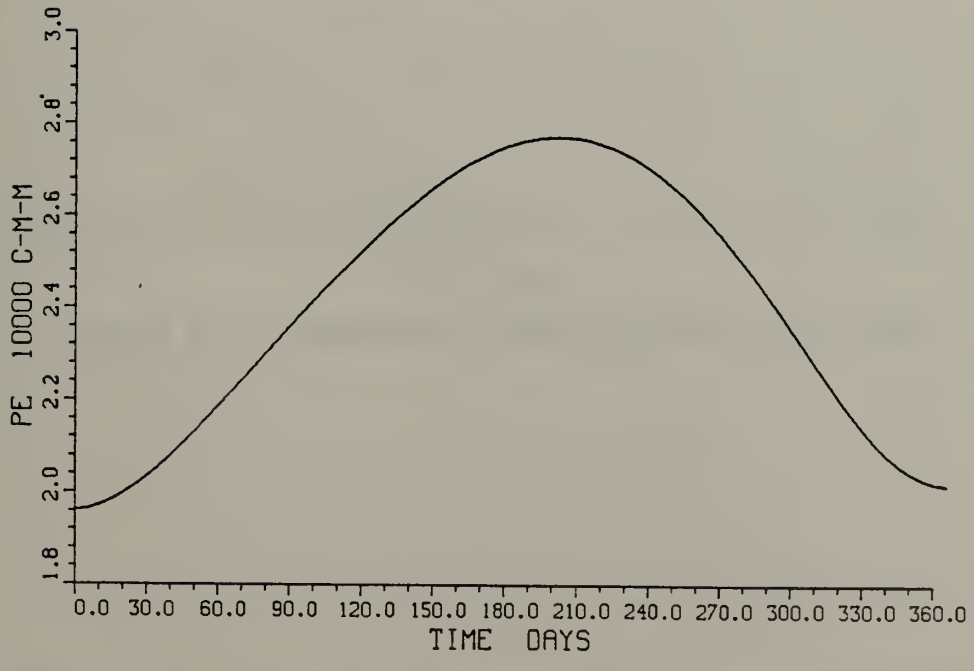

Figure A.7 Potential Energy, No Interior Motion.

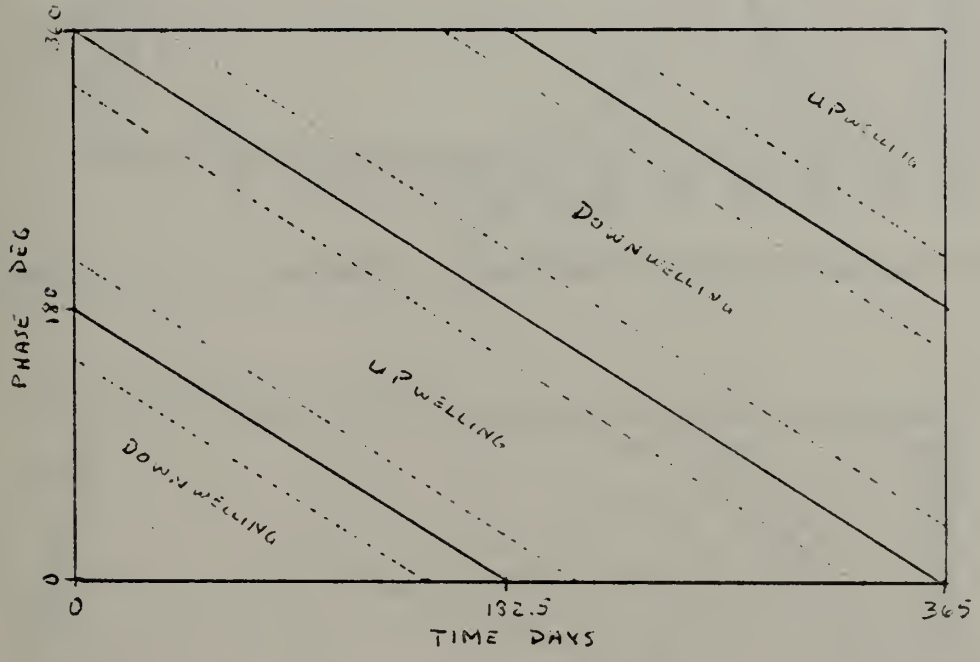

Figure A.8 One-Year Period Interior Motion.

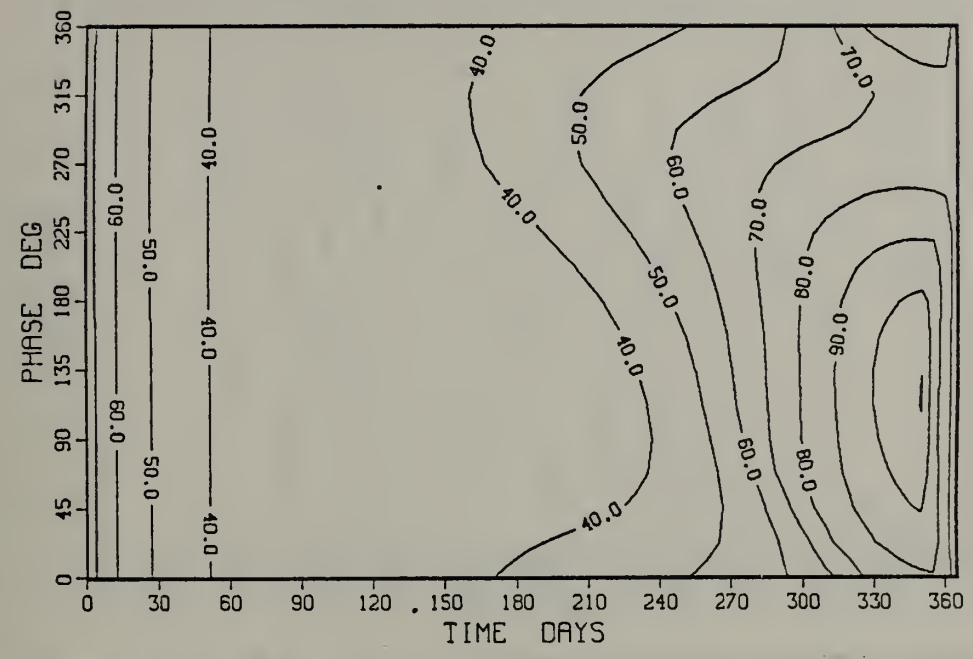

Figure A.9 h (meters), One-Year Period Interior Motion.

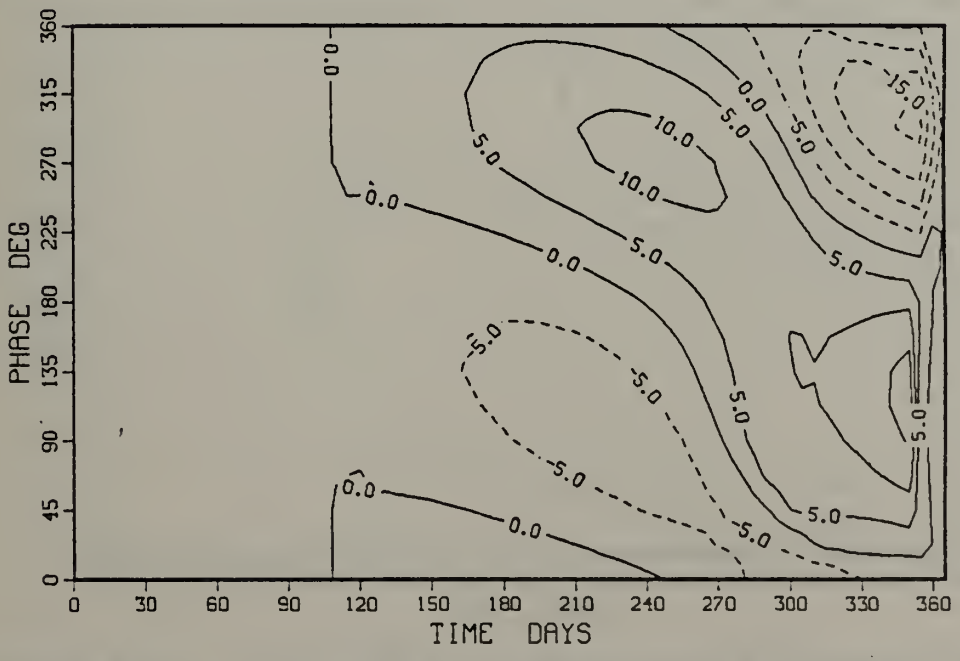

Figure A.10 Δh (meters), One-Year Period Interior Motion.

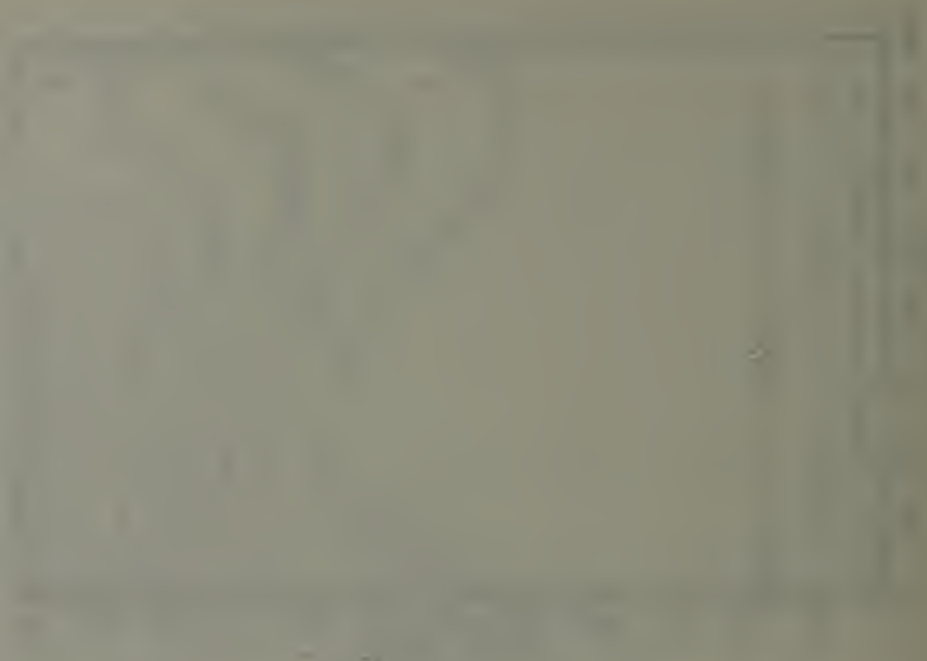

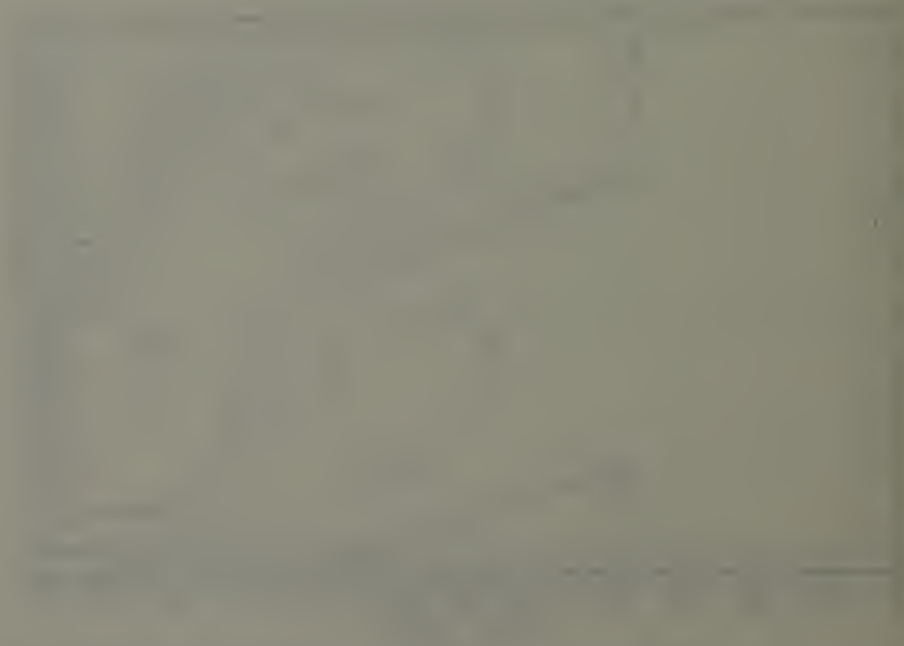

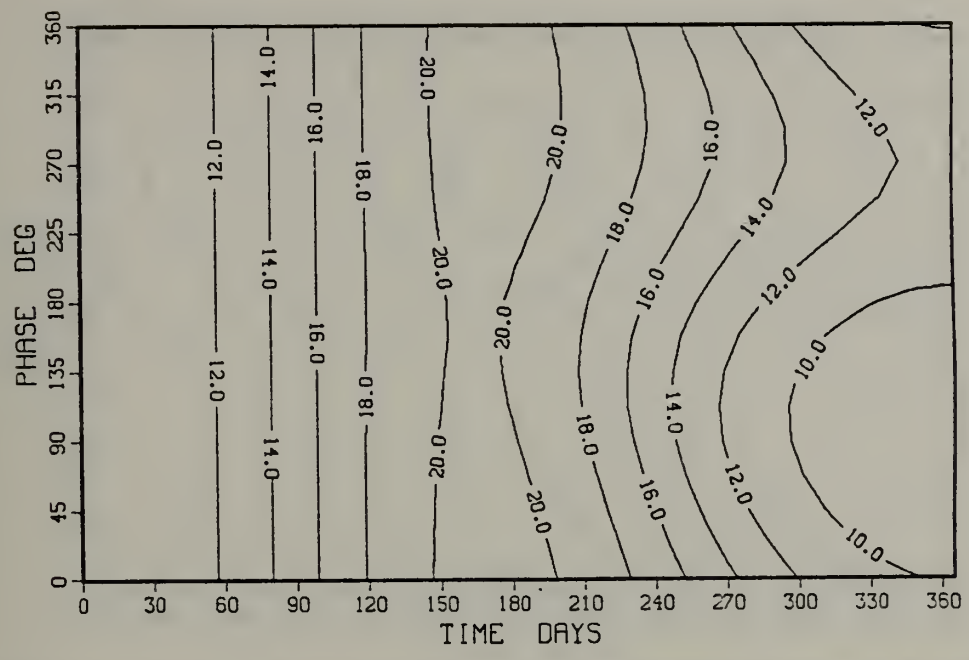

Figure A.11 $\bar{T}_{ML}$ (C), One-Year Period Interior Motion.

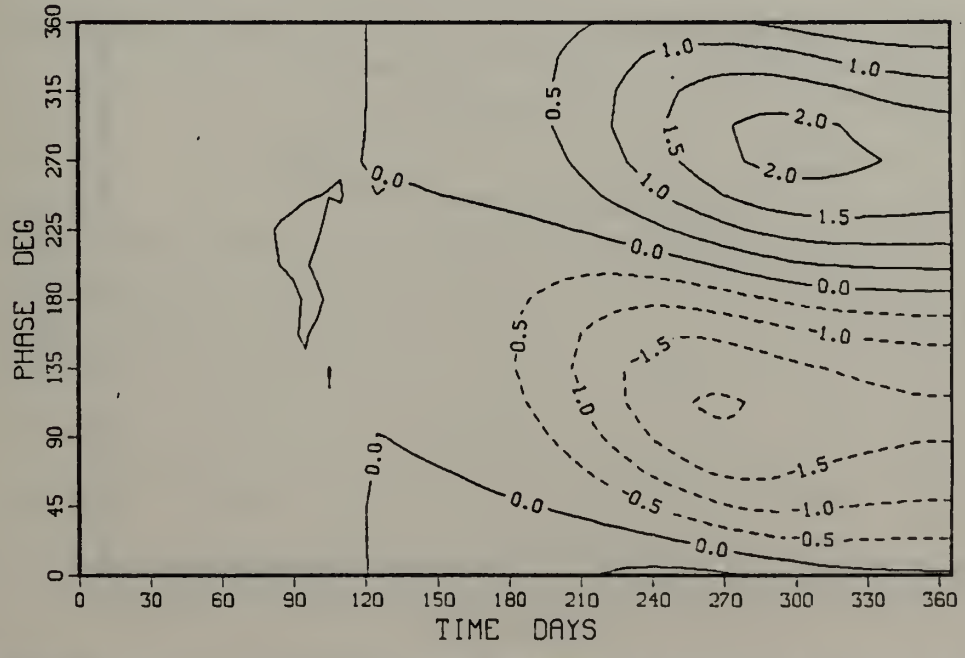

Figure A.12 $\Delta\bar{T}_{ML}$ (C), One-Year Period Interior Motion.

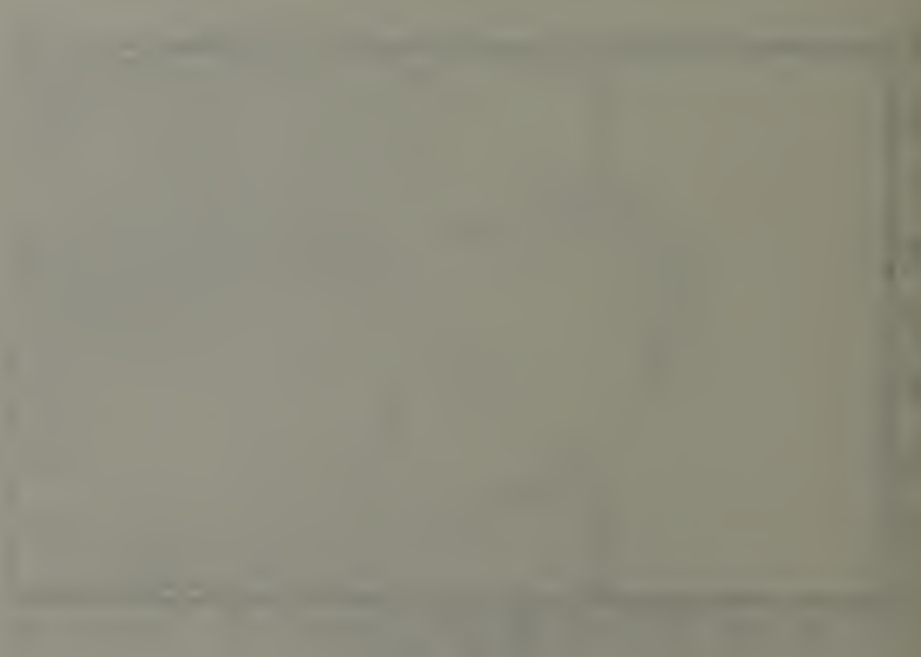

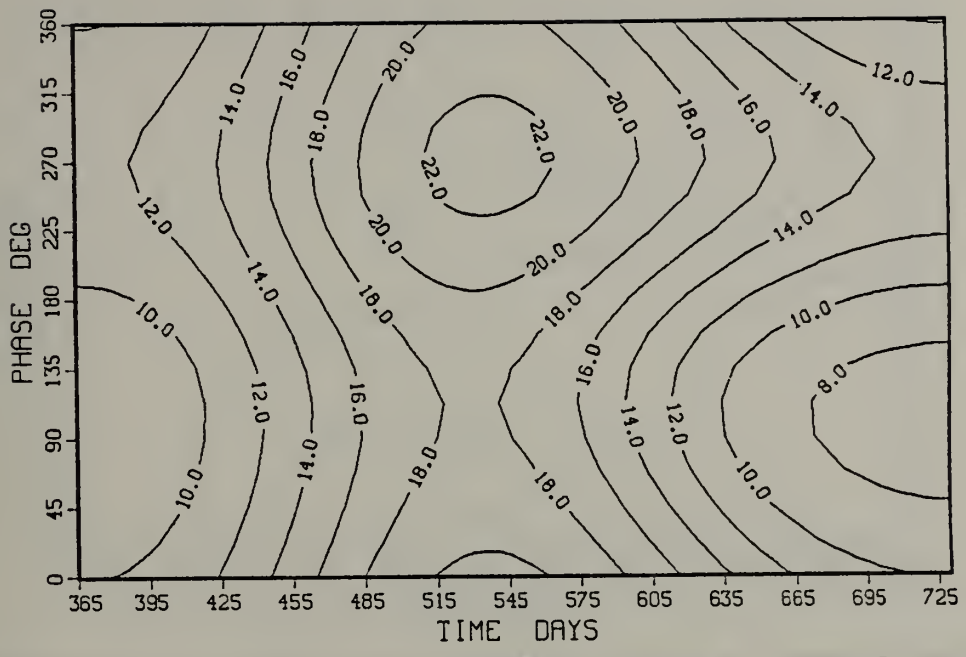

Figure A.13 $\bar{T}_{ML}$ (C), One-Year Period, Second Year.

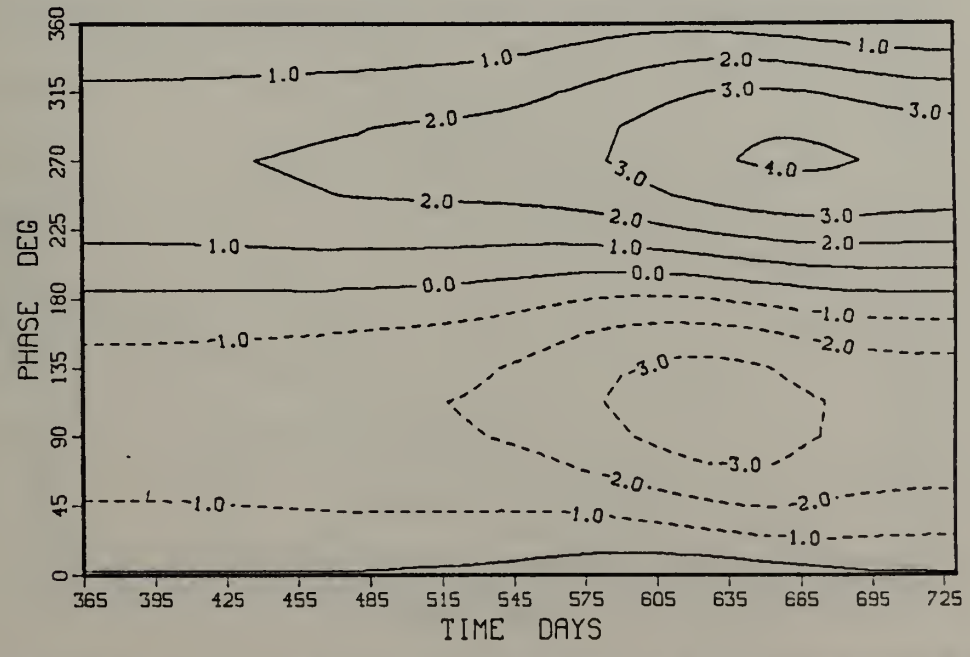

Figure A.14 $\Delta \bar{T}_{ML}$ (C), One-Year Period, Second Year.

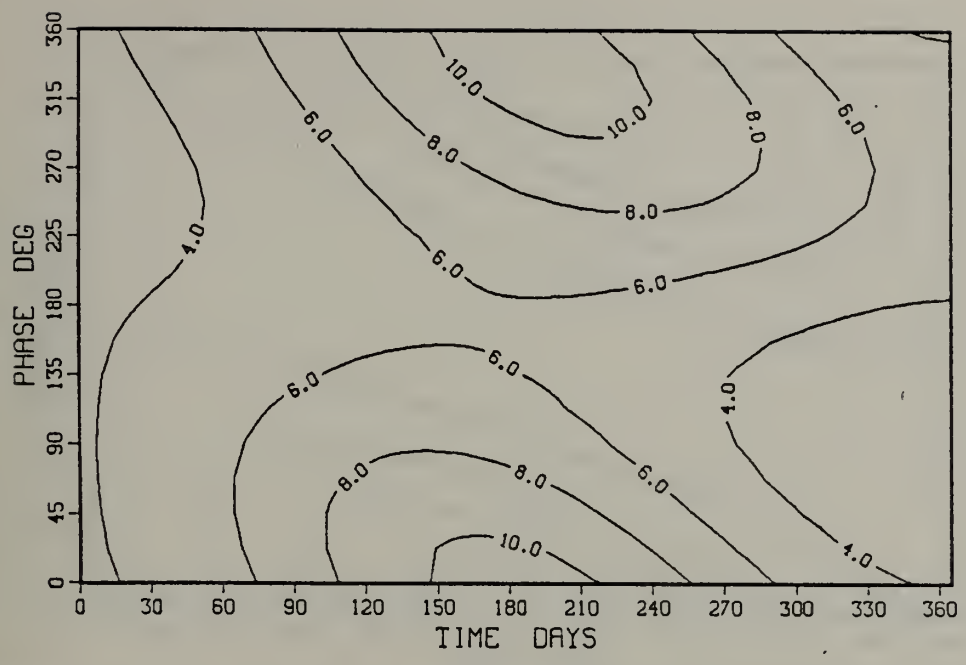

Figure A.15 H (100°C m), One-Year Period Interior Motion.

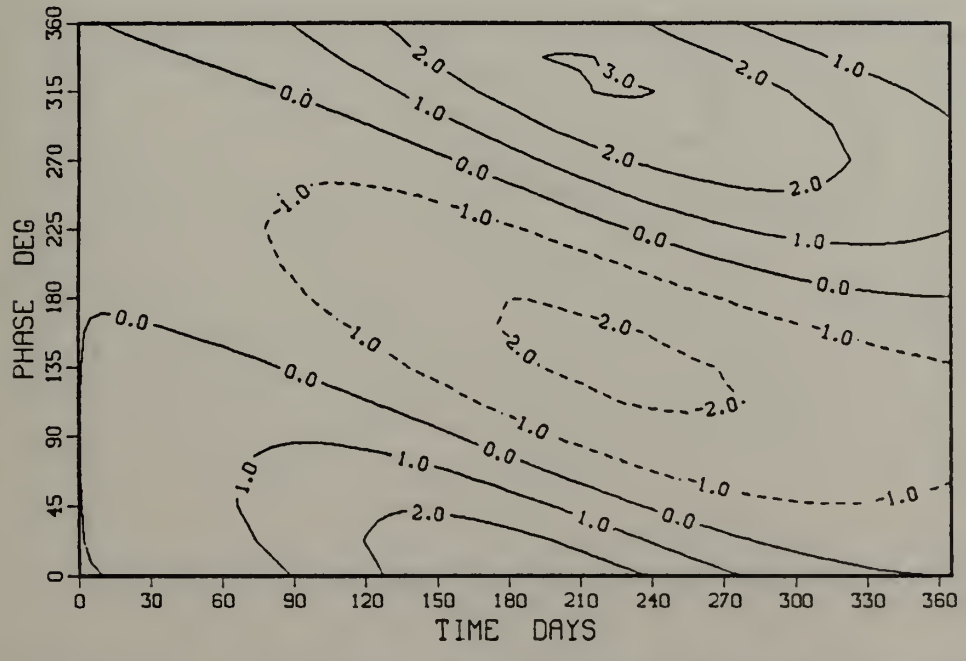

Figure A.16 ΔH (100°C m), One-Year Period Interior Motion.

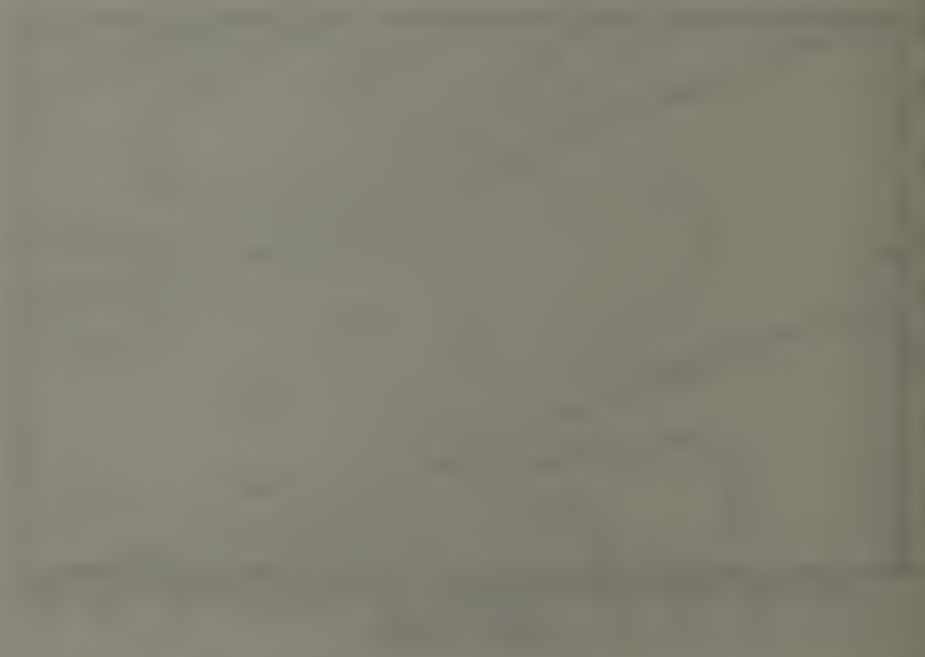

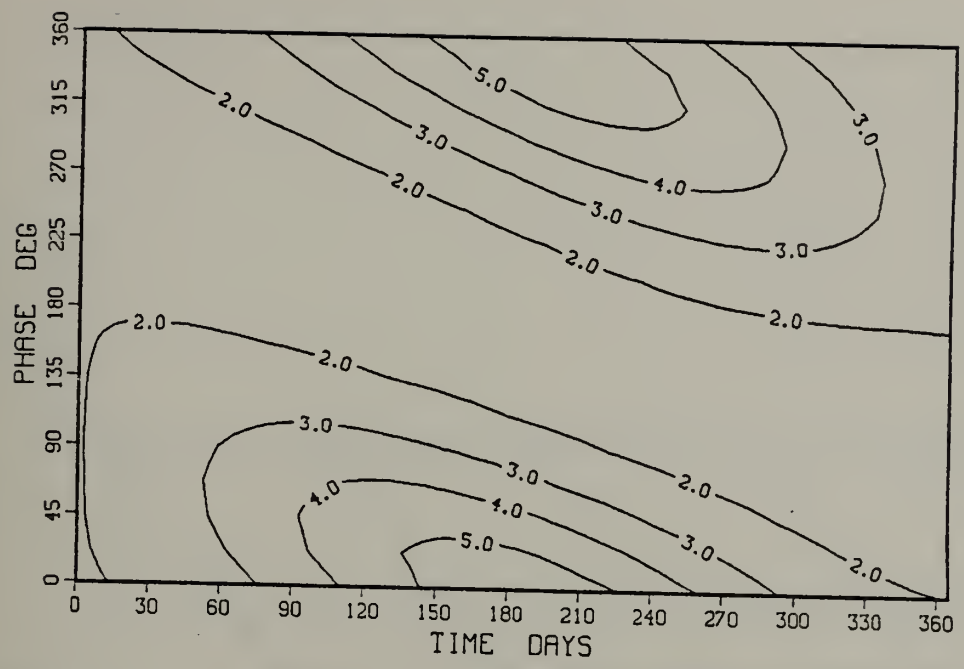

Figure A.17 P (10^4 °C m²), One-Year Period Interior Motion.

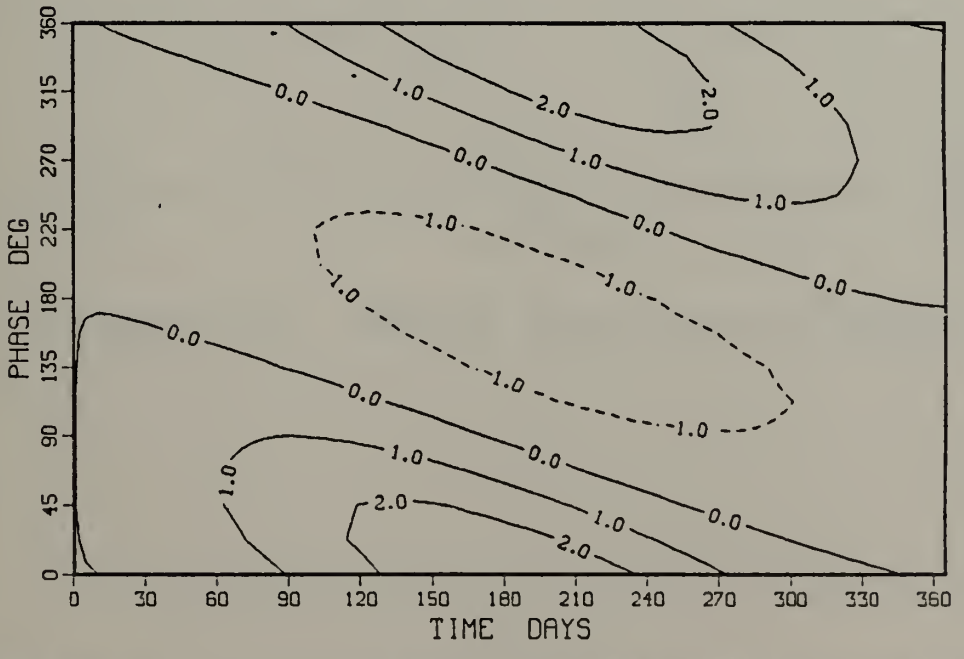

Figure A.18 ΔP (10^4 °C m²), One-Year Period Interior Motion.

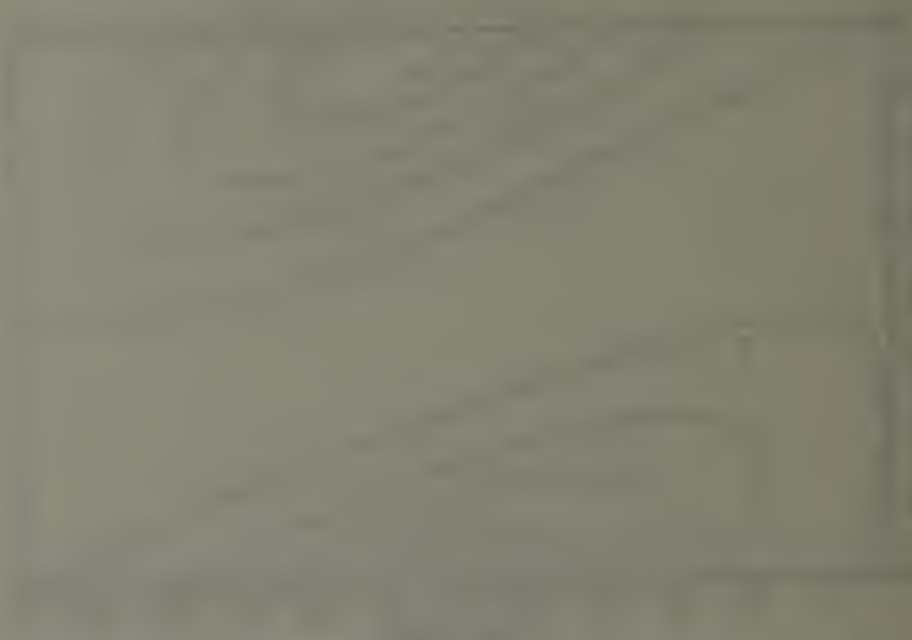

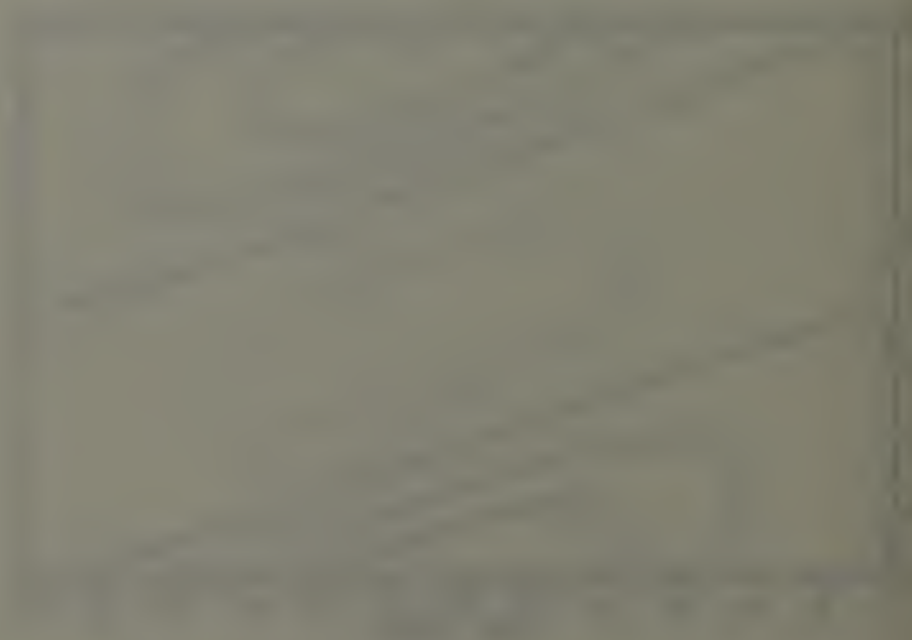

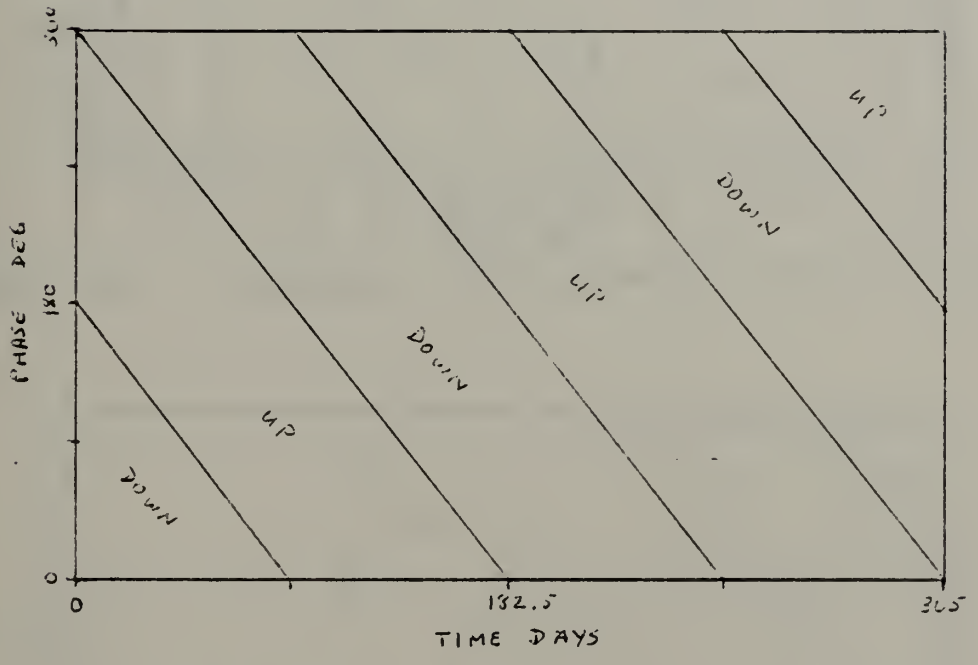

Figure A.19 1/2-Year Period Interior Motion.

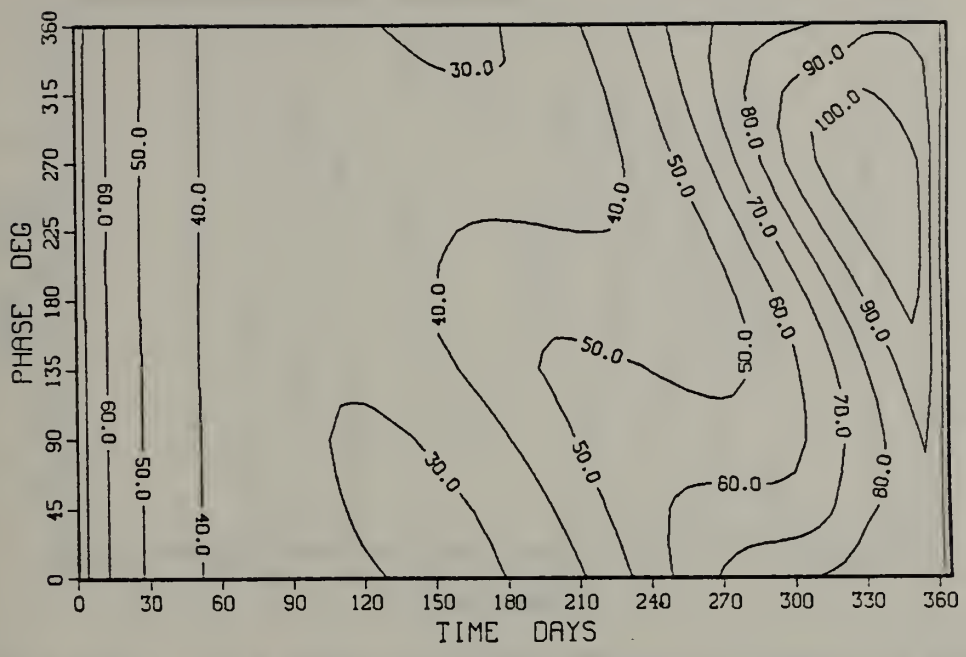

Figure A.20 h (meters), 1/2-Year Period Interior Motion.

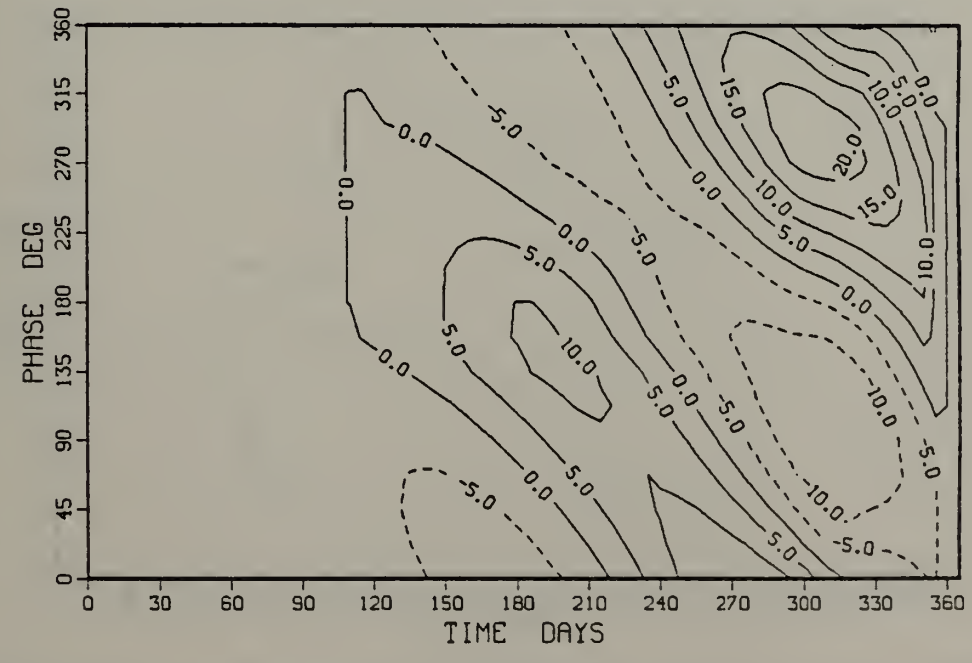

Figure A.21 Δh (meters), 1/2-Year Period Interior Motion.

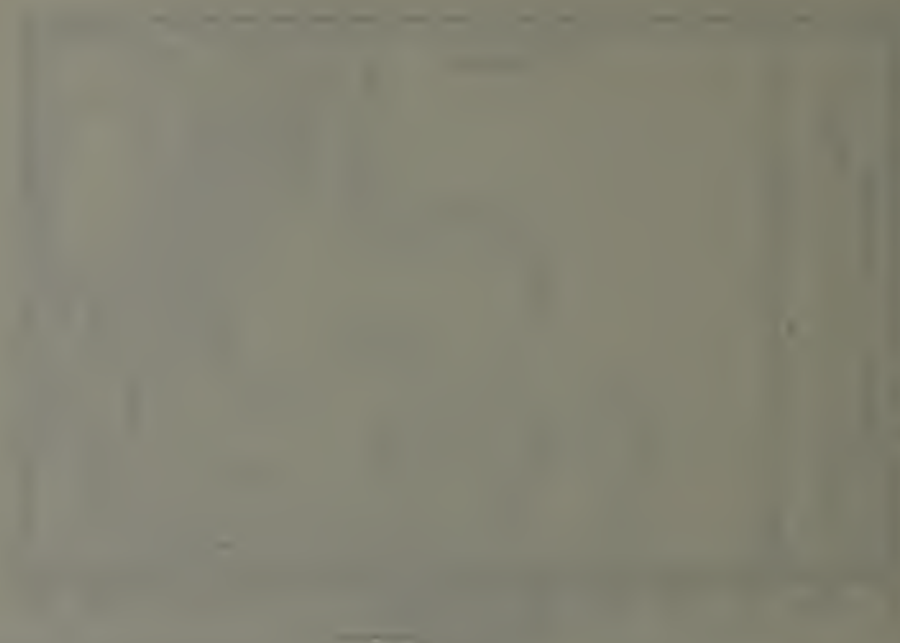

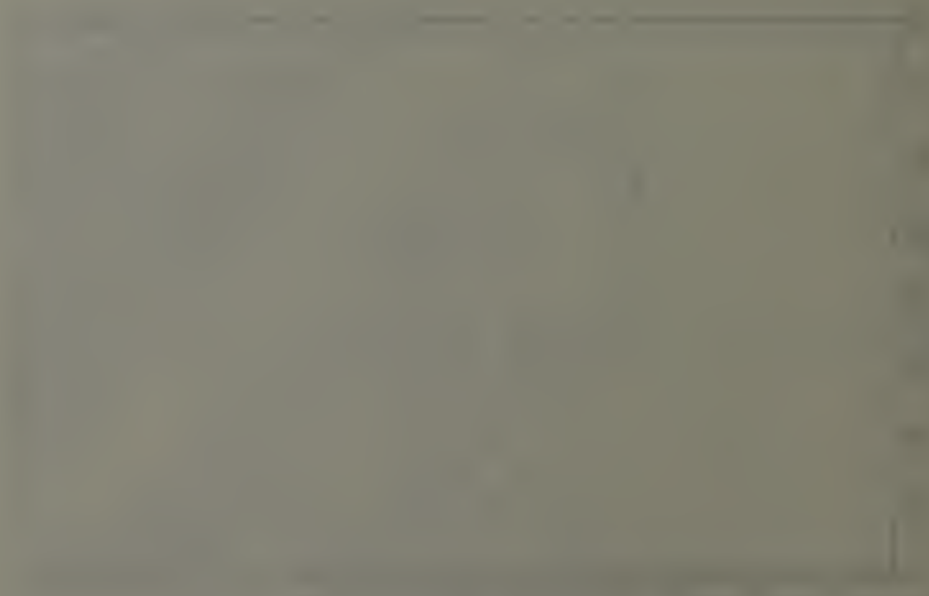

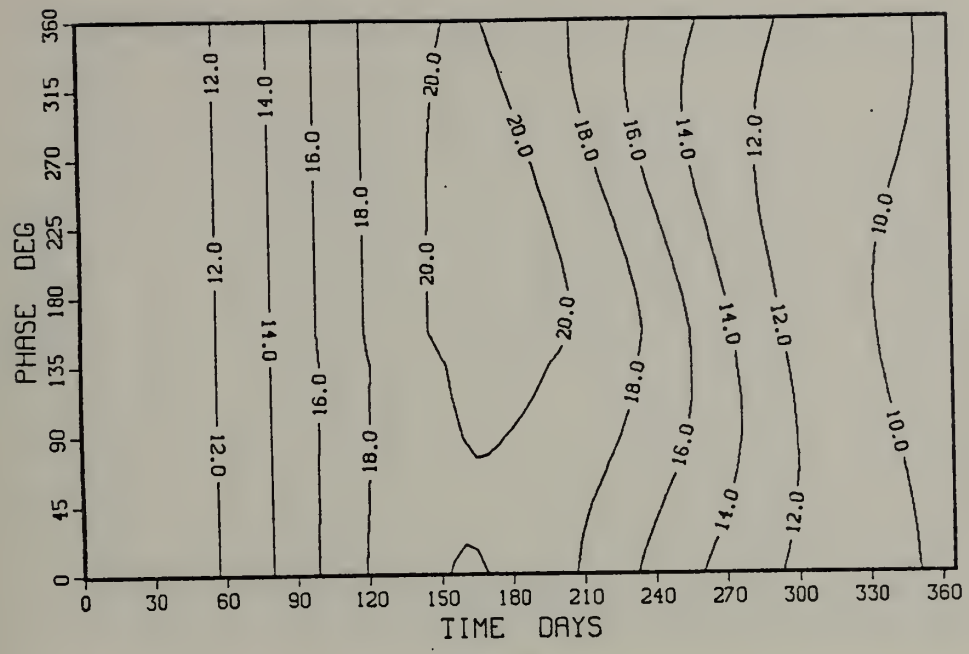

Figure A.22 $\bar{T}_{ML}$ (C), 1/2-Year Period Interior Motion.

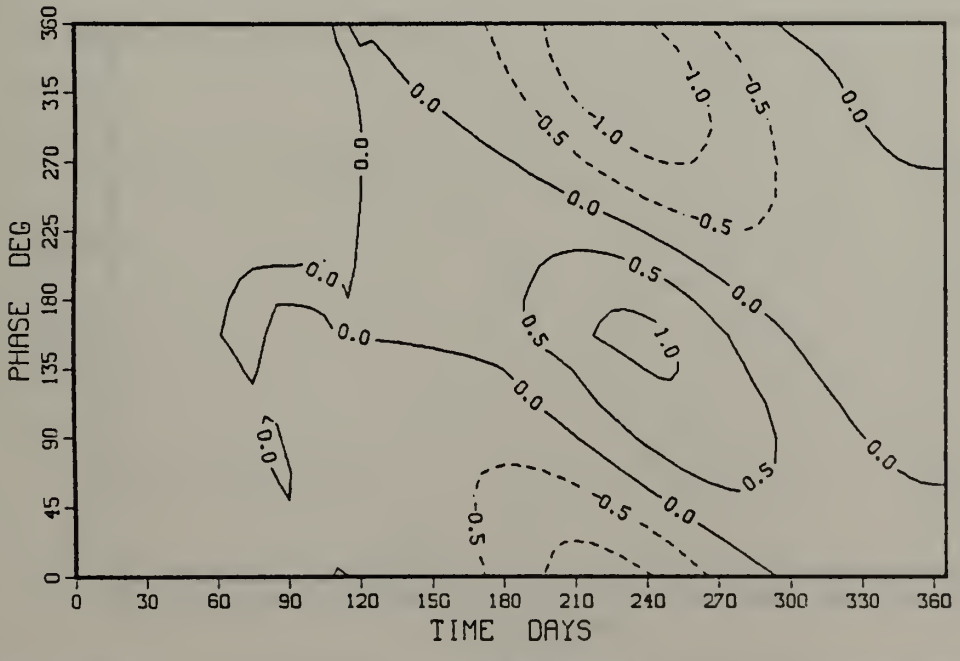

Figure A.23 $\Delta \bar{T}_{ML}$ (C), 1/2-Year Period Interior Motion.

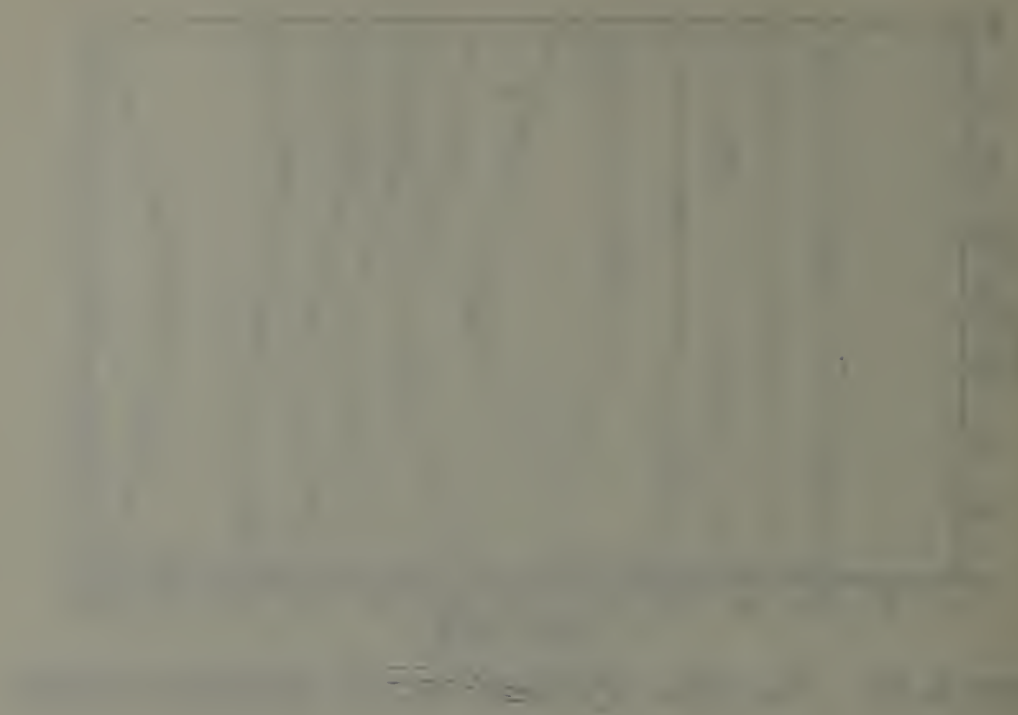

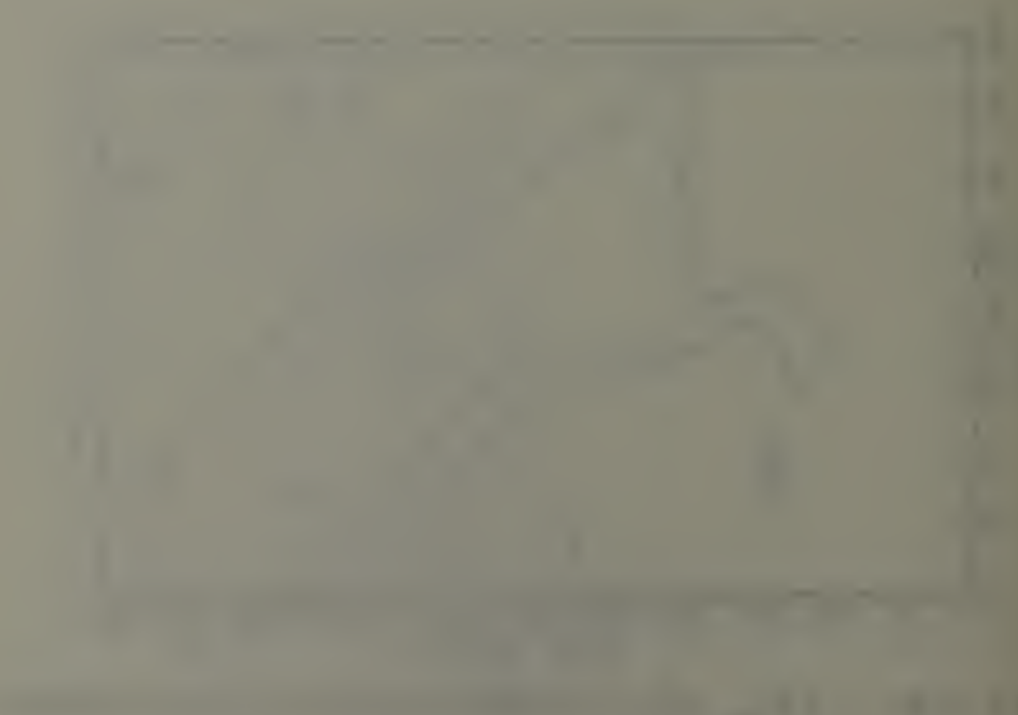

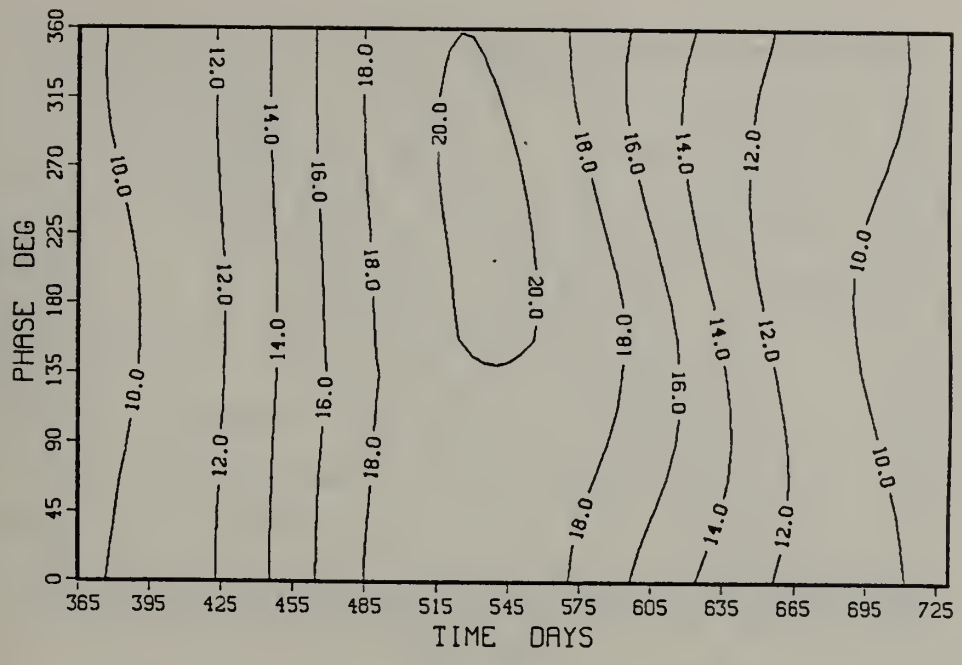

Figure A.24 $\bar{T}_{ML}$ (C), 1/2-Year Period, Second Year.

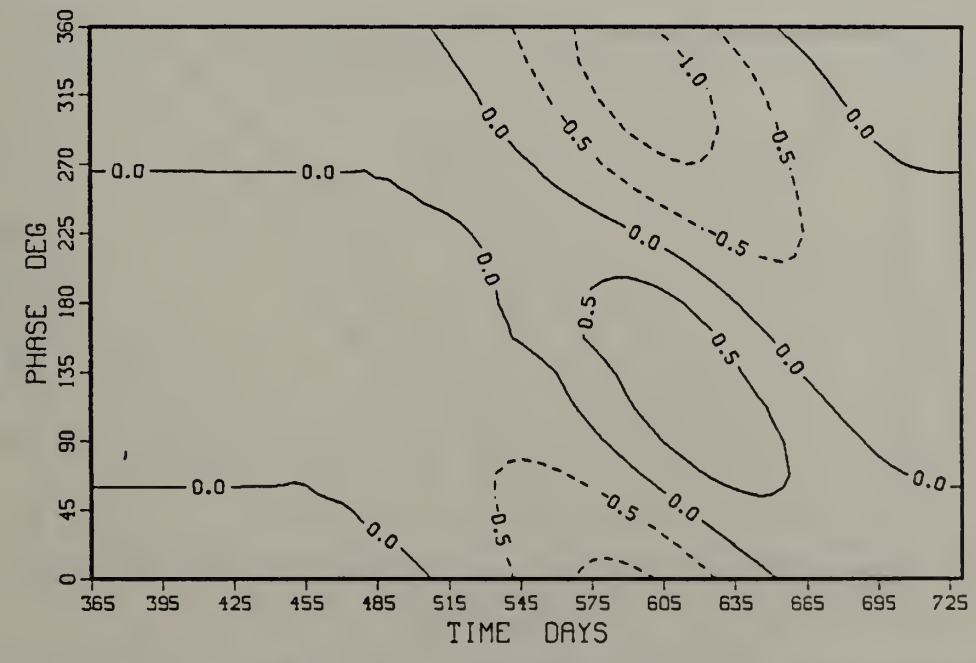

Figure A.25 $\Delta \bar{T}_{ML}$ (C), 1/2-Year Period, Second Year.

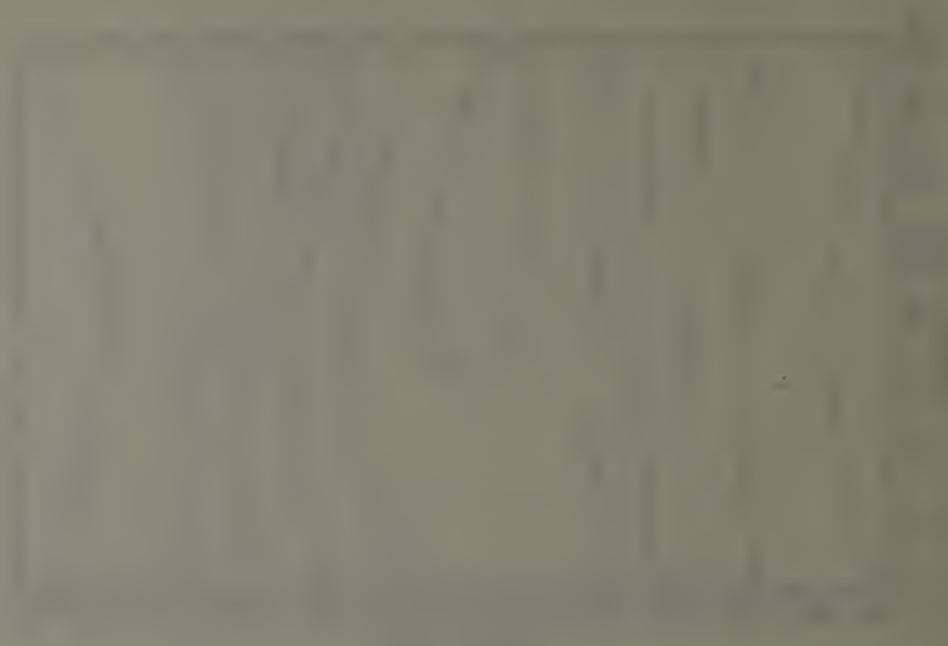

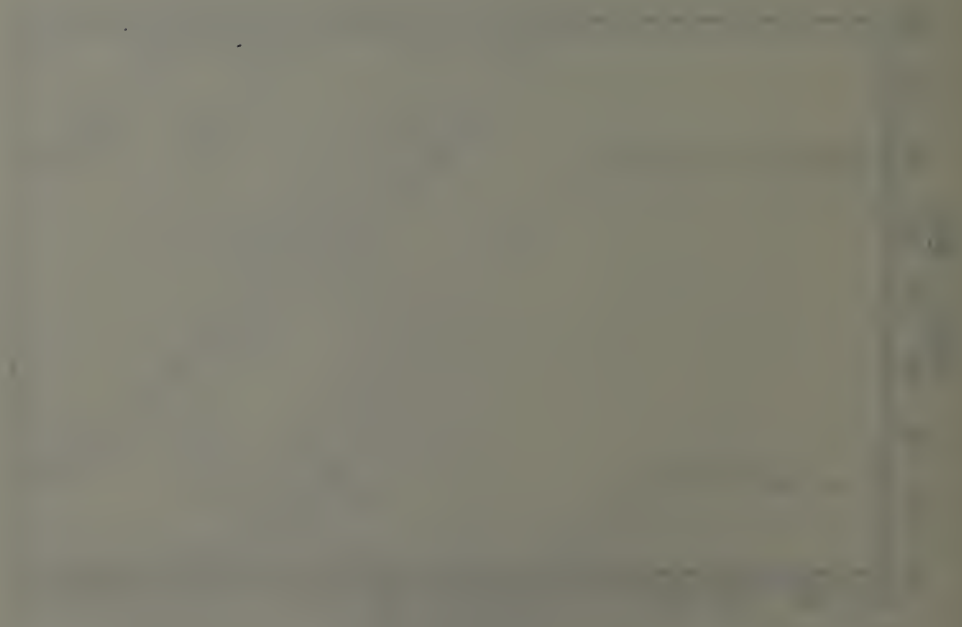

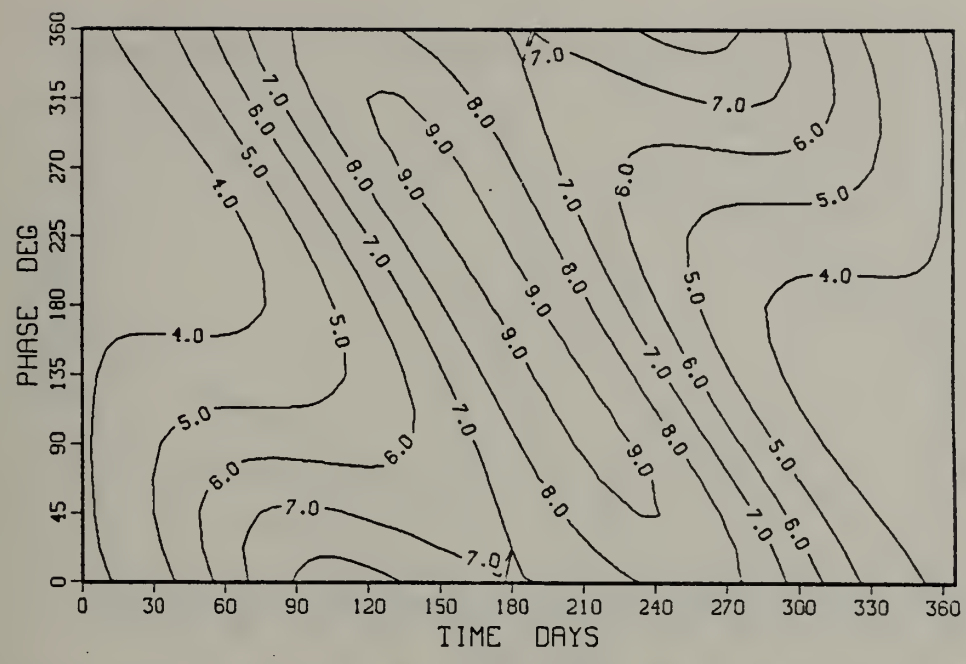

Figure A.26 H (100 °C m), 1/2-Year Period Interior Motion.

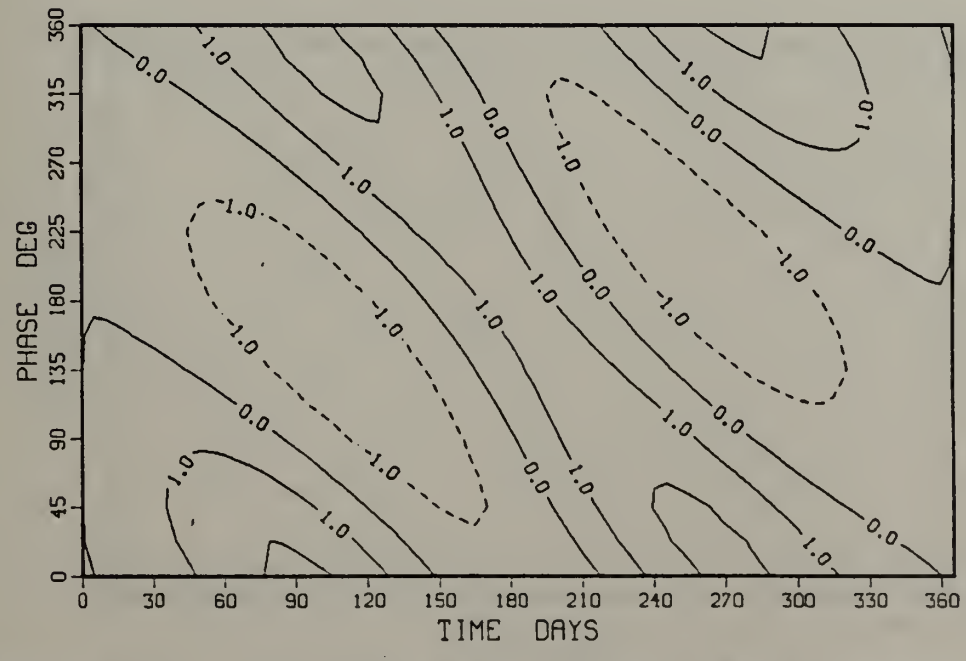

Figure A.27 ΔH (100 °C m), 1/2-Year Period Interior Motion.

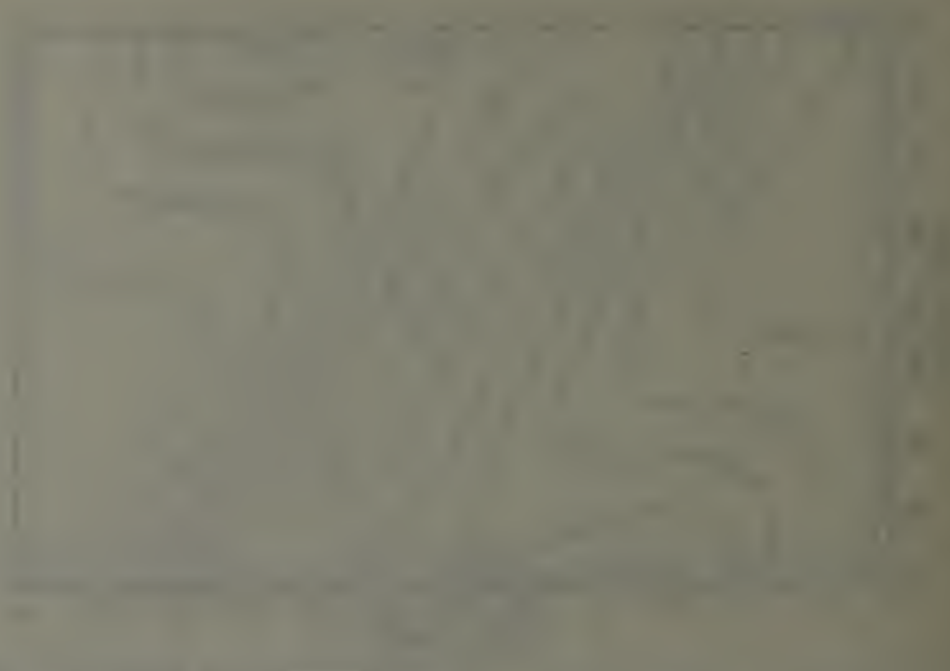

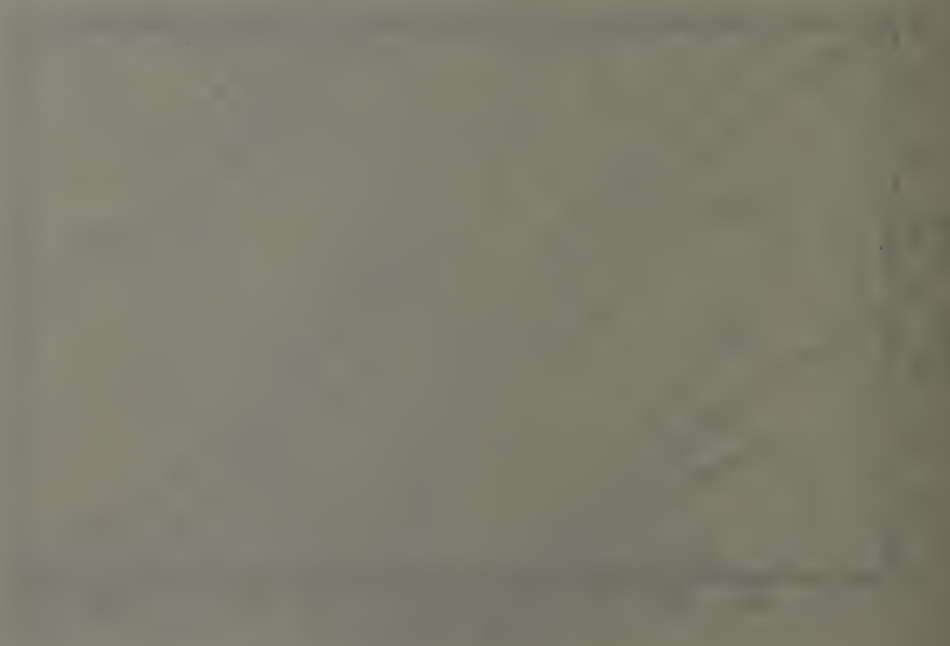

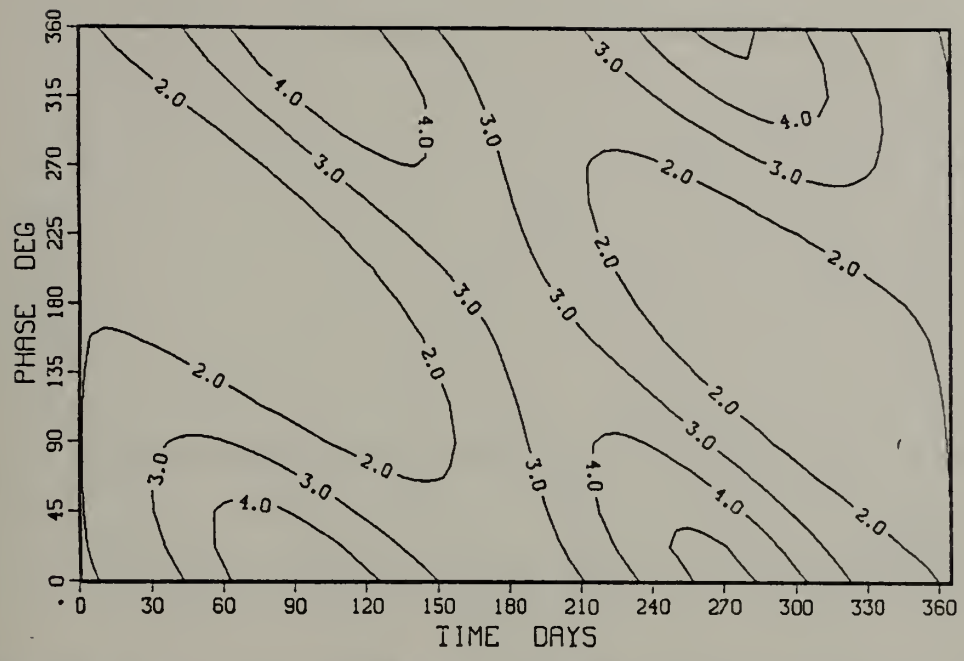

Figure A.28 P ($10^{\blacklozenge}$ °C m²), 1/2-Year Period Interior Motion.

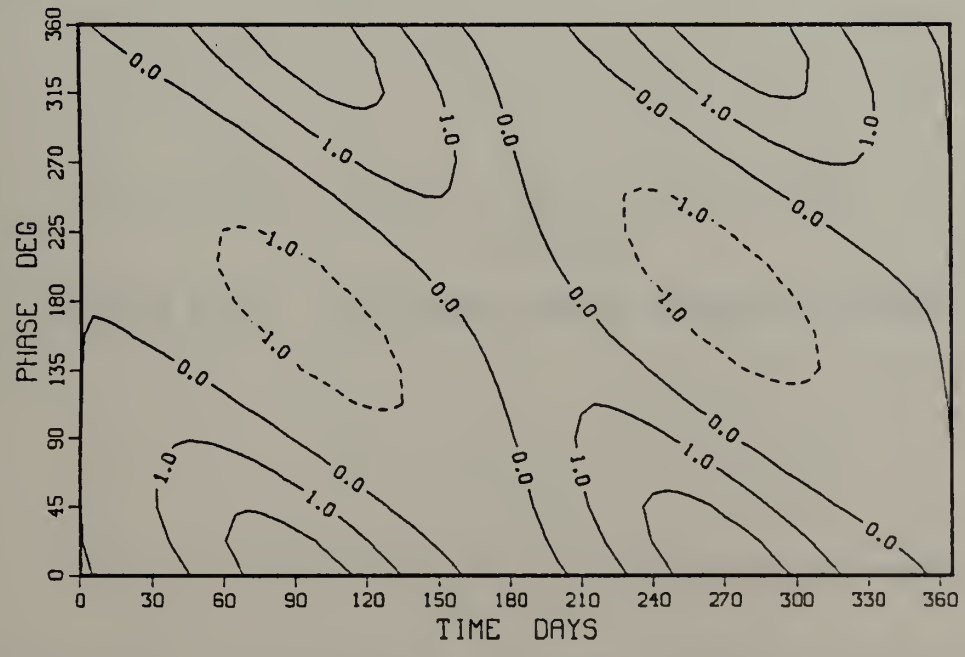

Figure A.29 ΔP ($10^{\blacklozenge}$ °C m²), 1/2-Year Period Interior Motion.

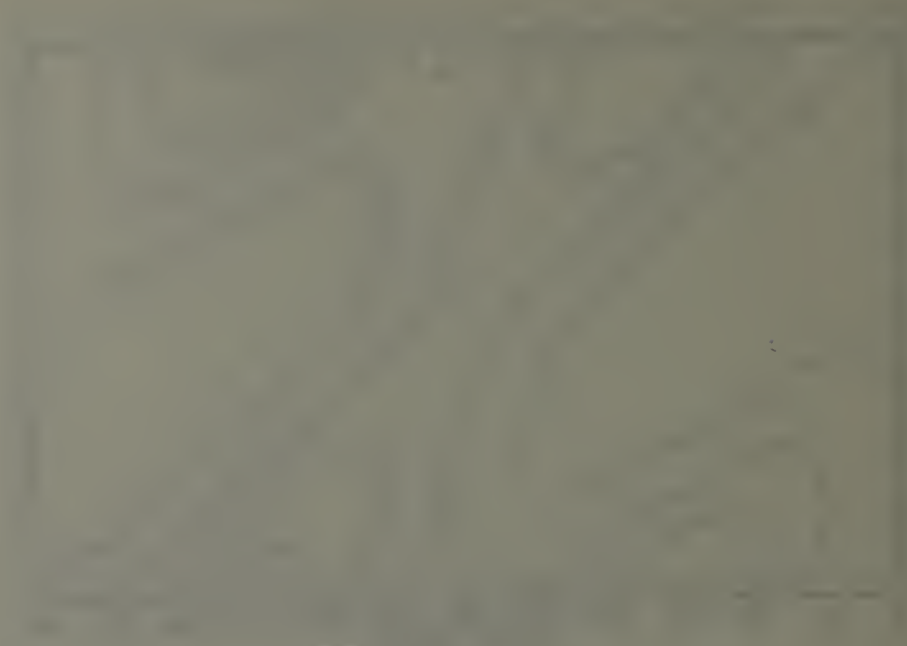

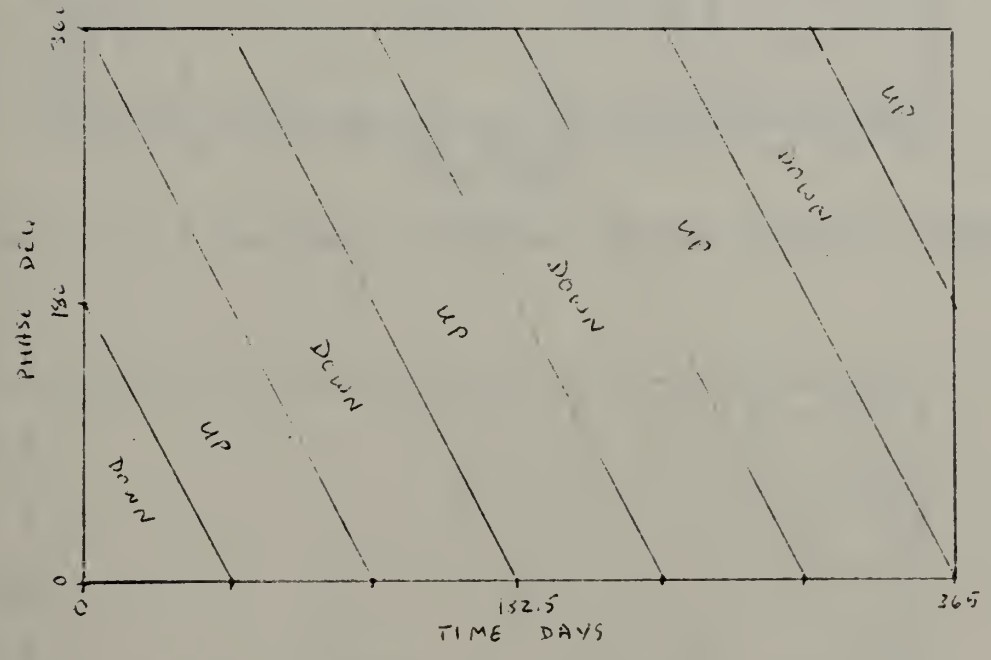

Figure A.30 1/3-Year Period Interior Motion.

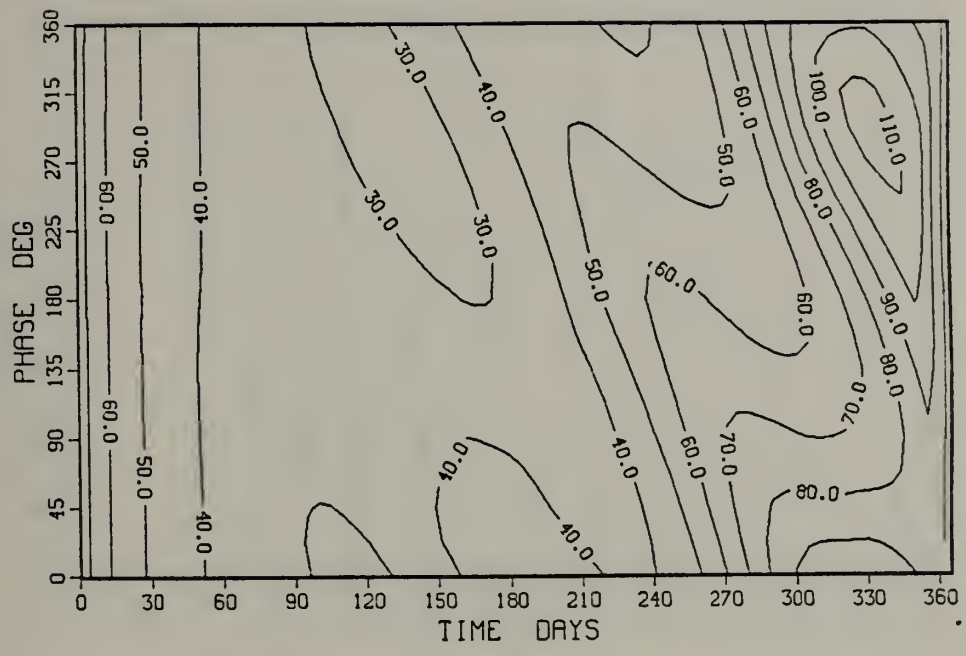

Figure A.31 h (meters), 1/3-Year Period Interior Motion.

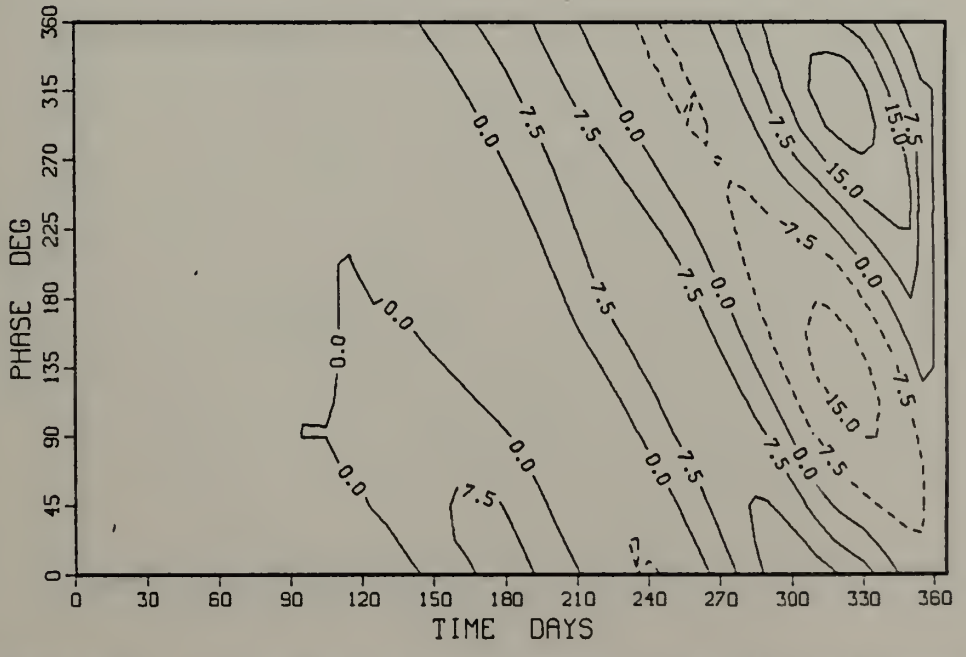

Figure A.32 Δh (meters), 1/3-Year Period Interior Motion.

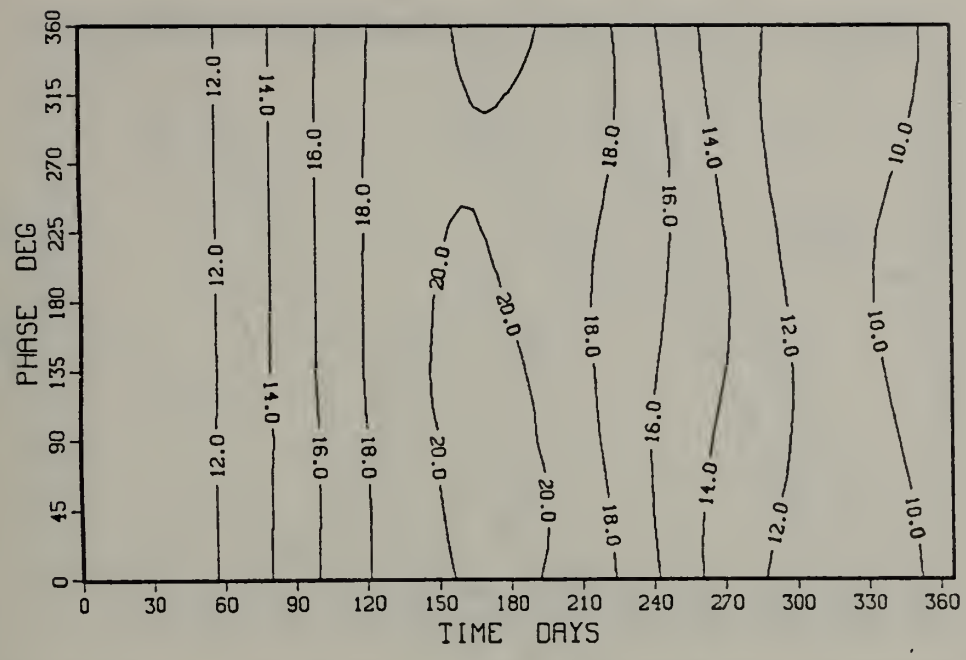

Figure A.33 $\bar{T}_{ML}$ (C), 1/3-Year Period Interior Mction.

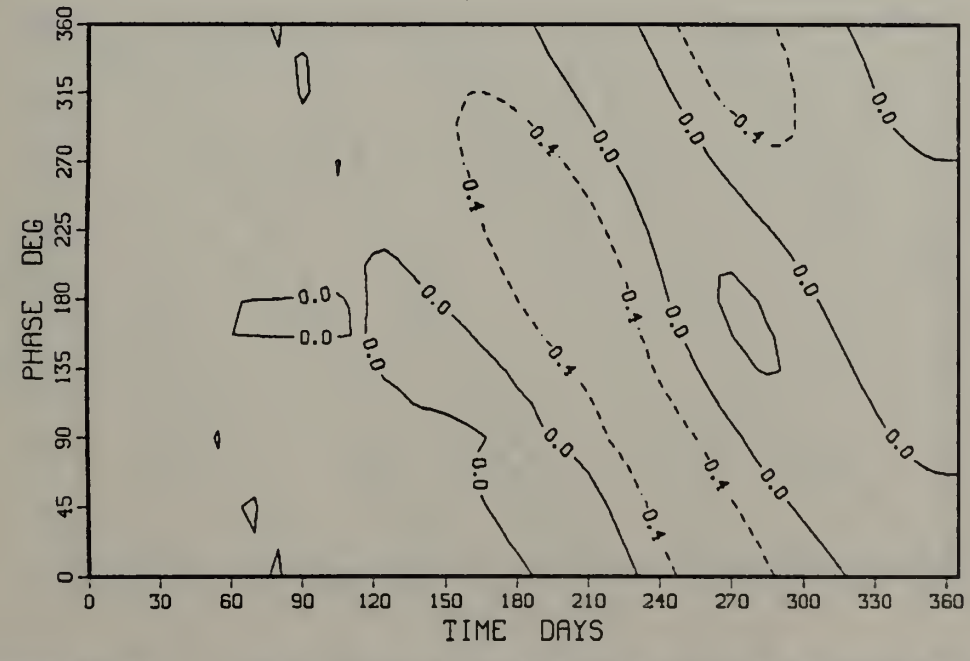

Figure A.34 $\Delta\bar{T}_{ML}$ (C), 1/3-Year Period Interior Motion.

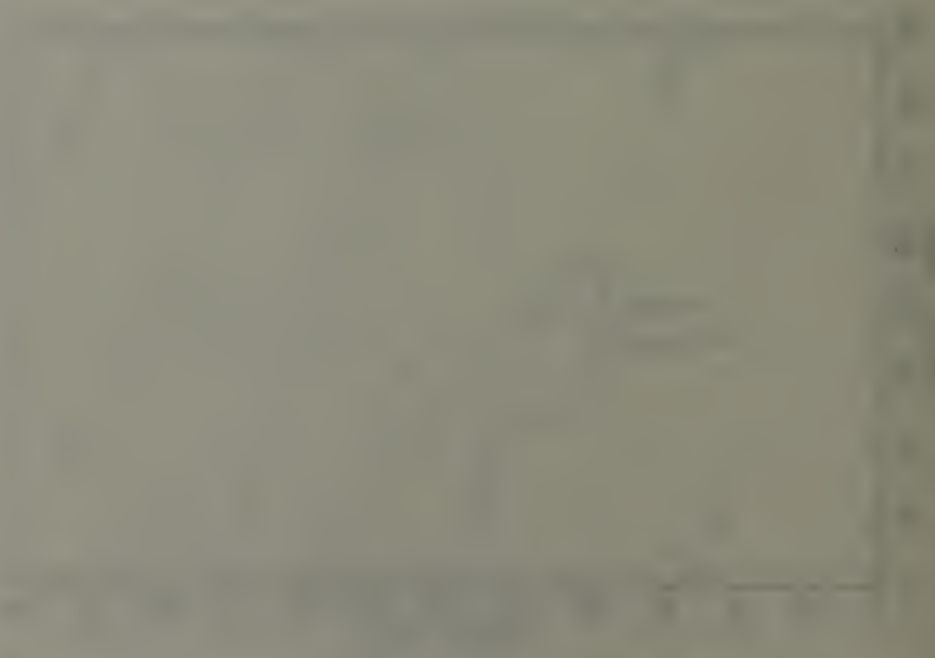

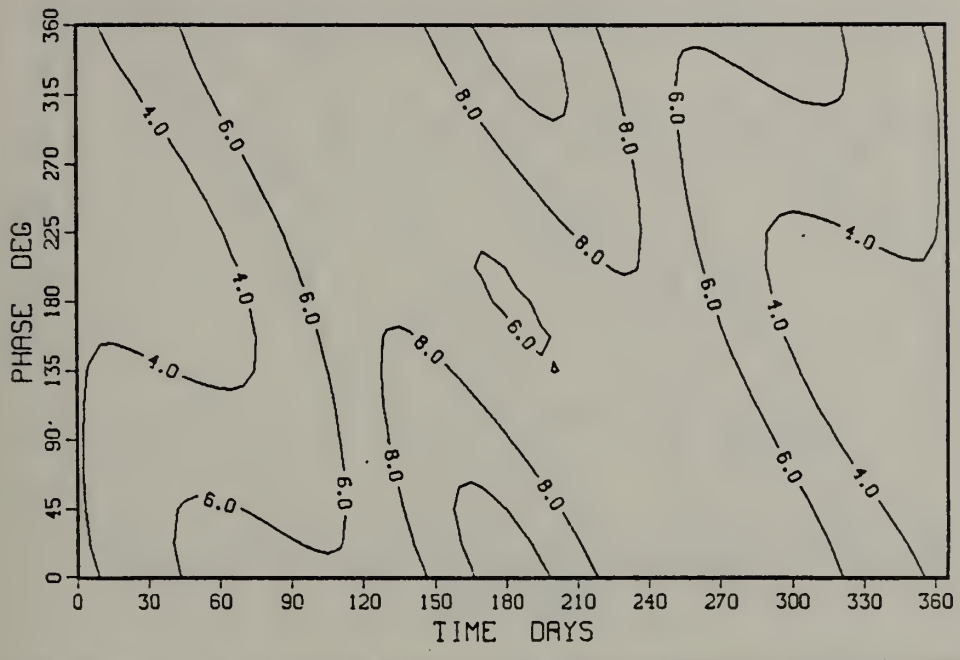

Figure A.35 H (100 °C m), 1/3-Year Period Interior Motion.

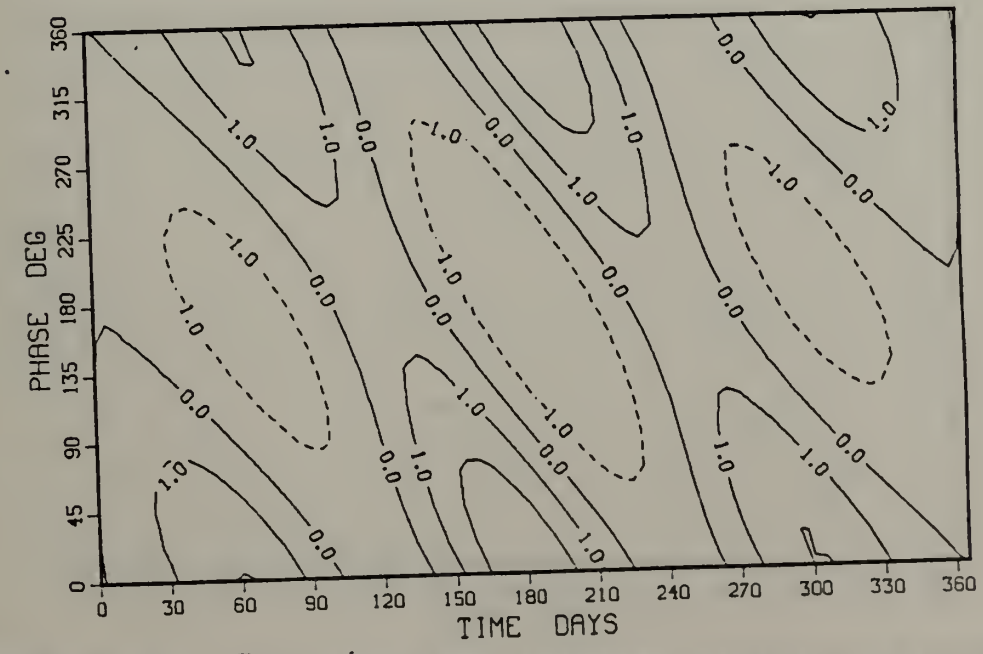

Figure A.36 $\Delta\bar{H}$ (100 °C m), 1/3-Year Period Interior Motion.

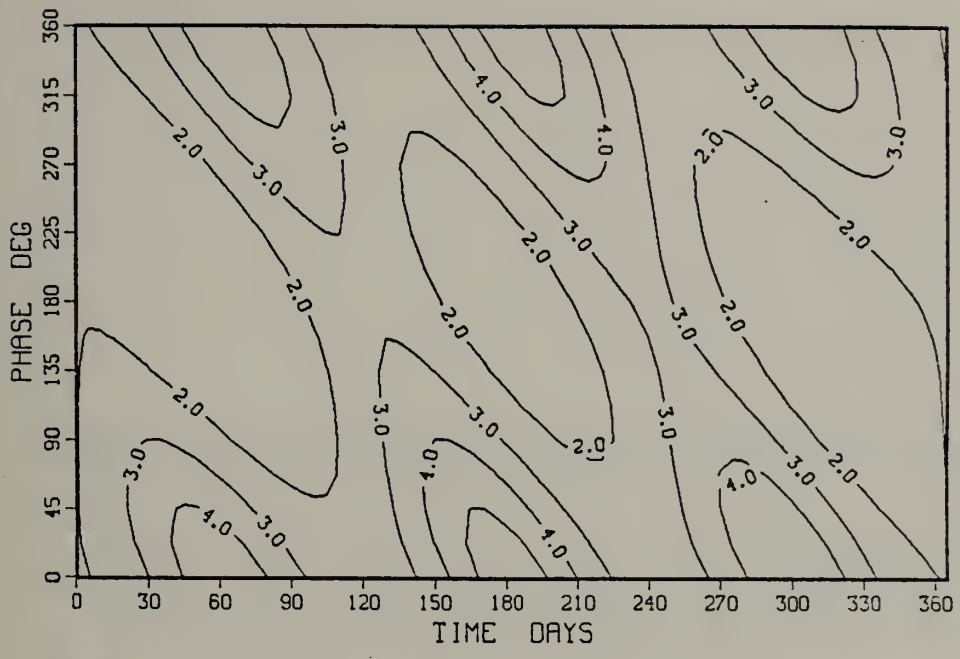

Figure A.37 P (10^4 °C m²), 1/3-Year Period Interior Motion.

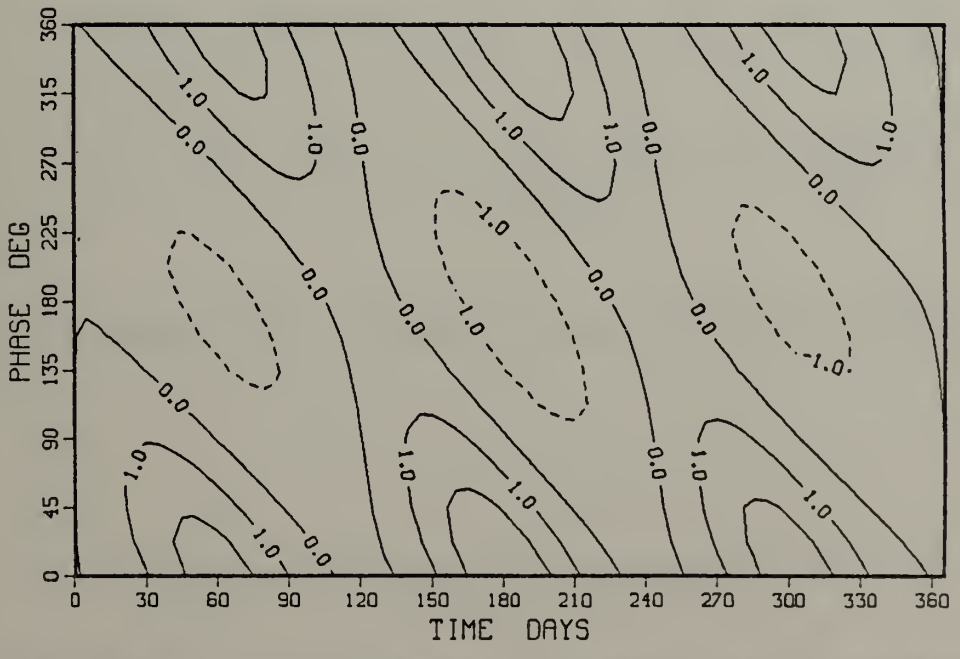

Figure A.38 ΔP (10^4 °C m²), 1/3-Year Period Interior Motion.

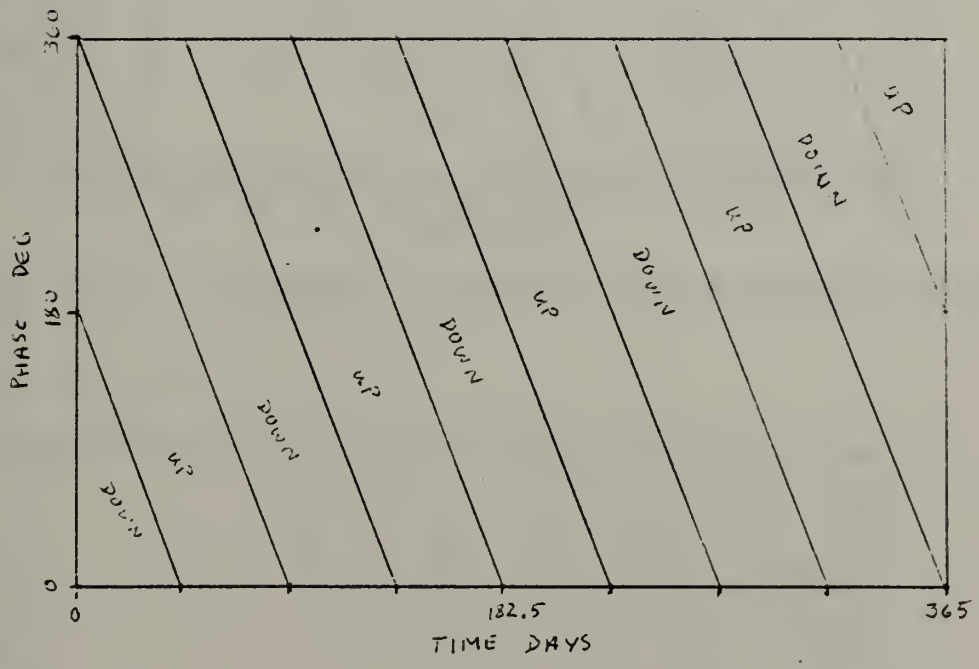

Figure A.39 1/4-Year Period Interior Motion.

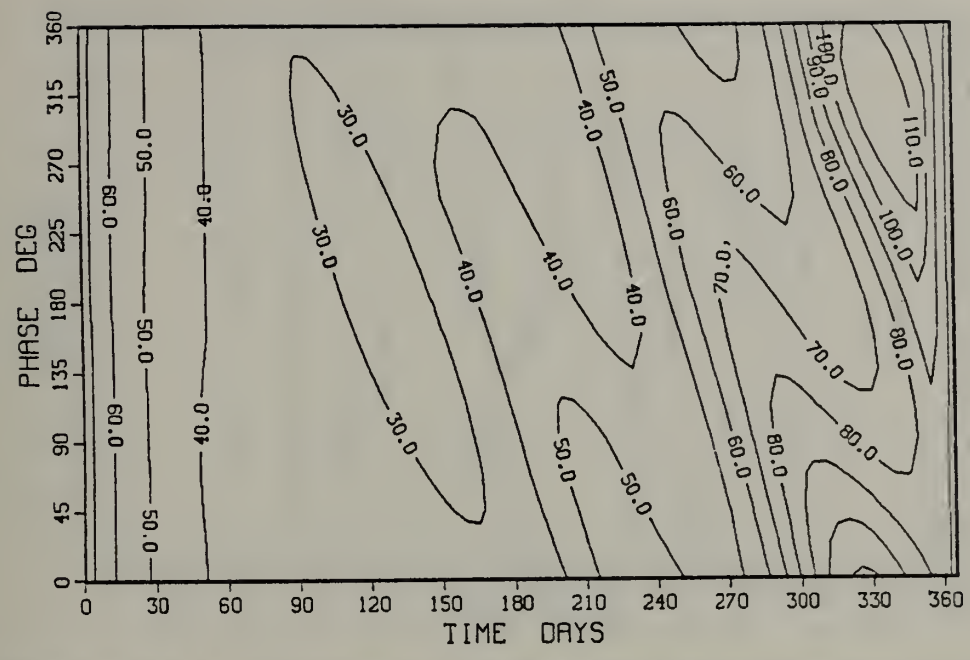

Figure A.40 h (meters), 1/4-Year Period Interior Motion.

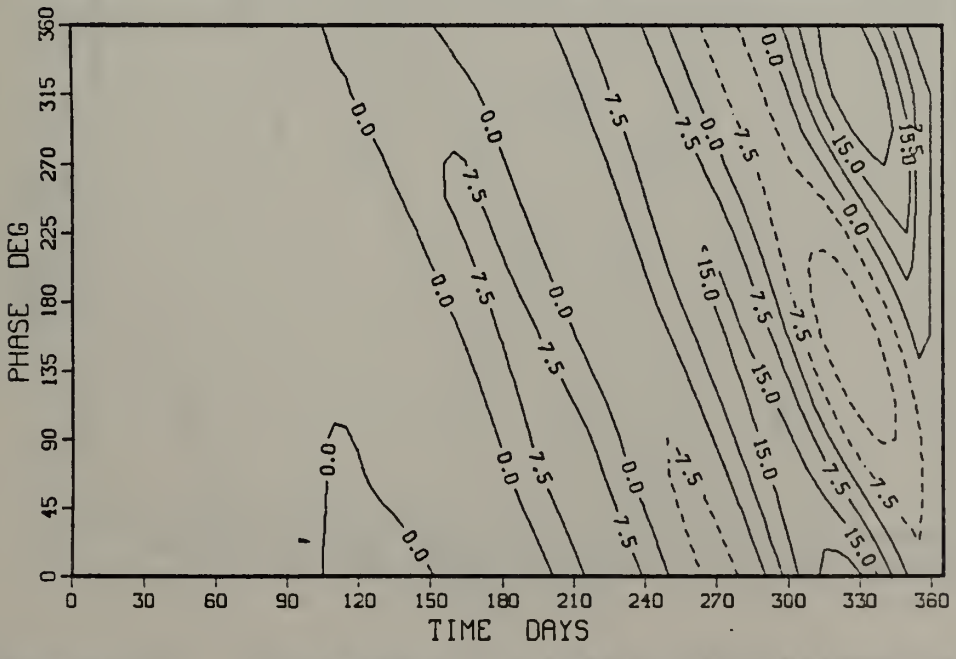

Figure A.41 Δh (meters), 1/4-Year Period Interior Motion.

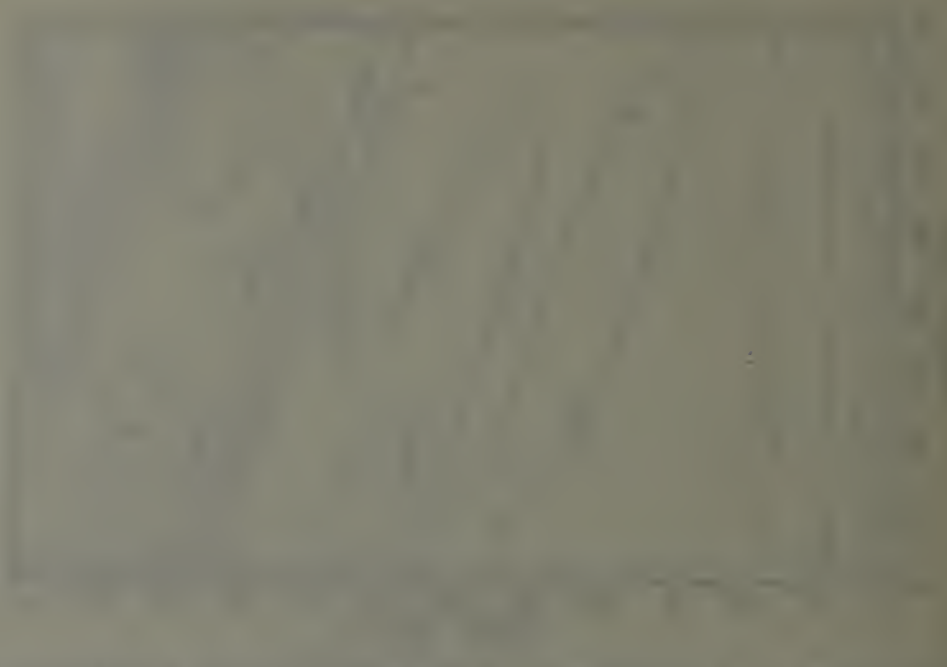

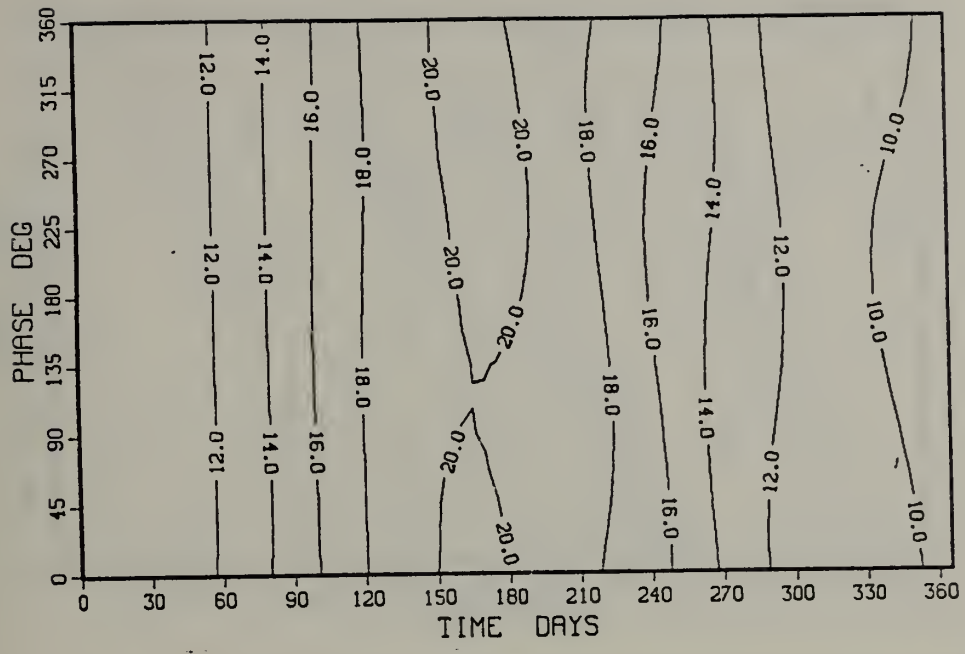

Figure A.42 $\bar{T}_{ML}$ (C), 1/4-Year Period Interior Motion.

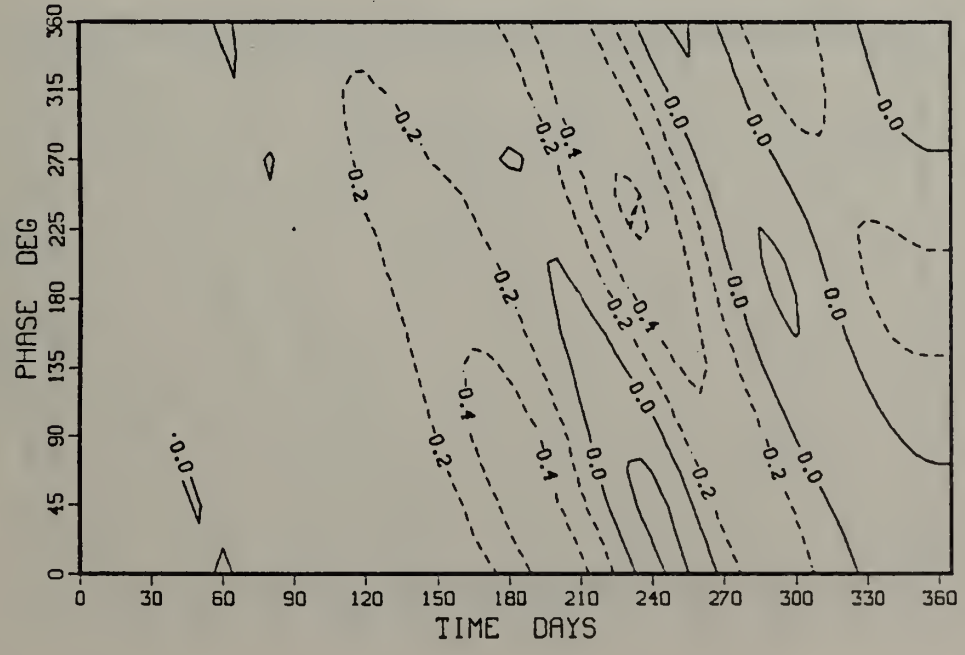

Figure A.43 $\Delta\bar{T}_{ML}$ (C), 1/4-Year Period Interior Motion.

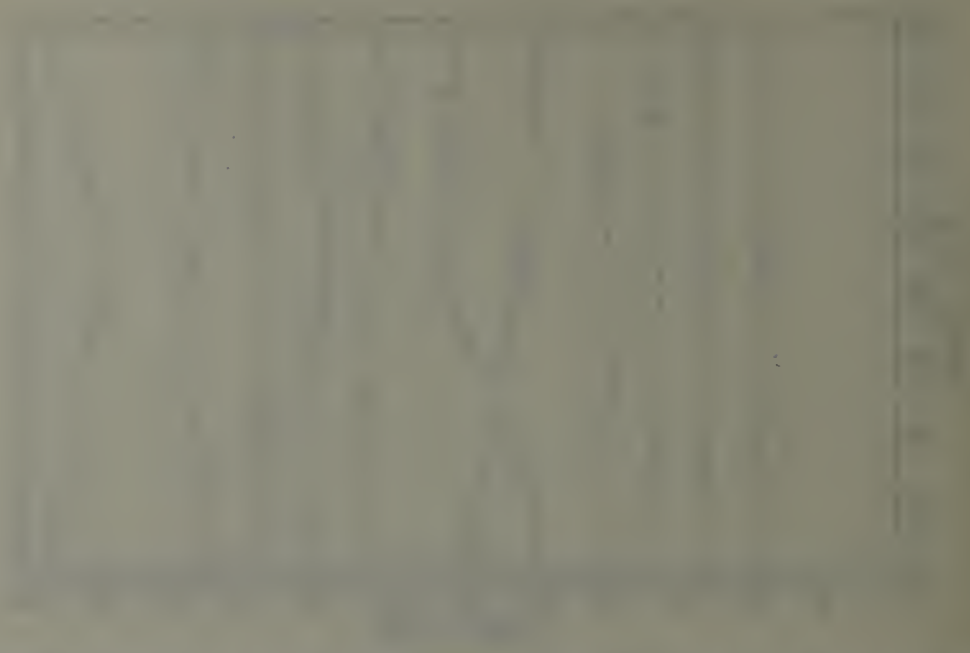

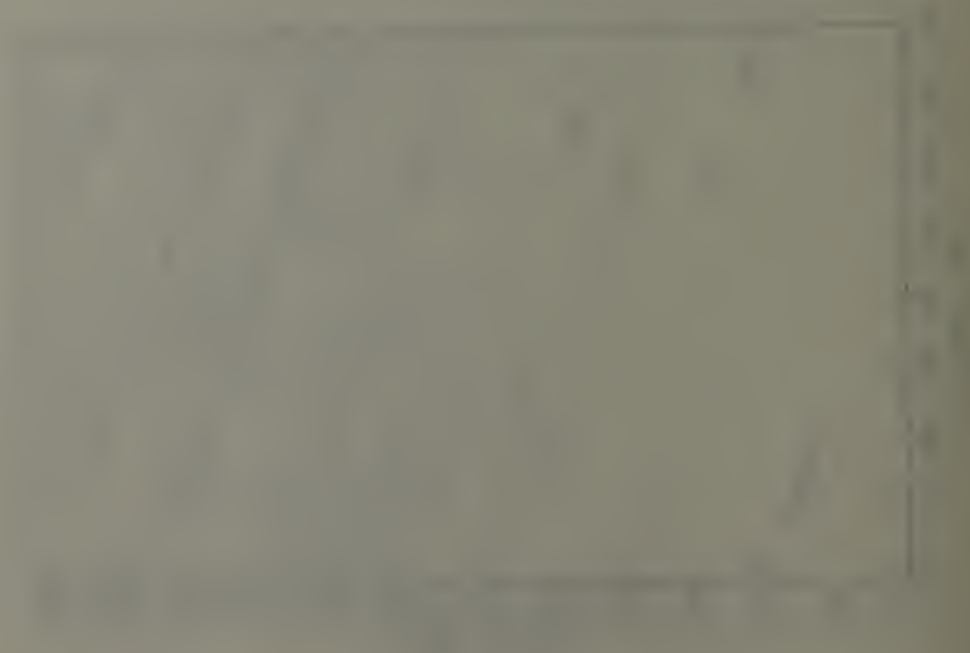

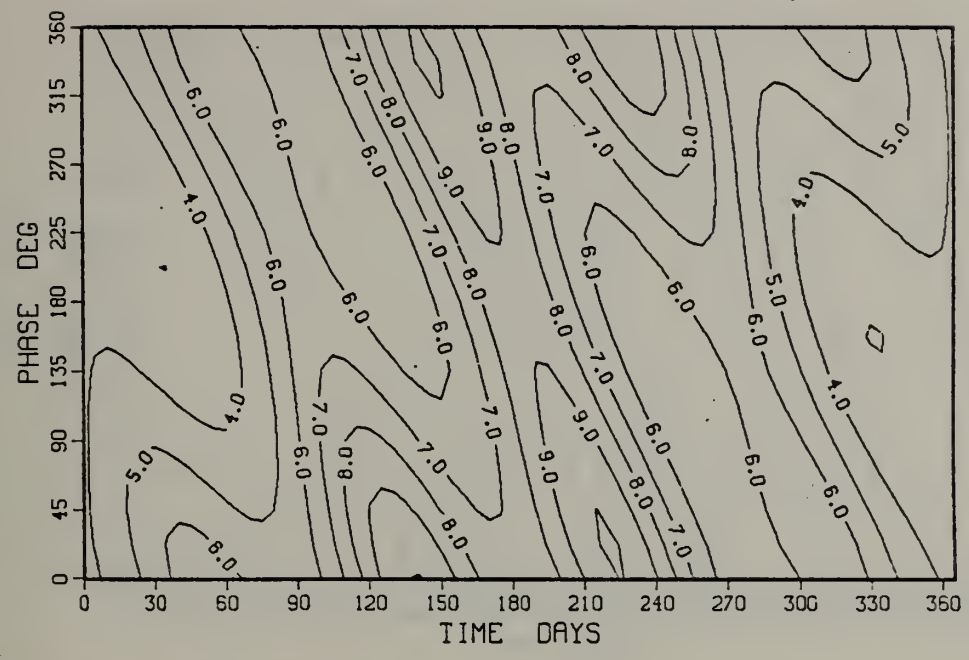

Figure A.44 H (100°C m), 1/4-Year Period Interior Motion.

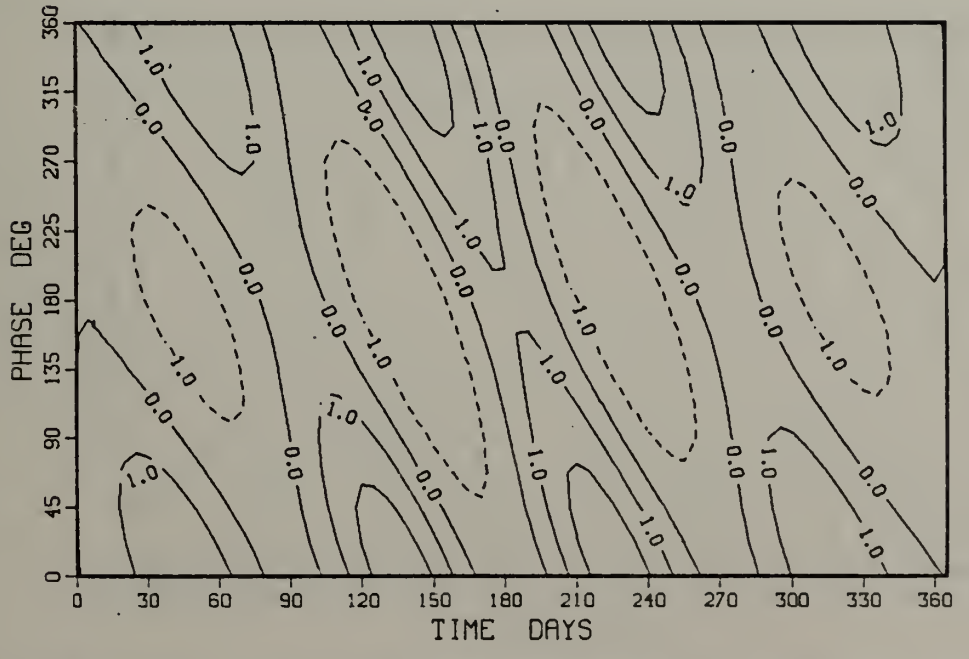

Figure A.45 ΔH (100°C m), 1/4-Year Period Interior Motion.

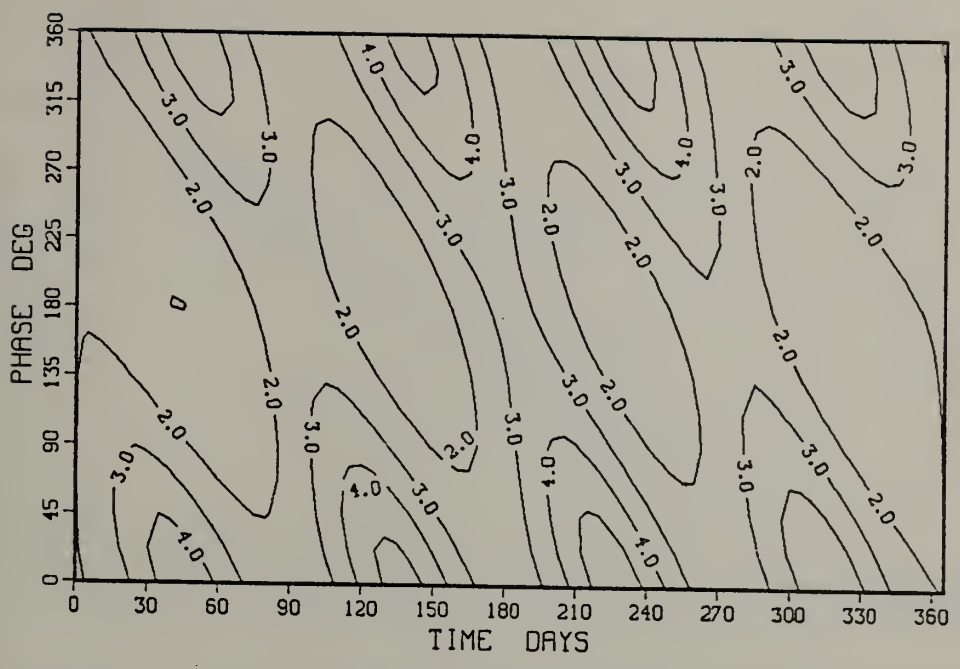

Figure A.46 P (10^4 °C m²), 1/4-Year Period Interior Motion.

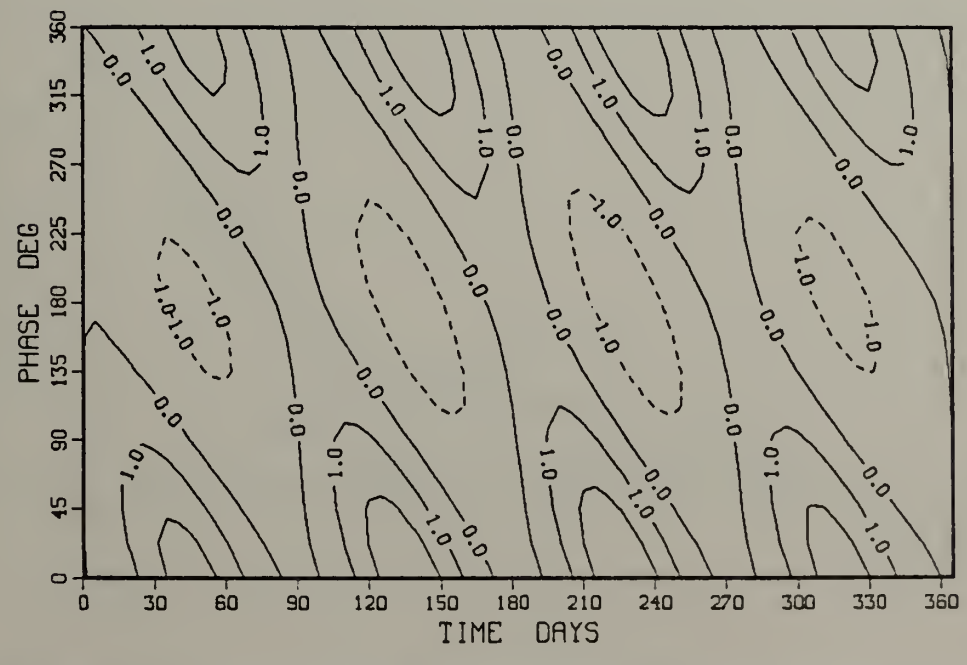

Figure A.47 △P (10^4 °C m²), 1/4-Year Period Interior Motion.

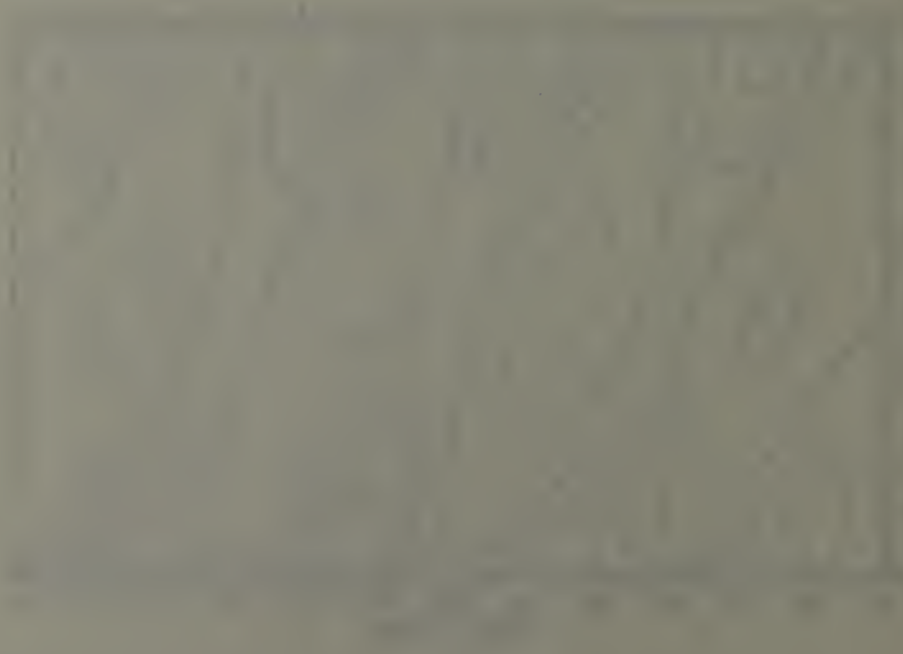

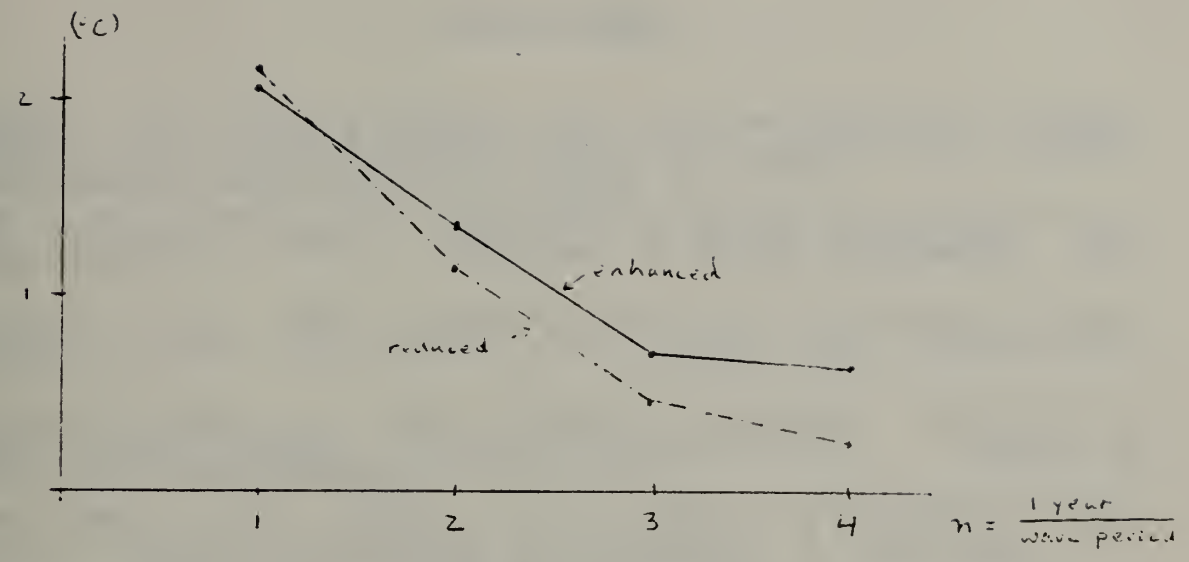

Figure A.48 Peak Enhanced and Reduced Cooling Values, Year 1.

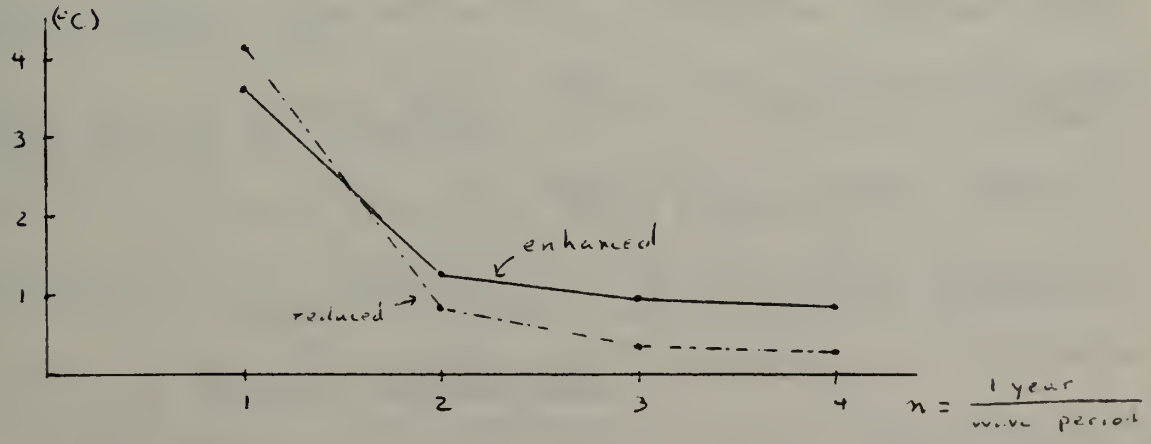

Figure A.49 Peak Enhanced and Reduced Cooling Values, Year 2.

BIBLIOGRAPHY

Adamec, D., R.L. Elsberry, R.W. Garwood and R.L. Haney, 1981: An embedded mixed-layer--ocean circulation model. Dynamics of Atmospheres and Oceans, 6, 69-96.

Bell, T.H., 1978: Radiation damping of inertial oscillations in the upper ocean. Journal of Fluid Mechanics, 88, 289-308.

Burger, R.J., 1982: Oceanic mixed layer response to tidal period internal wave motion. M.S. thesis, Naval Postgraduate School.

Cushman-Roisin, B., 1981: Effects of horizontal advection on upper ocean mixing: a case of frontogenesis. Journal of Physical Oceanography, 10, 1345-1356.

De Szceke, R.A., 1980: On the effects of horizontal variability of wind stress on the dynamics of the ocean mixed layer. Journal of Physical Oceanography, 9, 1439-1454.

Garwood, R.W., 1976: A general model of the ocean mixed layer using a two-component turbulent kinetic energy budget with mean turbulent field closure. Ph.D. thesis, University of Washington, (NOAA Tech. Rep. ERL 384-PMEL 27).

Garwood, R.W., 1977: An oceanic mixed layer model capable of simulating cyclic states. Journal of Physical Oceanography, 7, 455-468.

Greatbatch, R.J., 1983: On the response of the ocean to a moving storm: the sea-surface temperature response (unpublished manuscript).

Kang, Y.Q. and L. Magaard, 1980: Annual baroclinic Rossby waves in the central north Pacific. Journal of Physical Oceanography, 10, 1159-1167.

Linden, P.F., 1975: The deepening of a mixed layer in a stratified fluid. Journal of Fluid Mechanics, 7, 385-405.

Price, J.F., C.N.K. Mooers and J.C. Van Leer, 1978: Observation and simulation of storm-induced mixed-layer deepening. Journal of Physical Oceanography, 8, 582-599.

Price, J.F., 1981: Upper ocean response to a hurricane. Journal of Physical Oceanography, 11, 153-175.

Stevenson, J.W., 1980: Response of the surface mixed layer to quasi-geostrophic oceanic motions. Ph.D. thesis, Harvard University.

Stevenson, J.W., 1981: The seasonal variation of the surface mixed layer response to the vertical motions of linear Rossby waves (unpublished manuscript).

Willmott, A.J. and L.A. Mysak, 1980: Atmospherically forced eddies in the northeast Pacific. Journal of Physical Oceanography, 10, 1769-1791.

INITIAL DISTRIBUTION LIST

		No. Copies
1.	Defense Technical Information Center Cameron Station Alexandria, VA 22314	2
2.	Library, Code 0142 Naval Postgraduate School Monterey, CA 93943	2
3.	Professor C.N.K. Mooers (Code 68Mr) Chairman Department of Oceanography Naval Postgraduate School Monterey, CA 93943	1
4.	Professor R.J. Renard (Code 63Rd) Chairman Department of Meteorology Naval Postgraduate School Monterey, CA 93943	1
5.	Professor R.W. Garwood (Code 68Gd) Department of Oceanography Naval Postgraduate School Monterey, CA 93943	1
6.	Professor A.J. Willmott Department of Mathematics University of Exeter North Park Road Exeter EX4 4QE England	1
7.	Professor R.L. Elsberry (Code 63Es) Department of Meteorology Naval Postgraduate School Monterey, CA 93943	1
8.	Professor K.L. Davidson (Code 63Ds) Department of Meteorology Naval Postgraduate School Monterey, CA 93943	1
9.	Professor G.L. Geernaert (Code 63) Department of Meteorology Naval Postgraduate School Monterey, CA 93943	1
10.	LT J.P. Garner Naval Oceanography Command Center, Guam Box 12 FPO San Francisco, CA 96630	1
11.	Director Naval Oceanography Division Naval Observatory 34th and Massachusetts Avenue NW Washington, DC 20390	1

12. Commander 1
Naval Oceanography Command
NSTL Station
Bay St. Louis, MS 39522

13. Commanding Officer 1
Naval Oceanographic Office
NSTL Station
Bay St. Louis, MS 39522

14. Commanding Officer 1
Fleet Numerical Oceanography Center
Monterey, CA 93940

15. Commanding Officer 1
(Attn: S. Piacsek)
Naval Ocean Research and Development Activity
NSTL Station
Bay St. Louis, MS 39522

16. Commanding Officer 1
Naval Environmental Prediction Research Facility
Monterey, CA 93940

17. Chairman, Oceanography Department 1
U. S. Naval Academy
Annapolis, MD 21402

18. Chief of Naval Research 1
800 N. Quincy Street
Arlington, VA 22217

19. Office of Naval Research (Code 420) 1
Naval Ocean Research and Development Activity
800 N. Quincy Street
Arlington, VA 22217

20. Scientific Liaison Office 1
Office of Naval Research
Scripps Institute of Oceanography
La Jolla, CA 92037

21. Library 1
Scripps Institute of Oceanography
P.O. Box 2367
La Jolla, CA 92037

22. Library 1
Department of Oceanography
University of Washington
Seattle, WA 98105

23. Library 1
CICESE
P. O. Box 4803
San Ysidro, CA 92073

24. Library 1
School of Oceanography
Oregon State University
Corvallis, OR 97331

25. Commander 1
Oceanography Systems Pacific
Box 1390
Pearl Harbor, HI 96860

26. Richard J. Greatbatch 1
GFDI, NOAA
P.O. Box 308
Princeton, NJ 08542

27. Professor Peter Muller 1
Department of Oceanography
Univeristy of Hawaii
1000 Pope Rd.
Honolulu, HI 96822

28. Professor R.L. Haney 1
Department of Oceanography
Univeristy of Hawaii
1000 Pope Rd.
Honolulu, HI 96822

206375

Thesis
G1943 Garner
c.1 The offect of interior motion on seasonal thermocline evolution.